Copyright Warning & Restrictions

The copyright law of the United States (Title 17, United States Code) governs the making of photocopies or other reproductions of copyrighted material.

Under certain conditions specified in the law, libraries and archives are authorized to furnish a photocopy or other reproduction. One of these specified conditions is that the photocopy or reproduction is not to be "used for any purpose other than private study, scholarship, or research." If a, user makes a request for, or later uses, a photocopy or reproduction for purposes in excess of "fair use" that user may be liable for copyright infringement,

This institution reserves the right to refuse to accept a copying order if, in its judgment, fulfillment of the order would involve violation of copyright law.

Please Note: The author retains the copyright while the New Jersey Institute of Technology reserves the right to distribute this thesis or dissertation

Printing note: If you do not wish to print this page, then select "Pages from: first page # to: last page #" on the print dialog screen

ABSTRACT

COMMUNICATIONS WITH SPECTRUM SHARING IN 5G NETWORKS VIA DRONE-MOUNTED BASE STATIONS

by
Liang Zhang

The fifth generation wireless network is designed to accommodate enormous traffic demands for the next decade and to satisfy varying quality of service for different users. Drone-mounted base stations (*DBS*s) characterized by high mobility and low cost intrinsic attributes can be deployed to enhance the network capacity. In-band full-duplex (*IBFD*) is a promising technology for future wireless communications that can potentially enhance the spectrum efficiency and the throughput capacity. Therefore, the following issues have been identified and investigated in this dissertation in order to achieve high spectrum efficiency and high user quality of service.

First, the problem of deploying DBSs is studied. Deploying more DBSs may increase the total throughput of the network but at the expense of the operation cost. The droNe-mounted bAse station PlacEment (*NAPE*) problem with consideration of IBFD communications and DBS backhaul is then formulated. The objective is to minimize the number of deployed DBSs while maximizing the total throughput of the network by incorporating IBFD-enabled communications for both access links and backhaul links via DBSs as relay nodes. A heuristic algorithm is proposed to solve the NAPE problem, and its performance is evaluated via extensive simulations.

Second, the 3-D DBS placement problem is investigated as the communication efficiency is greatly affected by the positions of DBSs. Then, the DBS placement with IBFD communications (*DSP-IBFD*) problem for downlink communications is formulated, and two heuristic algorithms are proposed to solve the DSP-IBFD problem based on different DBS placement strategies. The performance of the proposed algorithms are demonstrated via extensive simulations.

Third, the potential benefits of jointly optimizing the radio resource assignment and 3-D DBS placement are explored, upon which the Drone-mounted Base Station Placement with IBFD communications (*DBSP-IBFD*) problem is formulated. Since the DBSP-IBFD problem is NP-hard, it is then decomposed into two sub-problems: the joint bandwidth, power allocation and UE association problem and the DBS placement problem. A $\frac{1}{2}(1-\frac{1}{2^l})$-approximation algorithm is proposed to solve the DBSP-IBFD problem based on the solutions to the two sub-problems, where l is the number of simulation runs. Simulation results demonstrate that the throughput of the proposed approximation algorithm is superior to benchmark algorithms.

Fourth, the uplink communications is studied as the mobile users need to transmit and receive data to and from base stations. The Backhaul-aware Uplink communications in a full-duplex DBS-aided HetNet (*BUD*) problem is investigated with the objective to maximize the total throughput of the network while minimizing the number of deployed DBSs. Since the BUD problem is NP-hard, it is then decomposed into three sub-problems: the joint UE association, power and bandwidth assignment problem, the DBS placement problem and the problem of determining the number of DBSs to be deployed. The AA-BUD algorithm is proposed to solve the BUD problem with guaranteed performance based on the solutions to the three sub-problems, and its performance is demonstrated via extensive simulations.

The future work comprises two parts. First, a DBS can be used to provide both communications and computing services to users. Thus, how to minimize the average latency of all users in a DBS-aided mobile edge computing network requires further investigation. Second, the short flying time of a drone limits the deployment and the performance of DBSs. Free space optics (*FSO*) can be utilized as the backhaul link and the energizer to provision both communication and energy to a DBS. How to optimize the charging efficiency while maximizing the total throughput of the network requires further investigation.

COMMUNICATIONS WITH SPECTRUM SHARING IN 5G NETWORKS VIA DRONE-MOUNTED BASE STATIONS

by
Liang Zhang

A Dissertation
Submitted to the Faculty of
New Jersey Institute of Technology
in Partial Fulfillment of the Requirements for the Degree of
Doctor of Philosophy in Electrical Engineering

Helen and John C. Hartmann Department of
Electrical and Computer Engineering

May 2020

APPROVAL PAGE

COMMUNICATIONS WITH SPECTRUM SHARING IN 5G NETWORKS VIA DRONE-MOUNTED BASE STATIONS

Liang Zhang

Dr. Nirwan Ansari, Dissertation Advisor — Date
Distinguished Professor, Department of Electrical and Computer Engineering, NJIT

Dr. Abdallah Khreishah, Committee Member — Date
Associate Professor, Department of Electrical and Computer Engineering, NJIT

Dr. Qing Liu, Committee Member — Date
Assistant Professor, Department of Electrical and Computer Engineering, NJIT

Dr. Yuanqiu Luo, Committee Member — Date
Principal Engineer, FutureWei Technologies

Dr. Roberto Rojas-Cessa, Committee Member — Date
Professor, Department of Electrical and Computer Engineering, NJIT

BIOGRAPHICAL SKETCH

Author: Liang Zhang

Degree: Doctor of Philosophy

Date: May 2020

Undergraduate and Graduate Education:

- Doctor of Philosophy in Electrical Engineering,
  New Jersey Institute of Technology, Newark, NJ, 2020.
- Master of Engineering Information and Communication Engineering,
  University of Science and Technology of China, Hefei, China, 2014.
- Bachelor of Electronic Science and Technology,
  Huazhong University of Science and Technology, Hubei, China, 2006.

Major: Electrical Engineering

Presentations and Publications:

Journal Articles:

N. Ansari and **L. Zhang**, "Flexible backhaul-aware DBS-aided HetNet with IBFD communications," *ICT Express*, vol. 6, no. 1, pp. 48-56, Mar. 2020 (Invited Paper).

L. Zhang and N. Ansari, "Optimizing the deployment and throughput of DBSs for uplink communications," *IEEE Open Journal of Vehicular Technology (OJVT)*, vol. 1, pp. 18-28, Jan. 2020 (Invited Paper).

N. Ansari, Q. Fan, X. Sun and **L. Zhang**, "SoarNet," *IEEE Wireless Communications*, vol. 26, no. 6, pp. 37-43, Dec. 2019.

L. Zhang and N. Ansari, "A framework for 5G Networks with in-band full-duplex enabled drone-mounted base-stations," *IEEE Wireless Communications*, vol. 26, no. 5, pp. 121-127, Oct. 2019.

L. Zhang and N. Ansari, "Approximate algorithms for 3-D placement of IBFD enabled drone-mounted base-stations," *IEEE Transactions on Vehicular Technology*, vol. 68, no. 8, pp. 7715-7722, Jun. 2019.

L. Zhang and N. Ansari, "On the number and 3-D placement of in-band full-duplex enabled drone-mounted base-stations," *IEEE Wireless Communications Letters*, vol. 8, no. 1, pp. 221-224, Feb. 2019.

L. Zhang, Q. Fan and N. Ansari, "3-D drone-base-station placement with in-band full-duplex communications," *IEEE Communications Letters*, vol. 22, no. 9, pp. 1902-1905, Sept. 2018.

L. Zhang, T. Han and N. Ansari, "Energy-aware virtual machine management in inter-datacenter networks over elastic optical infrastructure," *IEEE Transactions on Green Communications and Networking*, vol. 2, no. 1, pp. 305-315, Mar. 2018.

L. Zhang, N. Ansari and A. Khreishah, "Anycast planning in space division multiplexing elastic optical networks with multi-core fibers," *IEEE Communications Letters*, vol. 20, no. 10, pp. 1983-1986, Oct. 2016.

P. Lu, **L. Zhang**, X. Liu, J. Yao and Z. Zhu, "Highly efficient data migration and backup for big data applications in elastic optical inter-data-center networks," *IEEE Network*, vol. 29, no. 5, pp. 36-42, Sept. 2015.

L. Zhang and Z. Zhu, "Spectrum-efficient anycast in elastic optical inter-datacenter networks," *Optical Switching and Networking (Elsevier)*, vol. 14, no. 3, pp. 250-259, Aug. 2014.

Z. Zhu, W. Lu, **L. Zhang** and N. Ansari, "Dynamic service provisioning in elastic optical networks with hybrid single-/multi-path routing," *IEEE/OSA Journal of Lightwave Technology*, vol. 31, no. 1, pp. 15-22, Jan. 2013.

Z. Zhu, X. Chen, F. Ji, **L. Zhang**, F. Farahmand and J. P. Jue, "Energy efficient translucent optical transport networks with mixed regenerator placement," *IEEE/OSA Journal of Lightwave Technology*, vol. 30, no. 19, pp. 3147-3156, Oct. 2012.

Conference Papers

L. Zhang and N. Ansari, "Backhaul-aware uplink communications in full-duplex DBS-aided HetNets," *Proc. 2019 IEEE Global Communications Conference (GLOBECOM 2019)*, Waikoloa, HI, USA, Dec. 9-13, 2019.

L. Zhang, Y. Luo, N. Anwari, B. Gao, X. Liu and F. Effenberger, "Enhancing next generation passive optical network stage2 (NG-PON2) with channel bonding," *International Conference on Networking, Architecture, and Storage*, pp. 1-6, Aug. 2017.

L. Zhang, Y. Luo, N. Ansari, B. Gao, X. Liu and F. Effenberger, "Channel bonding for next generation passive optical network stage 2 (NG-PON2)," *International Conference on Computer, Information and Telecommunication Systems (CITS)*, pp. 103-107, Jul. 2017.

Y. Luo, **L. Zhang**, N. Ansari, B. Gao, X. Liu and F. Effenberger, "Wavelength channel bonding for 100 Gb/s next generation passive optical networks," *Wireless and Optical Communication Conference (WOCC)*, pp. 1-6, Apr. 2017.

L. Zhang, Y. Luo, B. Gao, X. Liu, F. Effenberger and N. Ansari, "Channel bonding design for 100 Gb/s PON based on FEC codeword alignment," *Optical Fiber Communications Conference and Exhibition (OFC)*, pp. 1-3, Mar. 2017.

L. Zhang, T. Han and N. Ansari, "Revenue driven virtual machine management in green datacenter networks towards big data," *IEEE Global Communications Conference (GLOBECOM)*, pp. 1-6, Dec. 2016 (NSF Travel Grant).

L. Zhang, T. Han and N. Ansari, "Renewable energy-aware inter-datacenter virtual machine migration over elastic optical networks," *IEEE International Conference on Cloud Computing Technology and Science (CloudCom)*, pp. 440-443, Dec. 2015.

X. Liu, **L. Zhang**, M. Zhang and Z. Zhu, "Joint defragmentation of spectrum and computing resources in inter-datacenter networks over elastic optical infrastructure," *IEEE International Conference on Communications (ICC)*, pp. 3289-3294, Jun. 2014.

L. Zhang and Z. Zhu, "Dynamic anycast in inter-datacenter networks over elastic optical infrastructure," *International Conference on Computing, Networking and Communications (ICNC)*, pp. 1-5, Feb. 2014 (Best Paper Award).

L. Zhang, W. Lu, X. Zhou, and Z. Zhu, "Dynamic RMSA in spectrum-sliced elastic optical networks for high-throughput service provisioning," *International Conference on Computing, Networking and Communications (ICNC)*, pp. 380-384, Jan. 2013.

People might not get all they work for in this world, but they must certainly work for all they get.

Frederick Douglass

ACKNOWLEDGMENT

My deepest gratitude is to my advisor, Dr. Nirwan Ansari. He had supported me in the past six years, and helped me overcome difficulties and frustration in my research and life. Without his efforts, this dissertation would not have been possible. I extremely appreciate his help, guidance, and encouragement.

This dissertation is based on the work supported by National Science Foundation under Grant No. CNS-1320468 and No. CNS-1814748.

To my committee members, Dr. Abdallah Khreishah, Dr. Qing Liu, Dr. Roberto Rojas-Cessa, and Dr. Yuanqiu Luo, I really appreciate them for their time and advisement.

I want to thank my friends –– Tao Han, Mina Taheri, Xueqing huang, Abbas Kiani, Xiang Sun, Xilong Liu, Qiang Fan, Ali Shahini, Di Wu, Jingjing Yao, Shuai Zhang, and many others, who have given me support and encouragement in the past six years.

I would like to appreciate other faculty and staff members in the ECE department for their help and support during my doctoral studies.

Finally, I greatly appreciate my family for their unwavering support.

TABLE OF CONTENTS

TABLE OF CONTENTS
(Continued)

Chapter **Page**

LIST OF TABLES

LIST OF FIGURES

Figure **Page**

CHAPTER 1

INTRODUCTION

The fifth generation (5G) of mobile communication systems has attracted much attention from both industry and academia to meet the 1000× wireless traffic increment in the next decade [1]. Future 5G wireless networks are designed to meet various user quality of service (QoS) requirements such as data rate and latency, and to provide dense hotspot coverage with high capacity in metropolitan areas [2]. Monthly global mobile data traffic reached 7 exabytes (EB) in 2016, and this number is expected to reach 49 EB by 2021; moreover, future 5G networks will provide high bandwidth ($>= 1Gbps$), wider coverage, and ultra-low latency to mobile terminals as compared to 4G networks [3, 4]. It is expected to provide throughput 1000 times and spectrum efficiency 10 times those of 4G networks; therefore, some new communications techniques such as cognitive radio, device-to-device communications, in-band full-duplex ($IBFD$) communications, non-orthogonal multiple access ($NOMA$), and Long Term Evolution on unlicensed spectrum ($LTE\text{-}U$) should be leveraged [5].

Unmanned aerial vehicles (UAVs) have recently been used to mount base stations to improve the QoS of wireless networks by increasing the network capacity and enhancing the coverage area; for example, more user equipment (UEs) can be provisioned by moving the UAV-mounted base station, viz. drone-mounted base station (DBS), close to the UEs [6]. DBSs can be deployed to provide wireless services with high mobility and low cost [7]. DBS presents several advantages: i) it can fly across a hazardous area, ii) it can be easily mobilized (high mobility), iii) it incurs low cost, and iv) it can change its altitude to provide guaranteed QoS based on UE intensity [8]. DBSs are especially useful for provisioning communications for temporary large-scale or unexpected events such as Olympic games, football games,

concerts, and some other application scenarios such as public safety, rescue missions, and reconnaissance for disaster recovery [9, 10].

Industry has started developing DBS; for examples, ATT's Cell Tower on Wings (*COW*) project [11] targeted to provide emergency service or to enhance the network coverage for large events; Nokia and UK mobile operator Everything Everywhere (*EE*) built DBS prototypes in 2016, and they demonstrated that DBSs flying in the air were able to provide 4G coverage [12]; Facebook's Aquila project and Google's SkyBender project focused on leveraging the solar powered DBSs to provide internet connections through millimeter wave radio transmissions [8].

Communications can be simplex or duplex, and duplex communications can be half duplex (*HD*) or full duplex (*FD*); simplex communications implies one way communications (either transmitting or receiving), and duplex communications refers to bi-directional communications; either frequency division duplex (*FDD*) or time division duplex (*TDD*) can be used in HD communications to separate the transmission and the reception [13].

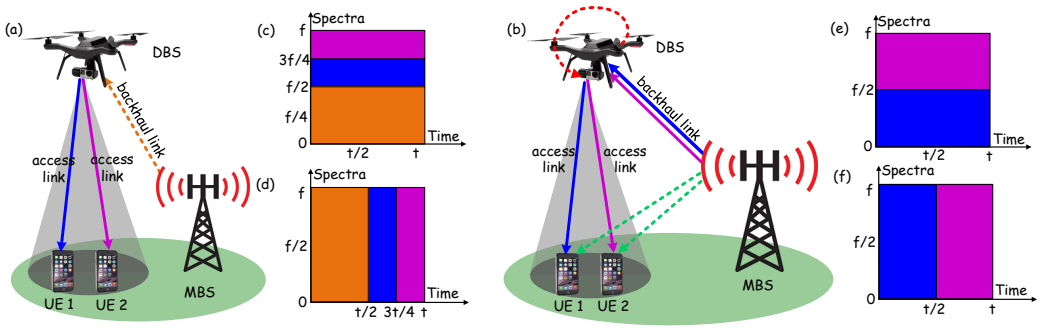

Transmission \ Communications	Resource Allocation	Half Duplex			Full Duplex		
		MBS-DBS	DBS-UE1	DBS-UE2	MBS-DBS	DBS-UE1	DBS-UE2
FDD	Frequency	(0, f/2)	(f/2, 3f/4)	(3f/4, f)	(0, f)	(0, f/2)	(f/2, f)
	Time	(0, t)	(0, t)	(0, t)	(0, t)	(0, t)	(0, t)
TDD	Frequency	(0, f)	(0, f)	(0, f)	(0, f)	(0, f)	(0, f)
	Time	(0, t/2)	(t/2, 3t/4)	(3t/4, t)	(0, t)	(0, t/2)	(t/2, t)

Backhaul interference

Self interference

Figure 1.1 Half duplex (a) and full duplex (b) communications in DBS-assisted HetNet; resource allocation with FDD (c) and TDD (d) in half duplex communications; resource allocation with FDD (e) and TDD (f) in full duplex communications.

Figure 1.1(a) shows a DBS-assisted HD cellular network, which includes a MBS (HD-enabled), a DBS (HD-enabled), two UEs (HD-enabled), the backhaul link (from the MBS to the DBS), and access links (from the DBS to UEs) [4]. Resource can be allocated in a FDD manner as shown in Figure 1.1(c) and in a TDD manner as shown in Figure 1.1(d). Figure 1.1(c) describes the frequency spectra allocation by utilizing FDD, where the backhaul link uses half of the total available frequency spectra f over time t, and two access links equally share the remaining half of the total available frequency spectra over time t. Figure 1.1(d) illustrates the time resource allocation by utilizing TDD, where the backhaul link uses half of the total available time t over frequency spectra f, and two access links equally share the remaining half of available time t over frequency spectra f.

In order to illustrate the differences between HD and FD communications, we use an example to show the time and frequency resource allocation of FD communications. Figure 1.1(b) illustrates a DBS-assisted FD cellular network, which includes a MBS (HD-enabled), a DBS (FD-enabled), two UEs (HD-enabled), the backhaul link and access links. Figure 1.1(e) describes the frequency spectra allocation by utilizing FDD, where the backhaul link uses the total available frequency spectra f over time t, and two access links equally share the total available frequency spectra f over time t. Figure 1.1(f) illustrates the time resource allocation by utilizing TDD, where the backhaul link uses the total available time t over frequency spectra f, and two access links equally share the total available time t over frequency spectra f. Figure 1.1 shows that FD can roughly double the spectrum efficiency (throughput) without consideration of the self-interference (SI).

In-band full-duplex ($IBFD$) is able to transmit and receive data through the same radio frequency; it is a promising technology for future wireless networks and can potentially double the spectrum efficiency and the throughput capacity as compared to conventional half-duplex (HD) systems [13]. In the past, it seems impossible to

realize IBFD because of the severe self-interference (SI) from the transmitter to the co-located receiver. SI is the interference to the received signals from the radiated power of the transmission that limits the performance of the full-duplex (FD) system [14]. However, recent creative hardware design of SI cancellation techniques has been demonstrated to efficiently suppress SI power, thus making FD communications feasible for wireless communications [14]. Note that SI is the received interfering signals from the wireless terminal's own transmitter while receiving desired signals, and IBFD communications induces severe SI from the transmitter to the co-located receiver [13]. Recent works demonstrate that SI power can be suppressed by SI cancellation techniques by as much as 150 dB [15], thus making IBFD communications feasible [14]. Since IBFD has the potential to improve the throughput and DBSs can improve the QoS of the wireless network, we focus on the DBS placement and communications of IBFD enabled DBSs in a heterogeneous network ($HetNet$).

Although many works have been reported related to DBS communications, many issues still require investigation to efficiently utilize the radio resources in the DBS-assisted HetNet.

1) How many DBSs should be deployed to provide guaranteed quality of service to users? The operation cost increases if more DBSs are deployed. Then, it is important to minimize the number of DBSs to be deployed while the throughput of the network is maximized.

2) How to allocate/manage radio resources and the DBS placement in a DBS-aided HetNet? Inefficient radio resource assignment limits the throughput performance of the network and thus user quality of service cannot be satisfied. The throughput of the DBSs can also be affected by the DBS placement. Hence, it is important to place the DBSs in the appropriate positions and carefully assign the radio resources to users to improve the throughput performance of the network. How to manage the interferences in a HetNet with IBFD-enabled DBSs? Note that IBFD

communications can improve the spectrum efficiency but it brings more interference to the network, etc., the severe SI and the backhaul interference.

3) How to maximize the total throughput for the uplink communications while minimizing the number of deployed DBSs? Uplink communications is different from downlink communications. The user-BS interference is in the access link (DBS to users) in downlink communications but that interference exists in the backhaul link (DBS to the MBS) in uplink communications. Meanwhile, a high operation cost is incurred if more DBS are deployed. Then, it is important to minimize the number of deployed DBSs while maximizing the total throughput of the network.

The rest of this dissertation is organized as follows. In Chapter 2, we study the problem of deploying DBSs for the downlink communications and the objective is to minimize the number of required DBSs while maximizing the total throughput of the network. In Chapter 3, the three dimensional DBS Placement with in-band full-duplex communications is investigated. In Chapter 4, an approximation algorithm with low complexity is designed to solve the joint radio resource assignment and DBS placement problem and this algorithm is proved to provide guaranteed performance. In Chapter 5, the backhaul-aware uplink communications in a full-duplex DBS-aided HetNet (BUD) problem with the target to maximize the total throughput of the network and minimize the number of deployed DBSs is investigated. In Chapter 6, two future research endeavors are briefly described: i) DBS-aided/UAV-aided mobile edge computing: DBSs are deployed to provide both communications and computing to users, and ii) laser for both charging and communications. Free space optics (FSO) can be used to provide energy and backhaul communications to a DBS. In other words, an FSO beam is utilized as both the backhaul and energizer for a DBS in the DBS-aided HetNet. The conclusion is summarized in Chapter 7.

CHAPTER 2

OPTIMIZING THE DEPLOYED NUMBER OF DRONE-MOUNTED BASE STATIONS

Alzenad *et al.* [16] studied the UAV base stations placement problem to maximize the number of covered UEs; Kalantari *et al.* [17] investigated the problem of 3-D placement of a DBS with consideration of the data rate of the wireless backhaul and the DBS; Chen *et al.* [18] studied the optimum UAV placement for maximum reliability in a hotspot; Mozaffari *et al.* [19] investigated optimal 3-D UAV placement based on the circle packing theory without overlapping coverage areas in a hotspot; Siddique *et al.* [20] focused on IBFD and out of band FD backhauling in providing services to small base stations (*SBSs*) in downlink communications; Goyal *et al.* [21] proposed a distributed resource allocation to maximize the throughput of a FD multi-small-cell system.

Since DBSs can be deployed for many applications and IBFD can significantly improve the spectrum efficiency, we propose to investigate the droNe-mounted bAse-station PlacEment (*NAPE*) problem with IBFD communications and DBS backhaul. To our best knowledge, this is the first work to minimize the number of required DBSs and maximize the total throughput of the network in providing services to UEs while incorporating IBFD-enabled DBSs communications for both access links and backhaul links of DBSs. Solving the DBS placement by incorporating IBFD-enabled DBSs communications, UE assignment, and power and bandwidth allocation for access links and backhaul links is the main contribution of this letter. By leveraging IBFD-DBSs, the total throughput of the network has been increased and the data rate block ratio has been decreased.

2.1 System Model

In this research, a macro base-station (*MBS*) (half duplex (*HD*) enabled) and a DBS (IBFD-enabled) are employed to form a heterogeneous network. Figure 2.1(a) shows that the access links (from DBS to UEs) and backhaul link (from MBS to DBS) utilize different frequency spectra in HD operations, and different UEs utilize different frequency spectra. Figure 2.1(b) illustrates the IBFD operations, in which the backhaul link and an acces link employ the same frequency spectra for communications, and different UEs use different frequency spectra for the access links. Take UE 2 as an example: it receives data from DBS 1 and backhaul interference from the MBS. DBS 1 receives SI while transmitting data to UE 2 and receiving data from the MBS on the same frequency, which is different from HD operations. All DBSs are located at the MBS before our optimization, and then they will fly to their destinations after the optimization, and provide services to UEs. We focus on the downlink communications, i.e., from the MBS to UEs directly or via a DBS.

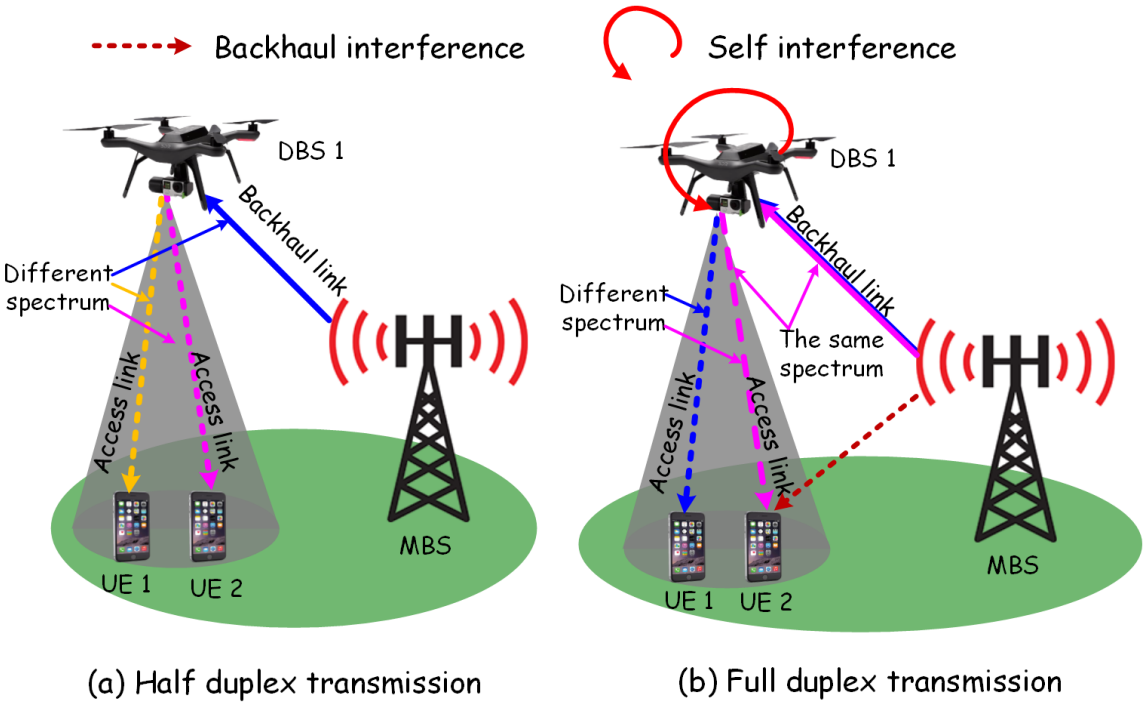

Figure 2.1 DBS communications with HD and FD.

Let $\mathcal{B} = \{1, 2, \cdots, n\}$ be the set of BSs including the MBS and DBSs, and $j = 1$ refers to the MBS. Denote $\mathcal{U} = \{1, 2, \cdots, k\}$ as the set of UEs. A Matérn cluster process is used to generate the spatial UE distribution with heterogeneity [17]. The parent points (centers of the clusters) are generated based on a Poisson process, and the daughter points (which represent the locations of UEs) are generated around the parent points according to a uniform distribution.

Two path loss models are considered in this research: air-to-ground ($A2G$) (ground-to-air ($A2G$)) path loss model and ground-to-ground ($G2G$) path loss model. The A2G (G2A) path loss consists of line-of-sight (LoS) path loss and none-line-of-sight ($NLoS$) path loss [16, 22, 23]. The probability of experiencing a LoS by a UE (DBS) is ψ_L, and that of NLoS is ψ_N:

$$\begin{cases} \psi_L + \psi_N = 1, \\ \psi_L = [1 + a * exp(-b(180\theta/\pi - a))]^{-1}, \end{cases} \tag{2.1}$$

where a and b are weights associated with the environment (rural, urban, etc.), h is the height of the DBS, r is the horizontal distance, and $\theta = arctan(\frac{h}{r})$ is the elevation angle, respectively [17, 24]. It is hard to ascertain whether the path loss is LoS or NLoS in the absence of the terrain knowledge. Hence, the path loss is calculated by the mean path loss instead of the exact path loss of LoS or NLoS:

$$\Psi = \eta_L \psi_L + \eta_N \psi_N + 20log(4\pi f_c \kappa / c), \tag{2.2}$$

where η_L is the additional mean loss of the LoS link, η_N is the additional mean loss of the NLoS link, f_c is the center of frequency spectra, c represents the light transmission speed, and $\kappa = (h^2 + r^2)^{1/2}$ is the 3-D distance between a UE and a DBS [17]. Equation (2.2) includes the excessive path loss of LoS, the excessive path loss of NLoS, and the mean free-space path loss.

By substituting ψ_L and ψ_N into Equation (2.2), we have

$$\Psi = \frac{\eta_L - \eta_N}{1 + a * exp(-b(\frac{180\theta}{\pi} - a))} + 20log(r/cos\theta) + A, \tag{2.3}$$

where $r = \kappa cos\theta$, $A = 20log(4\pi f_c/c) + \eta_N$ and $log(4\pi f_c d/c) = log(r/cos\theta) + log(4\pi f_c/c)$.

Let $b_{i,j}$, $p_{i,j}$, and $S_{i,j}$ be the frequency bandwidth, the power, and the signal to interference plus noise ratio ($SINR$) of the ith UE associated with the jth BS, respectively. Thus, SINR is

$$S_{i,j} = \begin{cases} \frac{p_{i,j}|\gamma_{i,j}|^2}{\sigma_{i,j}^2}, & \forall i \in \mathcal{U}, j = 1, \\ \frac{p_{i,j}\Psi_{i,j}}{\sigma_{i,j}^2 + p_{i,1}|\gamma_{i,1}|^2}, & \forall i \in \mathcal{U}, j \in \mathcal{B}, j > 1, \end{cases} \tag{2.4}$$

where $\gamma_{i,1}$ is the channel gain (loss) between the ith UE and the MBS, $\Psi_{i,j} (j \geq 1)$ is the channel gain between the ith UE and the jth DBS, N_0 is the thermal noise power spectral density, and $\sigma_{i,j}^2 = b_{i,j} * N_0$ is the thermal noise power. Different UEs are assigned with different frequency spectra, implying that the UE assigned to a DBS experiences backhaul interference, and the UE assigned to the MBS does not receive backhaul interference.

The data rate, $R_{i,j}$, of the ith UE assigned to the jth BS, according to the Shannon Hartley theorem [25], is

$$R_{i,j} = b_{i,j} log_2(1 + S_{i,j}). \tag{2.5}$$

Thus, the required bandwidth, $b_{i,j}$, is

$$b_{i,j} = R_{i,j}/log_2(1 + S_{i,j}). \tag{2.6}$$

The backhaul data rate ϕ_j of the jth DBS is determined by the received power, the SI and the thermal noise power, as

$$\phi_j = \beta_j^B log_2(1 + \frac{P_{1,j}\Psi_{1,j}}{I_j^{SI} + \sigma_j^2}), \quad j \in \mathcal{B}, j > 1, \tag{2.7}$$

where β_j^B is the backhaul bandwidth assigned by the MBS towards the jth DBS; $P_{1,j}$ is the assigned power by the MBS towards the jth DBS; $\Psi_{1,j}$ is the path loss between the MBS and the jth DBS; $\sigma_j^2 = \beta_j^B * N_0$ is the thermal noise power; $I_j^{SI} = \sum_i p_{i,j}/c_0$ is the SI of the jth DBS, and $1/c_0$ is the residual SI power [20]. The value of the SI cancellation implies the ability to reduce the echo power at the receiver, and this value can be identified as the power loss from the transmitter to the co-located receiver.

2.2 Problem Formulation

We assume each BS's power spectral density is fixed [26], and then $p_{i,j}/b_{i,j} = \xi_j$, i.e., the allocated power and bandwidth to a UE has a linear relationship. Various notations and variables are summarized in Table 2.1.

The objective of the NAPE problem, as expressed in Equation (2.8), is to minimize the number of required DBSs while maximizing the total throughput of the network. C1 ensures that each UE is assigned to no more than one BS. C2 implies that a DBS is used when more than one UE is associated with this DBS. C3–C4 are the DBS location constraint in the XY-plane, and they ensure that all DBSs are placed within the coverage of the MBS. The location of the jth DBS is determined by q_j and h_j. Let $x(\cdot)$ and $y(\cdot)$ be the functions to get the X-coordinate and Y-coordinate of a location. Then, Equation (2.3) can be used to calculate the channel gain $\Psi_{i,j}(j \geq 1)$ between the ith UE and the jth DBS ($\kappa_j = (h_j^2 + r_j^2)^{1/2}, r_j = (x(q_j) - x_i^{ue})^2 + (y(q_j) - y_i^{ue})^2)^{1/2}$). C5 imposes the real data rate of the ith UE equal to its data rate requirement when it is associated with a BS. C6 is the backhaul data rate capacity constraint, which ensures that the total

Table 2.1 Important Notations and Variables of the NAPE Problem

Symbol	Definiton
N_{max}	the maximum number of available BSs, $N_{max} = \|\mathcal{B}\|$.
$\{x_i^{ue}, y_i^{ue}\}$	the 2-D location information of the ith UE.
d_i	the data rate requirement of the ith UE.
$\mathcal{Q}$	the set of candidate locations for DBSs in the horizontal plane.
P_M	the power capacity of the MBS.
P_D	the power capacity of a DBS.
ξ_j	the power spectral density of the jth BS.
β^M	the total bandwidth capacity of the MBS.
β_j^B	the backhaul bandwidth towards the jth DBS which is assigned by the MBS.
$P_{j,1}$	the assigned transmission power from the MBS to the jth DBS (backhaul).
f_j	a binary variable indicating whether the jth DBS is used ("1" is affirmative).
$\omega_{i,j}$	a binary variable indicating whether the ith UE is associated with the jth BS ("1" is affirmative).
$b_{i,j}$	the assigned bandwidth from the jth BS to the ith UE.
$p_{i,j}$	the assigned power from the jth BS to the ith UE.
q_j	the location of the jth BS in the horizontal plane, $q_j \in \mathcal{Q}$.
h_j	the height of the jth DBS.
T_j	the total throughput of the jth BS, $T_j = \sum_i R_{i,j}$.

data rate of the jth DBS's access link does not exceed that of the backhaul link. C7 imposes the total used power of a DBS not to exceed its maximum power. C8 implies that the total used power of a MBS does not exceed its maximum power.

$$\min \sum_{j} f_j \quad \& \quad \max_{\{f_j, q_j, h_j, \omega_{i,j}, b_{i,j}\}} \sum_{j} T_j$$

$$s.t.:$$

$$C1: \sum_{j} \omega_{i,j} \leq 1, \quad \forall i \in \mathcal{U},$$

$$C2: f_j \leq \sum_{i} \omega_{i,j} \leq f_j * |\mathcal{U}|, \quad \forall j \in \mathcal{B}, j > 1,$$

$$C3: q_j \in \mathcal{Q}, \quad \forall j \in \mathcal{B}, j > 1,$$

$$C4: h_{min} \leq h_j \leq h_{max}, \quad \forall j \in \mathcal{B}, j > 1,$$

$$C5: R_{i,j} = \omega_{i,j} * d_i, \quad \forall i \in \mathcal{U}, j \in \mathcal{B},$$

$$C6: \sum_{i} R_{i,j} \leq \phi_j, \quad \forall j \in \mathcal{B}, j > 1,$$

$$C7: \sum_{i} \omega_{i,j} * b_{i,j} * \xi_j \leq P_D, \quad \forall j \in \mathcal{B}, j > 1,$$

$$C8: \sum_{i} b_{i,1} * \xi_1 + \sum_{j \in \mathcal{B}, j > 1} P_{j,1} \leq P_M. \tag{2.8}$$

For the UE assignment, ω_{i,j^*} is pre-set as "1", as expressed in Equation (2.9), implying that each UE is assigned to the BS with the best SINR if it is provisioned; otherwise, it is "0".

$$\omega_{i,j^*} = 1, j^* = \arg\max_{j} S_{i,j}, \quad \forall i \in \mathcal{U}. \tag{2.9}$$

2.3 Heuristic Algorithm

The NAPE problem is composed of four subproblems: the DBS placement problem, the UE assignment problem, and power and bandwidth allocation problem. The NAPE problem is a non-convex and non-linear optimization problem, which is NP-

hard [21]. We propose a heuristic algorithm, named the Dynamic droNe-bAse-station-PlacEment (*D-NAPE*) algorithm, to solve the NAPE problem.

The D-NAPE algorithm is illustrated in *Algorithm* 1. D-NAPE provides the vertical coordinates of all DBSs as well as the horizontal locations in the xy-plane. Here, W_j denotes the total weight of the jth DBS and $\varsigma_{i,j}$ defines the weight for each UE by considering the distance to the DBS, the SINR to the MBS and the UE number:

$$W_j = \sum_i \varsigma_{i,j}. \tag{2.10}$$

$$\varsigma_{i,j} = ((x_i - x_j)^2 + (y_i - y_j)^2)^{-1} + 10 * (S_{i,1})^{-1/2} + 1. \tag{2.11}$$

C_d is the coverage of the jth DBS; l_{max} is the maximum number of loops used to match the total data rate of the jth DBS and that of its backhaul; ε is a small deviation value. *Algorithm* 1 includes: the DBS placement in the vertical plane (*Steps* $2-3$) and the horizontal plane (*Steps* $6-9$), stop conditions (when the maximum number of DBSs are used or all UEs are provisioned) (*Step* 4), power and bandwidth allocation for the MBS (*Step* 12) and that for all DBSs (*Step* 13). The complexity of Steps 1-4 is $O(\frac{h_{max}-h_{min}}{\Delta h}|\mathcal{B}|)$, where Δh is the altitude increment; that of Step 5 is $O(|\mathcal{U}|)$; that of Steps 6-9 is $O(|\mathcal{B}||\mathcal{Q}||\mathcal{U}|)$; that of Steps 10-12 is $O((|\mathcal{B}|-1)|\mathcal{U}| + |\mathcal{U}|^{|\mathcal{B}|} + |\mathcal{U}|)$. The complexity of Steps 3-14 of *Algorithm* 2 is $O(|\mathcal{B}|(|\mathcal{U}| + log(|\mathcal{U}|)))$; that of Steps 2-14 of *Algorithm* 2 is $O(l^{max}|\mathcal{B}|(|\mathcal{U}| + log(|\mathcal{U}|)))$ (can be repeated for at most l^{max} iterations). Therefore, the complexity of *Algorithm* 1 in the worst case is $O(\frac{h_{max}-h_{min}}{\Delta h}|\mathcal{B}|(|\mathcal{B}||\mathcal{Q}| + |\mathcal{B}| + 1)|\mathcal{U}| + |\mathcal{U}|^{|\mathcal{B}|} + l^{max}|\mathcal{B}|(|\mathcal{U}| + log(|\mathcal{U}|)))$.

Algorithm 1: D-NAPE Algorithm

Input : x_i^{ue},y_i^{ue} and parameters from Table 2.2;

Output: f_j, q_j, h_j, $\omega_{i,j}$, $b_{i,j}$, $p_{i,j}$;

$N_{bs} = 1$, $N_{block} = 1$ and $h = h_{min}$;

for $h \leq h_{max}$ **do**

  $h_j = h$;

  while $N_{bs} \leq N_{max} \& N_{block} = 1$ **do**

    calculate $S_{i,1}$ of all UEs;

    for $j \in \mathcal{B}$ & $q \in \mathcal{Q}$ **do**

      calculate W_j within C_d through Equations (2.10)-(2.11);

      get q_j where W_j is maximized;

      remove UEs within coverage q_j;

    get $S_{i,j}$ and calculate $\omega_{i,j}$ by Equation (2.9);

    allocate $P_{1,j}$ and β_j^B for backhaul links;

    allocate $b_{i,1}$ and $p_{i,1}$ to MBS' UEs;

    run D-NAPE Algorithm 2 ;

    update N_{block} and f_j ;

    $N_{bs} = N_{bs} + 1$;

  calculate throughput $T = \sum_j T_j$ and $h = h + \Delta h$;

  update f_j, q_j, h_j, $\omega_{i,j}$, $b_{i,j}$, $p_{i,j}$ associated with the maximum T.

Algorithm 2: D-NAPE Algorithm 2

Input : l, P_j^l and parameters from Table 2.2;

Output: N_{block} and f_j;

$l = 0$, $N_D = 1$, $N_D^j = 1$, $P_j^l = P_D/2^{l+1}, \forall j$;

while $N_D > 0$ & $l < l^{max}$ **do**

  set available power $P_j^{max} = \sum P_j^l$;

  for $j \in \mathcal{B}$ **do**

    sort UEs in descending order by SINR;

    allocate $b_{i,j}$ and $p_{i,j}$ to UEs;

    if $|(\sum_i R_{i,j} - \phi_j)/\phi_j| < \varepsilon$ **then**

      $N_D^j = 0$ and $N_D = \sum_j N_D^j$;

      continue;

    if $\sum_i R_{i,j} \geq \phi_j$ **then**

      set $P_j^{l+1} = P_D/2^{(l+1)+1}$;

    else

      set $P_j^{l+1} = -P_D/2^{(l+1)+1}$;

    $l = l + 1$ and $N_D = \sum_j N_D^j$;

if *all UEs are provisioned* **then**

  $N_{block} = 0$;

else

  $N_{block} = 1$;

Table 2.2 Parameters for Simulations of the NAPE Problem

(a, b), environment constants	$(9.61, 0.16)$
(η_L, η_N), additional mean losses of LoS, NLOS	$(1, 20)$ dB
C_m, MBS cell coverage	$500 * 500m^2$
C_d, DBS cell radius (only for DBS placement)	80 m
(h_{min}, h_{max}), the altitude range of a DBS	$(80, 200)$ m
ground to ground (MBS-UE) path loss	$34.5 + 35log_{10}(d[m])$ [23]
Shadow fading of MBS to UE	$N(0, 6^2)$ dB
N_0	-174 dBm/Hz
c_0	130 dB [15]
$\|\mathcal{U}\|$	$\{130, 170, \cdots, 190\}$
d_i	$\{0.5, 0.5, 1, 2\}$ Mbps
P_M	4 W
P_D	0.5 W
β^M	20 MHz
l^{max}	10
ε	0.0002
N_{max}	6

2.4 Performance Evaluation

We ran the Matlab simulation 200 times to obtain the simulation mean results. One MBS in an urban area (i.e., C_m is $500 * 500$ m^2) is considered and the maximum number of DBS that can be used is five. $P_M = 4$ W and $P_D = 0.5$ W, implying that the power capacity of a MBS and a DBS are 4W and 0.5W, respectively. The other parameters are defined in Table 2.2 [17].

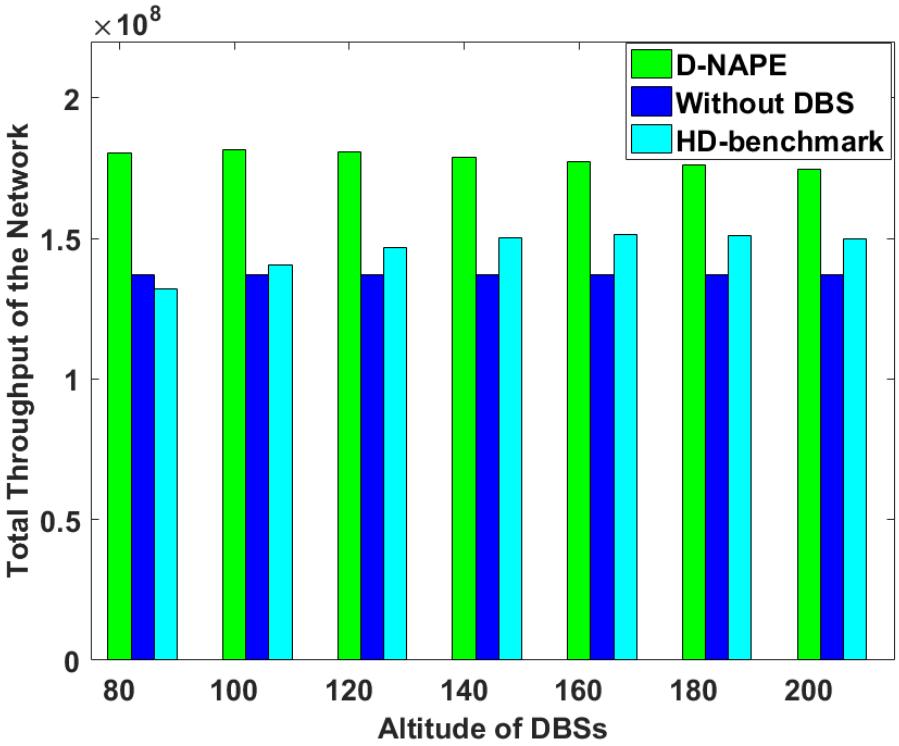

Figure 2.2 Throughput versus altitude.

A benchmark algorithm with half-duplex enabled DBSs (HD-benchmark) is also evaluated; it uses the same strategy as the D-NAPE algorithm in solving the four sub-problems. Figures 2.2-2.3 show the throughput performance versus altitude and the number of UEs of the D-NAPE algorithm, respectively. For a given number of UEs such as 190 UEs, the total network throughput of D-NAPE increases as the altitude increases when $h < 100$m; the total throughput of the network decreases as the altitude increases when $h > 100$m. For $h < 100$m, NLOS is the dominant

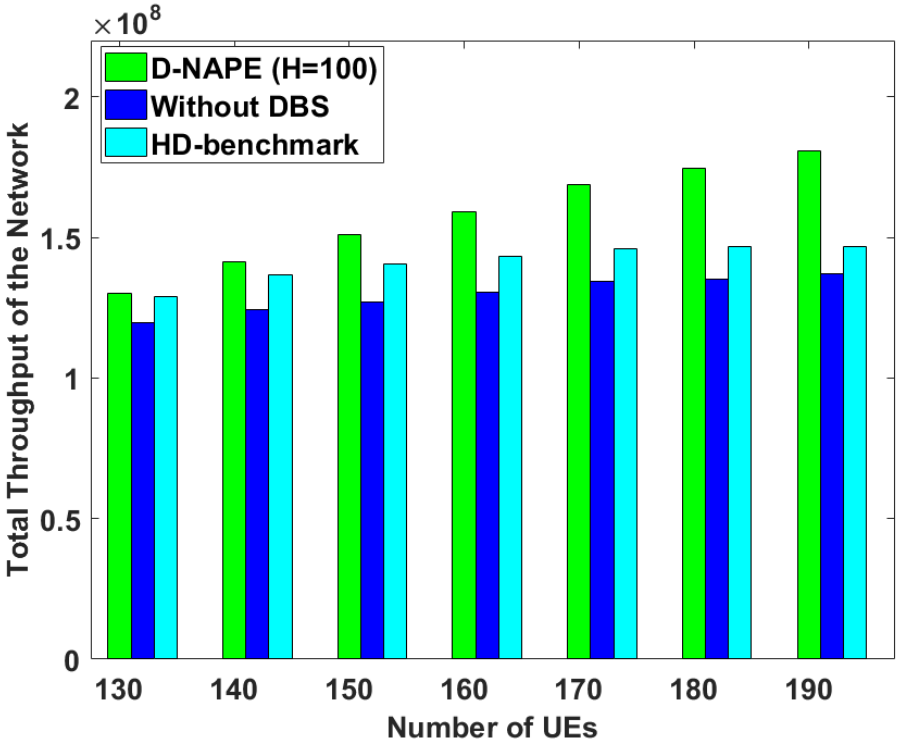

Figure 2.3 Throughput versus UEs.

path loss, and NLOS decreases as the altitude increases, thus resulting in the path loss decrease and the total network throughout increase; for $h > 100$m, LOS is the dominant path loss, and LOS increases as the altitude rises, thus increasing the path loss and decreasing the total network throughout. For a given altitude such as 100 m, the total network throughput also increases as the number of UE increases, and D-NAPE achieves up to 32% and 23% throughput increase as compared to that of without DBS strategy and HD-benchmark, respectively.

Figure 2.4 illustrates the results of the required number of DBSs, which increases as the number of UE increases because our algorithm tries to provide services to as many UEs as possible.

Figure 2.5 shows the results of the data rate block ratio, which is the total bandwidth of blocked UEs over the total required bandwidth of all UEs. The D-NAPE algorithm achieves the lowest data rate block ratio as compared to other strategies

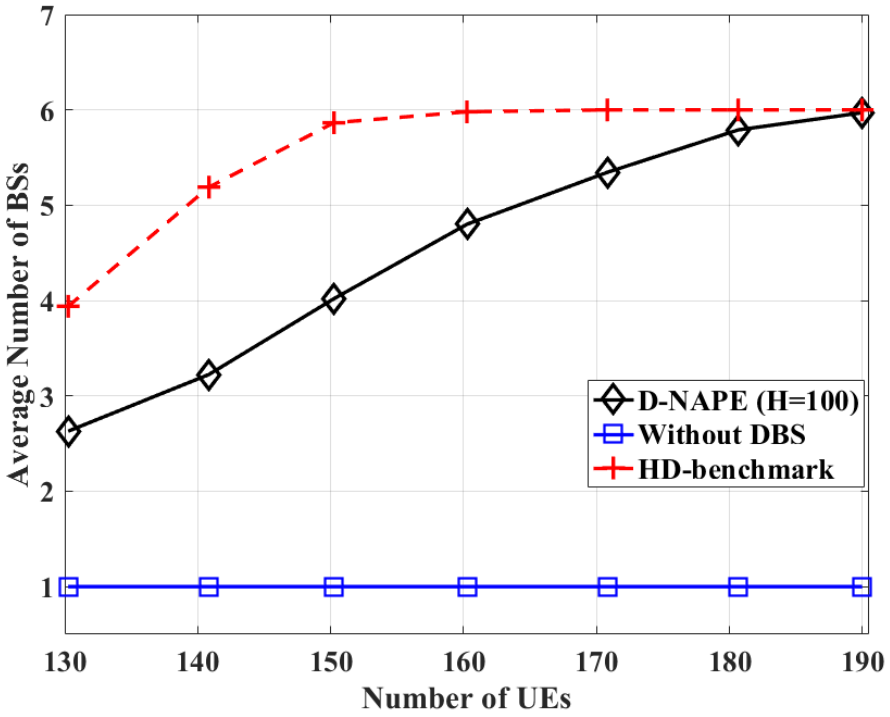

Figure 2.4 Required BSs versus UEs.

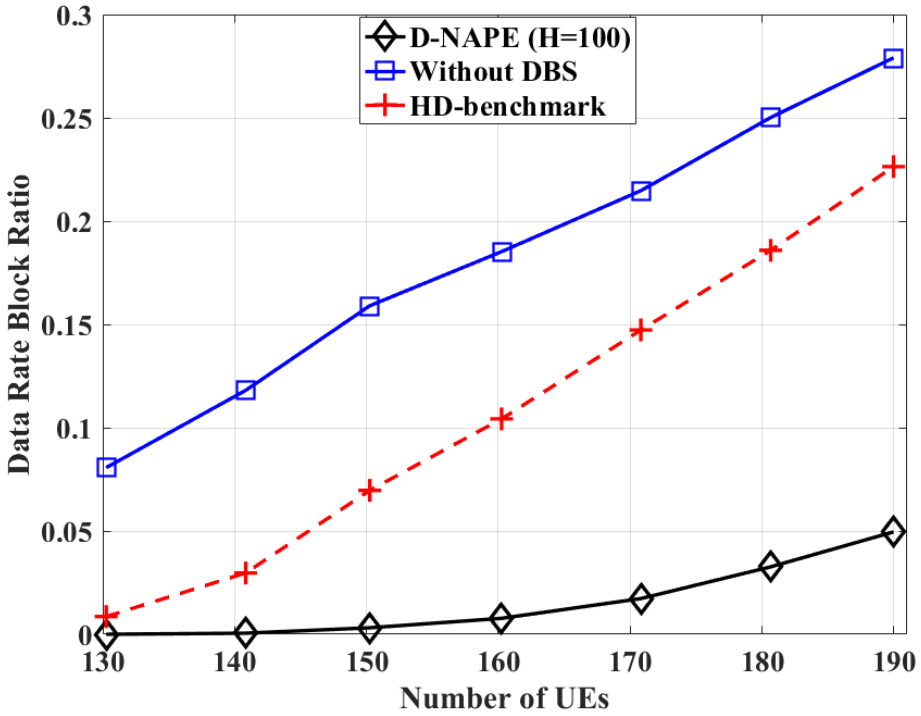

Figure 2.5 Data rate block ratio.

because IBFD-enabled DBSs can improve SINR and better balance the capacity of backhaul links and access links, and can thus provide service to more UEs.

CHAPTER 3

THREE-DIMENSIONAL DBS PLACEMENT

DBSs can be deployed to provide wireless services with high mobility and low cost [7]. Drone cells are especially useful for provisioning communications for temporary or unexpected events in sports, traffic jams, and emergency communications [27, 28]. DBSs can be used to overcome terrestrial BS failures, offload traffic from a congested macro base station (*MBS*), provide service to remote areas [17], and improve Quality of Service (QoS) of user equipments (*UE*s) [29].

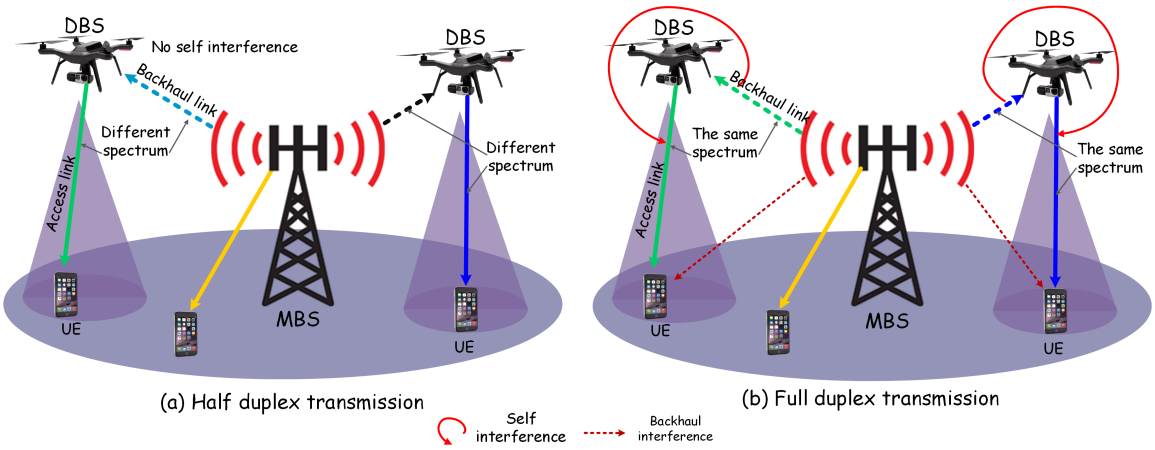

Figure 3.1 Half duplex and full duplex communications with DBSs.

Figure 3.1(a) shows a DBS assisted half-duplex (*HD*) cellular network, where separate frequency spectra are employed in the backhaul link (from the MBS to a DBS) and access link (from the DBS to the UE), but the spectrum efficiency of HD is low. In contrast, in-band full-duplex (*IBFD*) can potentially double the spectrum efficiency as compared to HD [21]. IBFD enables simultaneous communications in the backhaul link and access link in the same frequency band [20]. However, it is difficult to transmit and receive data on the same frequency owing to severe self-interference

(*SI*). Recent advances in SI cancellation, which can reduce SI by up to 150 dB [15], have enabled IBFD [20].

Kalantari *et al.* [17] addressed the DBS placement problem by maximizing the number of UEs covered by the DBS, and Sun *et al.* [29] minimized the total average latency ratio incurred by BSs; Wang *et al.* [30] determined the optimal drone position that minimizes the transmission power in provisioning a set of UEs; Goyal *et al.* [21] maximized the total average data rate of either downlink or uplink for FD enabled small base stations (*SBSs*); Siddique *et al.* [20] maximized the overall achievable rates of SBSs via access/backhaul spectrum allocation while considering both IBFD and out-of-band FD backhauling. Since IBFD can significantly improve the throughput of the DBS assisted cellular network, we formulate the *D*rone-base-*S*tation *P*lacement with *I*n-*B*and *F*ull-*D*uplex communication (*DSP-IBFD*) problem, which includes the DBS placement problem, and the bandwidth and power allocation (in the access link and the backhaul link) problem. We propose two heuristic algorithms based on different DBS placement strategies to solve the DSP-IBFD problem. One is the fixed DBS placement (benchmark), and the other is the dynamic DBS placement, which aims to achieve better performance. Meanwhile, the bandwidth and power allocation are optimized based on the DBS placement results.

3.1 System Model

We consider a heterogeneous network (*HetNet*) consisting of a MBS (HD-enabled) and a few DBSs (IBFD-enabled) deployed as small cells. Figure 3.1(b) shows the backhaul link and access link of a DBS sharing the same frequency. Meanwhile, different DBSs use different frequency spectra, thus not incurring BS-BS interference between each other. A UE associated with a DBS receives the interference from the backhaul link from the MBS to their DBS, which is different from Figure 3.1(a).

Denote $\mathcal{B} = \{1, 2, \cdots, k\}$ as the BS set, where $\mathcal{B}' = \{j \in \mathcal{B}, j \neq 1\}$ is the DBS set, and $j = 1$ refers to the MBS. $\mathcal{U} = \{u_1, u_2, \cdots, u_n\}$ is the UE set. We consider a MBS of coverage radius C_m overlapped with multiple DBSs. At the beginning, DBSs are located at the MBS, and then move to the target area, hovering there to provide services to UEs. We consider low-mobility DBSs (DBSs are hovering most of the time); both the MBS and DBSs dynamically allocate power and bandwidth to UEs. In this letter, we only focus on downlink communications from the MBS to UEs via a DBS or from the MBS to UEs.

When DBSs communicate with UEs on the ground, two types of path loss are considered, i.e., line-of-sight (LoS and non-line-of-sight ($NLoS$) [17, 22]. Probabilities of a LoS (Ψ_L) and NLoS (Ψ_N) transmission between a transmitter and a receiver are expressed in Equation (3.1). Here, a and b are constants, which are determined by the environment (rural, urban, etc.), $\theta = arctan(\frac{h}{r})$ is the elevation angle, h is the altitude of a DBS, and r is the horizontal distance, respectively [17, 24].

$$\begin{cases} \Psi_L = [1 + a \times exp(-b(\frac{180\theta}{\pi} - a))]^{-1} \\ \Psi_N = 1 - \Psi_L \end{cases} \tag{3.1}$$

Since it is difficult to determine the exact LoS or NLoS of a connection between a user and a DBS, we use the mean path loss Γ instead of the exact path loss of the LoS or NLoS, as detailed in Equation (3.2). Here, η_L and η_N are the additional mean losses of LoS and NLoS links, f_c is the carrier frequency, c is the speed of light, and $d = \sqrt{(h^2 + r^2)}$ is the distance between a DBS and a UE [17].

$$\Gamma = \eta_L \Psi_L + \eta_N \Psi_N + 20log(4\pi f_c d/c) \tag{3.2}$$

After substituting Ψ_L and Ψ_N into Equation (5.2), we can transform Equation (3.2) into Equation (3.3). As a result, Γ is a function of h and r, implying that the path loss is a function of the altitude and coverage of the DBS. For a given

Γ, the coverage radius r of a DBS is a function of its altitude h. Note that $20log(4\pi f_c d/c) = 20log(4\pi f_c/c) + 20log(r/cos\theta)$.

$$\Gamma = \frac{\eta_L - \eta_N}{1 + a \times exp(-b(\frac{180\theta}{\pi} - a))} + 20log(\frac{4\pi f_c d}{c}) + \eta_N \tag{3.3}$$

We assume the transmit power-spectral density of each BS is constant [31]. Let $p_{i,j}$ and $b_{i,j}$ be the allocated power and frequency bandwidth for the ith UE of the jth BS (note that each UE is associated with only one BS); denote $s_{i,j}$ as the signal to interference plus noise ratio ($SINR$) of the ith UE towards the jth BS, as detailed in Equation (3.4).

$$s_{i,j} = \begin{cases} \frac{p_{i,j}|h_{i,j}|^2}{\sigma^2}, & j = 1 \\ \frac{p_{i,j}\Gamma_{i,j}}{p_{i,j'}|h_{i,j'}|^2 + \sigma^2}, & j \in \mathcal{B}', j' = 1 \end{cases} \tag{3.4}$$

Here, $h_{i,j}$ is the channel gain between the kth BS and the ith UE; $\Gamma_{i,j}$ is the path loss of the ith UE when it is associated with the jth ($j > 1$) DBS; $\sigma^2 = b_{i,j} * N_0$ is the thermal noise power, and N_0 is the thermal noise power spectral density.

Let $\phi_{i,j}$ be the data rate of the ith UE from the jth BS. Then, a UE's data rate is determined by $s_{i,j}$ and $b_{i,j}$ according to the Shannon Hartley theorem [25], as shown in Equation (3.5). To reduce the problem complexity, we assume $p_{i,j} = b_{i,j} * \zeta_j$, where ζ_j is the power-spectral density [26]. Then, we only need to allocate the bandwidth for each UE.

$$\phi_{i,j} = b_{i,j} log_2(1 + s_{i,j}) \tag{3.5}$$

There are two types of interferences in our network: SI at the DBS, and backhaul interference [20, 21]; DBSs will experience SI, and a UE associated with a DBS will be affected by the transmission power of the backhaul from the MBS to this DBS. Then, the data rate of the backhaul f_j is formulated as Equation (3.6).

$$f_j = \beta_B log_2(1 + \frac{P_{1,j}\Gamma_{1,j}}{I_{SI} + \sigma_j^2}), \quad j \in \mathcal{B}' \tag{3.6}$$

Here, $P_{1,j}$ is the transmission power from the MBS to the jth DBS; $\Gamma_{1,j}$ is the path loss from the MBS to the jth DBS (by Equation (3.2)); β_B is the total backhaul bandwidth for a DBS, which is reused by both the DBS's backhaul link and its access links towards UEs (β_B is set to 3.3 MHz in the simulation); $\sigma_j^2 = \beta_B N_0$ is the thermal noise power; N_0 is the thermal noise power spectral density; $I_{SI} = \sum_i p_{i,j}/C_{SI}$ is the residual SI experienced at the DBS, and $1/C_{SI}$ is the residual self-interference power [20].

3.2 Problem Formulation

After the locations of all DBSs are determined, each UE is associated with the BS that has the highest SINR.

Notations (given):

N: the number of DBS, $N = |\mathcal{B}'|$.

x_i^{ue}, y_i^{ue}: the location of the ith UE.

P_M: the maximum transmission power of a MBS.

P_D: the maximum transmission power of a DBS.

d_{min}: the minimum data rate for each UE.

ζ_j: the power-spectral density of the jth BS.

$P_{j',j}(j' = 1)$: the transmission power of the MBS towards the jth DBS for the backhaul link.

Variables:

$\omega_{i,j}$: binary variable: 1 if the ith UE is associated with the jth BS; 0, otherwise.

$b_{i,j}$: the bandwidth of the jth BS allocated to the ith UE.

$p_{i,j}$: the transmission power of the jth BS allocated to the ith UE.

$\{x_j, y_j, h_j\}$: 3-D co-ordinates of the jth DBS; h_j is the altitude.

P_j: the total transmission power of the jth DBS towards its associated UEs, where

$P_j = \sum_i b_{i,j}\zeta_j\omega_{i,j}$.

Φ_j: the total throughput of the jth BS, $\Phi_j = \sum_i \phi_{i,j}$.

The objective of the DSP-IBFD problem is to maximize the throughput of the whole network as expressed in Equation (3.7).

$$\max_{x_j, y_j, h_j, \omega_{i,j}, b_{i,j}} \quad \sum_j \Phi_j \tag{3.7}$$

$s.t.:$

$$\sum_j \omega_{i,j} = 1, \quad \forall i \in \mathcal{U} \tag{3.8}$$

$$\omega_{i,j^*} = 1, j^* = \underset{j}{\text{argmax}}(s_{i,j}), \quad \forall i \in \mathcal{U} \tag{3.9}$$

$$\sum_i \phi_{i,j} \leq f_j, \quad \forall j \in \mathcal{B}' \tag{3.10}$$

$$P_j \leq P_D, \quad \forall j \in \mathcal{B}' \tag{3.11}$$

$$\sum_i b_{i,j'}\zeta_{j'} + \sum_{j, j \neq j'} P_{j',j} \leq P_M, \quad \forall j, j' = 1 \tag{3.12}$$

$$\phi_{i,j} \geq \omega_{i,j} d_{min}, \quad \forall i \in \mathcal{U}, j \in \mathcal{B} \tag{3.13}$$

$$h_{min} \leq h_j \leq h_{max}, \quad \forall j \in \mathcal{B}' \tag{3.14}$$

Equation (3.8) imposes each UE to be associated with only one BS, and Equation (3.9) ensures that each UE is associated with the BS with the best SINR. Equation (3.10) is the backhaul data rate capacity constraint, and it ensures that the total data rate of a DBS cannot exceed its backhaul capacity. Equation (3.11) is the power constraint of each DBS, and it ensures that the total transmission power of a DBS towards its associated UEs should not exceed the maximum available power. Equation (3.12) is the power constraint of the MBS, and it ensures that the aggregated transmission power of the MBS towards its associated UEs and all DBSs should not exceed the maximum available power. Equation (3.13) is the minimum data rate constraint, and it ensures that each UE's data rate should exceed the minimum threshold when it

is associated with a BS. Equation (3.14) is the altitude constraint for a DBS, and it provides the lower bound and upper bound altitudes for placing the DBS, respectively.

3.3 Heuristic Algorithm

The DSP-IBFD problem is a non-linear non-convex combinatorial optimization problem, which can be decomposed into the DBS placement problem and the resource allocation problem. The DBS placement problem is a set cover problem, which is NP-hard, and hence it is hard to find the optimal solution [21]. Hence, we propose two heuristic algorithms to solve this problem, namely, the Dynamic-DSP and Fixed-DSP algorithm.

The Dynamic-DSP algorithm is summarized in *Algorithm* 3. For each BS, the remaining bandwidth and power to the UE which has the best SINR. Here, Equation (3.15) defines the weight of the ith UE for the DBS placement; we assume the coverage of the DBS is C_j, which is only used for the DBS placement; the maximum loop number L_{max} is used to iteratively find the resource allocation of the DBS, which best matches the backhaul capacity and the data rate of UEs' access links; ε is a given small deviation value. Each BS provides the minimum data rate (500 kbps) to all associated UEs first, and the remaining power and bandwidth are then assigned to the UE which has the highest SINR to achieve the highest throughput. We first find the locations to place all DBSs (*Lines* 1-5), and then get the UE association and allocate bandwidth and power to UEs associated with the MBS (*Line* 6). Afterwards, power and bandwidth of each DBS are allocated to its associated UEs such that the aggregated data rate of these UEs is close to the DBS's backhaul capacity (*Lines* 7-20). The complexity of Steps 1-4 is $O(C_m/C_j|U||B|)$; that of Steps 5-6 is $O((h_{max} - h_{min})/\Delta h|B| + |U|^{|B|})$, where Δh is the increment of the altitude used in the iteration and $O(|U|^{|B|})$ is the complexity of calculating UE association; that of Steps 10-20 is $O(|B|(|U| + log(|U|)))$, and they can repeat for

Algorithm 3: Dynamic-DSP Algorithm

Input : (x_i^{ue}, y_i^{ue}) and other parameters in Table 3.1;

Output: $\{x_j, y_j, h_j\}$, $\omega_{i,j}$, $b_{i,j}$;

for $j \in \mathcal{B}'$ **do**
    calculate the weight of UEs in C_j by Equation (3.15);
    get x_j and y_j with the highest weight;
    remove UEs in the coverage of the jth DBS;
calculate $s_{i,j}$ and get h_j with the best average SINR of all UEs;
calculate $\omega_{i,j}$ based on the best SINR and allocate $b_{i,j}$ and $p_{i,j}$ to UEs in MBS;
assign the redundant bandwidth and power to MBS's UE with the best SINR;
$L = 0$, $D = 1$, $D_j = 1$, $P_j^L = P_D/2^{L+1}, \forall j$;
while $D > 0$ & $L < L_{max}$ **do**
    set maximum available power $P_j^{max} = \sum P_j^L, \forall j$;
    for $j \in \mathcal{B}'$ **do**
        allocate the bandwidth and power to UEs;
        if $|(\sum_i \phi_{i,j} - f_j)/f_j| < \varepsilon$ **then**
            $D_j = 0$, and $D = \sum_j D_j$;
            continue;
        if $\sum_i \phi_{i,j} \geq f_j$ **then**
            set $P_j^{L+1} = P_D/2^{(L+1)+1}$;
        else
            set $P_j^{L+1} = -P_D/2^{(L+1)+1}$;
    $L = L + 1$, and $D = \sum_j D_j$;
update $b_{i,j} = p_{i,j}/\zeta_j$, $\omega_{i,j}$, and P_j;

at most L_{max} times in the worst case. Thus, the complexity of Steps 9-20 can reach $O(L_{max}|B|(|U|+log(|U|)))$. Therefore, the complexity of the Dynamic-DSP algorithm is $O(C_m/C_j|U||B| + (h_{max} - h_{min})/\Delta h|B| + |U|^{|B|} + L_{max}|B|(|U| + log(|U|)))$.

$$\xi_i = 1 + ((x_i^{ue} - x_j)^2 + (y_i^{ue} - y_j)^2)^{-1} \tag{3.15}$$

For the Fixed-DSP algorithm, we place all DBS in fixed locations, and then execute *Lines* $6 - 21$ in *Algorithm* 3.

3.4 Performance Evaluation

In this research, we consider three DBSs and one MBS ($|\mathcal{B}'| = 3$) in an urban area (i.e., the coverage area of the MBS is 500×500 m^2). The frequency spectra of all BSs are around $f = 2$ GHz. We set the maximum transmission power of a DBS as $P_D = 1$ W, and that of the MBS as $P_M = 4$ W. The remaining parameters, such as a, b, η_L, and η_N, are listed in Table 3.1 [17].

Figure 3.2 shows the network throughput achieved by the Dynamic-DSP and the Fixed-DSP algorithms for different altitudes where the total number of UEs in the network is 100. The throughput achieved by the Dynamic-DSP strategy has been increased by 45% and 8% as compared to the strategy without DBS and the Fixed-DSP strategy, respectively. The throughput increases as the altitude increases. The NLoS path loss between a DBS and its associated UEs degrades with the increasing altitude of the DBS. Then, the network throughput decreases when the altitude is more than 120m because when the altitudes of DBSs are very high, the distances between UEs and DBSs become the dominant factor for the path loss, thus degrading the throughput of the network.

Figure 3.3 shows the network throughput when DBSs hover at the altitude of 120m as the number of UEs varies; both of the proposed strategies can provide a

Table 3.1 Simulation Parameters for the DSP-IBFD Problem

a, environment constant	9.61
b, environment constant	0.16
η_L, additional mean loss of LoS	1 dB
η_N, additional mean loss of NLoS	20 dB
C_m, MBS cell coverage	$500 \times 500\ m^2$
C_j, coverage of a DBS (used for DBS placement)	$70 * 70\ m^2$
h_{min}, the minimum altitude of a DBS	60 m
h_{max}, the maximum altitude of a DBS	200 m
path loss of MBS-UE	$34.5 + 35 \times log_{10}(d[m])$ [31]
Shadow fading of MBS-UE	$N(0, 8^2)$ dB
N_0, thermal noise power spectral density	-174 dBm/Hz
C_{SI}, SI cancellation value	130 dB [15]
β_M, the total bandwidth capacity of the MBS	20 MHz
β_B, the total backhaul bandwidth of a DBS	3.3 MHz
P_M, the maximum transmission power of a MBS	4 W
P_D, the maximum transmission power of a DBS	1 W
$\|\mathcal{U}\|$, the number of UEs	$\{100, 120, \cdots, 220\}$
The minimal data rate	500 kbps
L_{max}, the maximum loop number	60
ε, deviation of throughput and backhaul data rate	0.0002

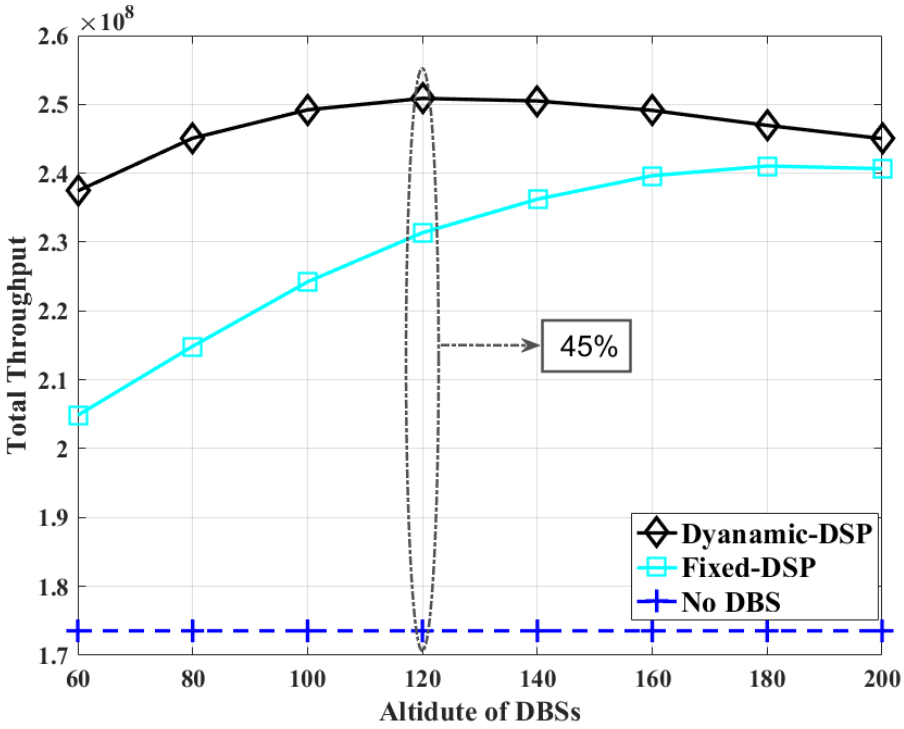

Figure 3.2 Throughput performance with 100 UEs.

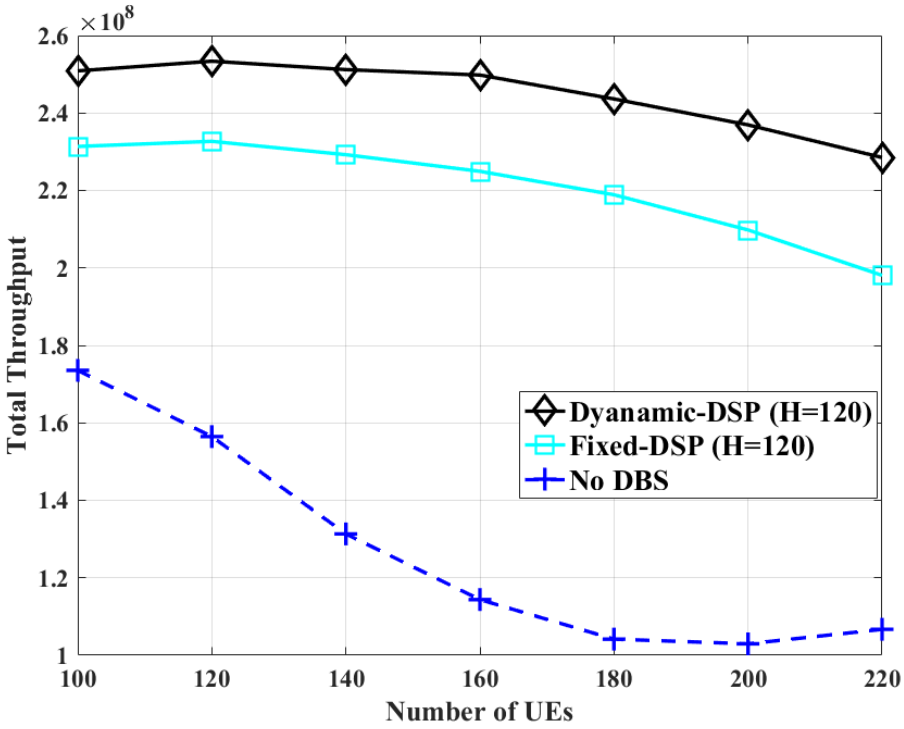

Figure 3.3 Throughput performance with fixed altitude.

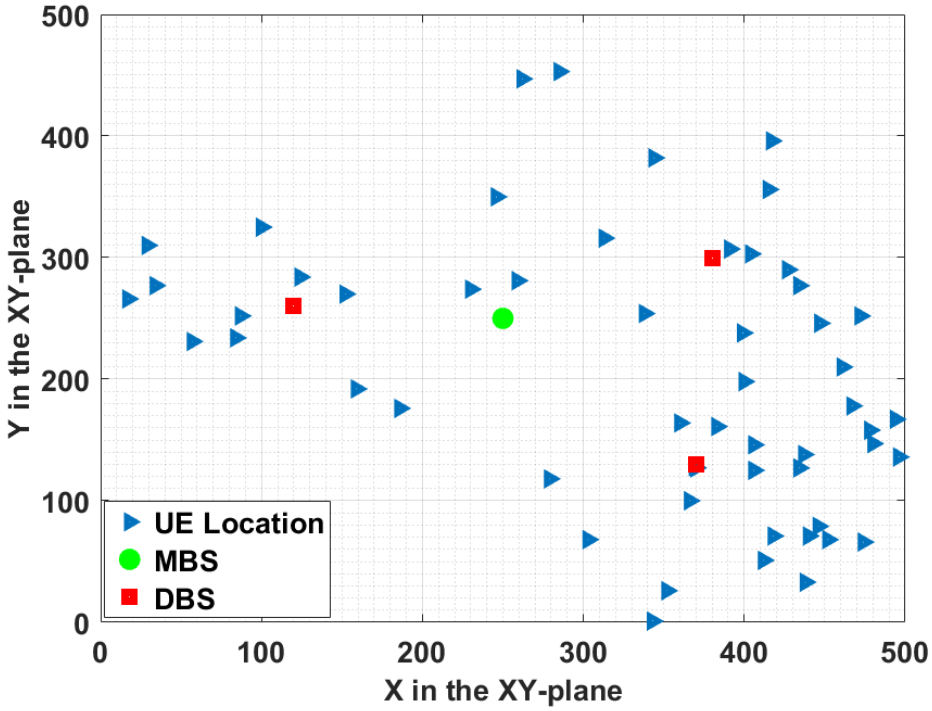

Figure 3.4 DBS placement by the Dynamic-DSP algorithm.

higher throughput as compared to the one without DBSs because the two proposed strategies can place DBSs close to UEs to improve the SINR of UEs. The throughout without DBSs decreases as the number of UEs increases because the MBS needs to allocate most bandwidth to UEs with bad channel conditions to maintain their minimum data rates, and thus the bandwidth allocated to UEs with high SINR is reduced. Figure 3.4 shows how DBSs are placed by Dynamic-DSP; note that DBSs hover close to regions with higher UE densities but not far away from the MBS.

CHAPTER 4

JOINT RADIO RESOURCE AND DBS PLACEMENT FOR DOWNLINK COMMUNICATIONS

Al-Hourani *et al.* [24] presented a path loss model for communications between a DBS (in the air) and a UE (on the ground), and they also built a model to obtain the optimum altitude of a low altitude platform (DBS) which can maximize the coverage area (of the DBS) for a given path loss threshold. Alzenad *et al.* [32] investigated the 3-D placement of one DBS in a hotspot area with the target to provide service to the maximum number of UEs. Sharma *et al.* [33] proposed to employ unmanned aerial vehicles (UAVs) as the relay between the macro and small cells to increase the throughput capacity of the network. Mozaffari *et al.* [19] investigated the deployment of multiple UAVs without overlapping coverage to provision ground UEs in a hotspot, and an efficient deployment is achieved by leveraging the circle packing theory. Chen *et al.* [18] investigated the vertical placement of a UAV as a relay to minimize reliability factors with consideration of a single UE at the cell edge; Sun *et al.* [29] focused on the 2-D placement of a DBS in the horizontal plane to minimize the average latency ratio of UEs in a HetNet. Alzenad *et al.* [16] studied the 3-D placement of one DBS in a hotspot area, and their objective is to maximize the number of UEs covered by the DBS with consideration of different QoS constraints.

Zhang *et al.* [34] studied the 3-D placement of multiple IBFD-enabled DBSs in a HetNet, and the objective is to minimize the number of DBSs while maximizing the total throughput. Siddique *et al.* [20] studied the access and backhaul (IBFD, out of band or hybrid) spectrum allocation of the downlink in a two-tier HetNet, and the objective is to maximize the minimum downlink data rate of all small BSs. Goyal *et al.* [21] presented the UE selection and power allocation problem in a multi-small-cell network to maximize the network utility with FD enabled BSs and HD enabled UEs.

Sharma *et al.* [35] proposed an IBFD self-backhauling HetNet with FD enabled small BSs, HD enabled MBS and HD enabled UEs, and the downlink data rate nearly double that of the conventional frequency division duplex (*FDD*) or time division duplex (*TDD*) network. Several UE association strategies, such as the maximum coverage [32], the best SINR [12], the maximum utility gain [21], the maximum average received biased power [35], and single MBS association [29] have been proposed.

Although there are works related to the placement of DBSs and works related to IBFD communications, few works focus on maximizing the throughput of a DBS-assisted HetNet with IBFD communications. In our previous work [23] (*IEEE CL*), we studied the 3-D DBS placement problem with IBFD communications, and the objective is to maximize the total throughput of the network. This work considered a light workload scenario, implying that no UE is blocked; each UE is provisioned by one BS with the minimum data rate first, and the remaining available bandwidth and power of a BS is assigned to the UE with the best SINR; two heuristic algorithms (without approximation ratio) were proposed to determine the locations of all DBSs first, and then solve the bandwidth and power allocation, UE association problem. In this work, we consider multiple DBSs and a MBS in provisioning services to ground UEs, while the MBS transmits signals to a DBS through the same frequency spectra as that between the DBS and ground UEs.

In this research, we formulate the *D*rone-mounted *B*ase-*S*tation *P*lacement with in-band full-duplex communications (*DBSP-IBFD*) problem [36]. The main contributions of this work are fourfold: 1) we formulate the DBSP-IBFD problem and consider power and bandwidth allocation in both access links and backhaul links that has not been addressed before; 2) we formulate the DBSP-IBFD problem for a general workload scenario (the workload can either be light or heavy); 3) we propose an approximation algorithm with low complexity to solve the DBSP-IBFD problem, and the algorithm is proved to provide guaranteed performance; 4) the optimal locations

of all DBSs are achieved. We have studied the DBSP-IBFD problem and preliminary results have been reported in our previous work [23] (*IEEE CL*). In [23], we did not consider bandwidth allocation constraints for backhaul links, the bandwidth capacity constraints of BSs, and the UE association constraints for blocked UEs. In other words, [23] considers a light workload scenario (no UE is blocked) while this work considers a general workload scenario (some UEs may be blocked with heavy workload).

4.1 System Model

In this research, we focus on the downlink communications, i.e., MBS-UE communications and MBS-DBS-UE communications. Figure 4.1(a) describes half duplex communications between UEs and BSs. All UEs, DBSs, and the MBS are half duplex enabled; an access link is the direct link from a BS to an UE; a backhaul link is the link between the MBS and the DBS; each UE can be provisioned by one BS; the access link and the backhaul link of one DBS use different frequency spectra; different DBSs use different frequency spectra. For example, the backhaul link (from the MBS to DBS 1) uses different spectrum from that of the access link (from DBS 1 to UE 1); UE 1 to UE 5 use different frequency spectra. Figure 4.1(b) exhibits FD communications. All DBSs are IBFD enabled; all UEs and the MBS are half duplex enabled. The backhaul link and the access link of a DBS use the same frequency spectrum; different BSs use different frequency spectra. UEs under the coverage of one BS (DBS or MBS) use different frequency spectra. For example, the backhaul link (from the MBS to DBS 1) uses the same spectrum from the access link (from DBS 1 to UE 1); UE 1 to UE 5 also use different frequency spectra. In this research, we consider two different time slots (a small time slot and a big time slot) for the DBS placement and power and bandwidth allocation, respectively [4]. The big time slot at the scale of minutes (depending on the mobile traffic) is used for the DBS placement, and the small time slot at the scale of seconds is used for the power and bandwidth

allocation [4]. All DBSs are located nearby the MBS before the optimization, and they will fly to the target area according to the results of the optimization. When a DBS arrives at the target location [37] in the beginning of a big time slot, it is hovering at that location to provide service to UEs till the end of this big time slot. Then, we allocate power and bandwidth for the backhaul links and access links in the small time slot, which only occupies a little time at the beginning of a big time slot.

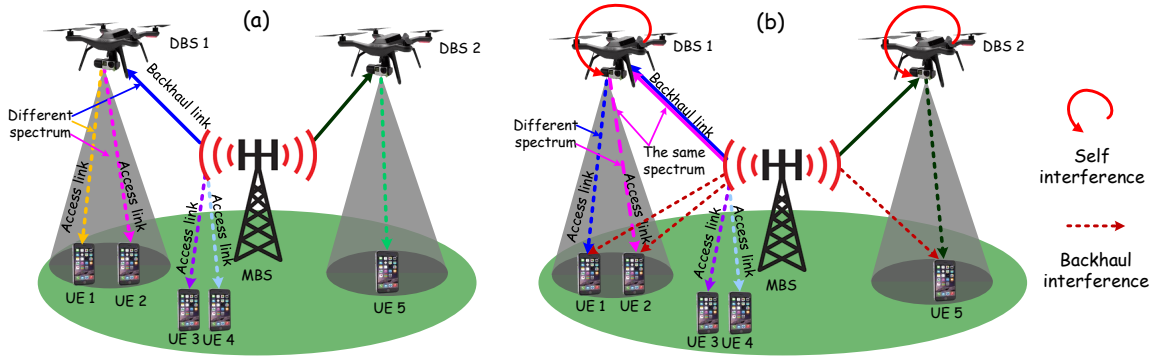

Figure 4.1 DBS-based half-duplex and full-duplex communications: (a) half duplex and (b) full duplex.

Denote $\mathcal{B} = \{1, 2, \cdots, n\}$ as the set of BSs with $j = 1$ representing the MBS; let $\mathcal{U} = \{1, 2, \cdots, k\}$ be the set of UEs. Although the Poisson Point Processes (PPP) is widely used in academia, it is not good enough to capture spatial coupling between UEs and BSs according to 3GPP simulation models while the Poisson Cluster Process (PCP) such as the Matérn cluster process is a good approach to capture the coupling problem [38]. The spatial UE distribution is generated according to a Matérn cluster process [34, 39]. The daughter points (representing UEs) are generated according to a uniform distribution around the parent points, and the parent points (representing the clusters) are generated according to a Poisson process.

In this research, we consider the air-to-ground ($A2G$) path loss model for the MBS-DBS and DBS-UE communications, and ground-to-ground ($G2G$) path loss model for the MBS-UE communications. Two types of path loss are considered in the A2G path loss model, i.e., line-of-sight (LoS) and none-line-of-sight ($NLoS$) [16, 22].

Given an access link between an UE located at (x_i^{ue}, y_i^{ue}) and a DBS located at (x_j, y_j, h_j), $\varphi_{i,j}^L$ and $\varphi_{i,j}^N$ are the A2G path loss for the LoS and NLoS of this link as defined below.

$$\begin{cases} \varphi_{i,j}^L = 20log(\frac{4\pi f_c d_{i,j}}{c}) + \eta^L, \\ \varphi_{i,j}^N = 20log(\frac{4\pi f_c d_{i,j}}{c}) + \eta^N. \end{cases} \tag{4.1}$$

Here, η^L and η^N are the average additional loss for the LoS and NLoS of an A2G link, f_c is the carrier frequency, $d_{i,j} = ((x_j - x_i^{ue})^2 + (y_j - y_i^{ue})^2 + h_j^2)^{1/2}$ is the distance between the ith UE and the jth DBS, and c is the speed of light [24].

The probability of an A2G link between the ith UE and the jth DBS experiencing LoS and that experiencing NLoS are $\zeta_{i,j}^L$ and $\zeta_{i,j}^N$ expressed respectively below.

$$\begin{cases} \zeta_{i,j}^L = [1 + a \cdot exp(-b(\frac{180\theta_{i,j}}{\pi} - a))]^{-1}, \\ \zeta_{i,j}^N = 1 - \zeta_{i,j}^L. \end{cases} \tag{4.2}$$

Here, $\theta_{i,j} = arctan(\frac{h_j}{z_{i,j}})$ is the elevation angle of the jth DBS, h is the height of the jth DBS, $z_{i,j} = ((x_j - x_i^{ue})^2 + (y_j - y_i^{ue})^2)^{1/2}$ is the horizontal distance between the ith UE and the jth DBS in the horizontal plane, and a and b are weights associated with the environment, i.e., suburban, urban and dense urban, respectively [16, 24].

Note that it is difficult to determine the accurate path loss type (i.e., LOS or NLoS) of an A2G link in the absence of terrain knowledge [32]. Hence, we employ the mean path loss $\psi_{i,j}$ instead of the exact LoS path loss or NLoS path loss of an A2G link between the ith UE and the jth DBS as expressed below.

$$\psi_{i,j}(h, z) = \varphi_{i,j}^L \zeta_{i,j}^L + \varphi_{i,j}^N \zeta_{i,j}^N. \tag{4.3}$$

Then, Equation (4.3) is transformed into Equation (4.4).

$$\psi_{i,j}(h,z) = \frac{\eta_L - \eta_N}{1 + a \cdot exp(-b(\frac{180\theta_{i,j}}{\pi} - a))} + G_1 + G_2, \tag{4.4}$$

where $G_1 = 20log(4\pi f_c/c) + \eta^N$, $G_2 = 20log(z/cos\theta_{i,j})$ and $G_1 + G_2 = 20log(4\pi f_c d_{i,j}/c) + \eta^N$. Equation (4.4) implies that the coverage radius C_j of the jth DBS is a function of its altitude h for a given ψ.

Denote $p_{i,j}$, $b_{i,j}$, $d_{i,j}$, and $s_{i,j}$ as the assigned power, the assigned frequency bandwidth, the data rate, and the signal to interference plus noise ratio (*SINR*) of the ith UE towards the jth BS, respectively. The data rate (according to the Shannon Hartley theorem [25]) and the SINR of the ith UE towards the jth BS are shown as Equation (4.5) and Equation (4.6).

$$d_{i,j} = b_{i,j} log_2(1 + s_{i,j}), \quad \forall i \in \mathcal{U}, j \in \mathcal{B} \tag{4.5}$$

$$s_{i,j} = \begin{cases} \frac{p_{i,j}|\gamma_{i,j}|^2}{\sigma_{i,j}^2}, & \forall i \in \mathcal{U}, j = 1, \\ \frac{p_{i,j}\psi_{i,j}}{p_{i,1}|\gamma_{i,1}|^2 + \sigma_{i,j}^2}, & \forall i \in \mathcal{U}, j \in \mathcal{B}, j > 1, \end{cases} \tag{4.6}$$

where $\gamma_{i,j} (j = 1)$ and $\psi_{i,j} (j > 1)$ are the channel gain from the MBS and the jth DBS to the ith UE, respectively; $\sigma_{i,j}^2 = b_{i,j} N_0$ is the thermal noise power and N_0 is the thermal noise power spectral density.

The backhaul data rate of the jth DBS (the data rate from the MBS to the jth DBS) is:

$$f_j = \beta_j log_2 \left(1 + \frac{P_{1,j}\psi'_{1,j}}{G_j^{SI} + \sigma_j^2}\right), \quad j \in \mathcal{B}, j > 1, \tag{4.7}$$

where $P_{1,j}$ and β_j are the assigned power and bandwidth assigned by the MBS towards the jth DBS, respectively; $\psi'_{1,j}$ is the channel gain from the MBS to the jth DBS; $\sigma_j^2 = \beta_j N_0$ is the thermal noise power and N_0 is the thermal noise power spectral

density; $G_j^{SI} = \sum_i p_{i,j}/G_0$ is the SI at the jth DBS and $1/G_0$ is the residual SI power (depending on the SI cancellation algorithm) [20].

4.2 Problem Formulation

We formulate the DBSP-IBFD problem in this section. Assume that N_{bs} is the number of required DBSs, which is known *a priori* (i.e., N_{bs} is estimated roughly based on the data rate capacity or by other methods similar to [34]). Notations and variables are summarized in Table 4.1.

The DBSP-IBFD problem is formulated as follows.

$$\max_{v_j, h_j, \omega_{i,j}, p_{i,j}, b_{i,j}, \beta_j} \quad \sum_j \sum_i d_{i,j}$$

$$s.t.:$$

$$C1: \sum_j \omega_{i,j} \leq 1, \quad \forall i \in \mathcal{U},$$

$$C2: \sum_i \omega_{i,j} b_{i,j} \leq \beta_j, \quad \forall i \in \mathcal{U}, j \in \mathcal{B}, j > 1,$$

$$C3: \sum_i \omega_{i,1} b_{i,1} + \sum_{j>1} \beta_j \leq \beta^M, \quad \forall i \in \mathcal{U},$$

$$C4: \sum_i \omega_{i,j} p_{i,j} \leq P^D, \quad \forall i \in \mathcal{U}, j \in \mathcal{B}, j > 1,$$

$$C5: \sum_i \omega_{i,1} p_{i,1} + \sum_{j>1} P_{1,j} \leq P^M, \quad \forall i \in \mathcal{U},$$

$$C6: d_{i,j} = \omega_{i,j} r_i, \quad \forall i \in \mathcal{U}, j \in \mathcal{B},$$

$$C7: \sum_i d_{i,j} \leq f_j, \quad \forall j \in \mathcal{B}, j > 1,$$

$$C8: v_j \in \Lambda, \quad \forall j \in \mathcal{B}, j > 1,$$

$$C9: h_j \in \Theta, \quad \forall j \in \mathcal{B}, j > 1,$$

$$C10: \omega_{i,j} \in \{0, 1\}, \quad \forall i \in \mathcal{U}, j \in \mathcal{B}. \tag{4.8}$$

The objective is to maximize the total throughput of all UEs, as expressed in Equation (4.8). C1 and C10 impose each UE to be provisioned with one BS (DBS or MBS) if it is served. C2–C3 are the bandwidth capacity constraints for DBSs and the MBS, which impose the total deployed bandwidth of a BS not to exceed the bandwidth capacity of the BS. C4–C5 are the power capacity constraints for DBSs and the MBS, which impose the total power consumed by a BS not to exceed the maximum power of the BS. C6 is the data rate requirement constraint of each UE. C7 is the backhaul data rate capacity constraint, which imposes the total data rate of provisioned UEs in the jth DBS not to exceed that from the MBS to the jth DBS. C8–C9 are the DBS placement constraints in the horizontal plane and vertical plane, respectively.

4.3 Problem Analysis

The (DBSP-IBFD) problem can be decomposed into two sub-problems: the joint bandwidth, power allocation and UE association (*joint-BPU*) problem and the DBS placement problem. The solutions of these two sub-problems are leveraged to solve the DBSP-IBFD problem. For analytical tractability, we assume $p_{i,j} = b_{i,j}\xi_j$, where ξ_j is the power-spectral density of the jth BS [26]. The bandwidth and the power are simultaneously provisioned to an UE. Then, $b_{i,j}$ and $p_{i,j}$ can be calculated based on $\omega_{i,j}$, v_j, h_j (the UE association and the DBS placement), Equation (4.5) and Equation (4.6). We also assume all DBSs and the MBS equally share the total available bandwidth in the network ($\beta_j = \beta^M/N$), i.e., fixed backhaul bandwidth allocation for all DBSs. Therefore, Equation (4.8) can be re-written as Equation (4.9).

4.3.1 The Joint-BPU Problem

For given locations of all DBSs, Equation (4.9) can be re-written as Equation (4.10). C3 in Equation (4.10) is the backhal data rate capacity constraint, and we try to

relax this constraint by adjusting β_j of C2 in Equation (4.10). The idea is to solve Equation (4.11) instead of solving Equation (4.10) by relaxing C3 step by step. In each step, β_j^{max} is used to replace β_j of C2 in Equation (4.10) ($\beta_j^{max} = \sum_l \beta_j^l$ and $\beta_j^1 = \frac{\beta_j}{2^l}$). In the lth step, we will update β_j^{l+1} when we achieve the results of Equation (4.11); $\beta_j^{l+1} = \frac{\beta_j}{2^{l+1}}$ if the total data rate of a DBS is smaller than the backhaul data rate capacity; otherwise, $\beta_j^{l+1} = -\frac{\beta_j}{2^{l+1}}$.

$$\max_{v_j, h_j, \omega_{i,j}} \quad \sum_j \sum_i \omega_{i,j} r_i$$

$$s.t.:$$

$$C1: \sum_j \omega_{i,j} \leq 1, \quad \forall i \in \mathcal{U},$$

$$C2: \sum_i \omega_{i,j} b_{i,j} \leq \beta_j, \quad \forall i \in \mathcal{U}, j \in \mathcal{B},$$

$$C3: \sum_i \omega_{i,j} r_i \leq f_j, \quad \forall j \in \mathcal{B}, j > 1,$$

$$C4: v_j \in \Lambda, \quad \forall j \in \mathcal{B}, j > 1,$$

$$C5: h_j \in \Theta, \quad \forall j \in \mathcal{B}, j > 1,$$

$$C6: \omega_{i,j} \in \{0, 1\}, \quad \forall i \in \mathcal{U}, j \in \mathcal{B}. \tag{4.9}$$

$$\max_{\omega_{i,j}} \quad \sum_j \sum_i \omega_{i,j} r_i$$

$$s.t.:$$

$$C1, C2, C3, C6 \quad in \quad (4.9) \tag{4.10}$$

Theorem 1. *Any solution* $\Omega = \{\omega_{i,j}^*\}$ *for Equation* (4.11) *is* $(1 - \frac{1}{2^l})$*-approximation for Equation* (4.10) *with* l *runs.*

Proof. Note that Equation (4.11) only relaxes C3 in Equation (4.10). Assume β_j^* ($0 \leq \beta_j^* \leq \beta_j$) is the optimal solution for Equation (4.10), then we need to calculate the variance between β_j^{max} and β_j^*. $|\beta_j^{max} - \beta_j^*| = |\sum_l \beta_j^l - \beta_j^*| = |\sum_l \frac{\beta_j}{2^l} - \beta_j^*| \leq |\sum_l \frac{\beta_j}{2^l} - \beta_j| = \beta_j|\sum_l \frac{1}{2^l} - 1| = \frac{1}{2^l}\beta_j$. Note that $\beta_j^{max} \leq \beta_j^*$ ensures a feasible solution. Let $\Phi(\cdot)$ be the function of β_j^{max} to achieve the objective value. Since Constraint C2 in Equation (4.11) is a linear constraint, we have $\Phi(\beta_j^*) - \Phi(\beta_j^{max}) = \Phi(\beta_j^* - \beta_j^{max}) \leq \Phi(\frac{1}{2^l}\beta_j) = \frac{1}{2^l}\Phi(\beta_j^*)$. Thus, $\Phi(\beta_j^{max}) \geq (1 - \frac{1}{2^l})\Phi(\beta_j^*)$. □

$$
\begin{aligned}
&\max_{\omega_{i,j}} \quad \sum_j \sum_i \omega_{i,j} r_i \\
&s.t.: \\
&\quad C1: \sum_j \omega_{i,j} \leq 1, \quad \forall i \in \mathcal{U} \\
&\quad C2: \sum_i \omega_{i,j} b_{i,j} \leq \beta_j^{max}, \quad \forall i \in \mathcal{U}, j \in \mathcal{B}, \\
&\quad C3: \omega_{i,j} \in \{0,1\}, \quad \forall i \in \mathcal{U}, j \in \mathcal{B}.
\end{aligned} \tag{4.11}
$$

$$
\begin{aligned}
&\max_{\omega_{i,j}} \quad \sum_j \sum_i \omega_{i,j} r_i \\
&s.t.: \\
&\quad C1: \sum_j \omega_{i,j} \leq 1, \quad \forall i \in \mathcal{U} \\
&\quad C2: \sum_i \omega_{i,j} b_{i,j} \leq \beta_j^{max}, \quad \forall i \in \mathcal{U}, j \in \mathcal{B}, \\
&\quad C3: 0 \leq \omega_{i,j} \leq 1, \quad \forall i \in \mathcal{U}, j \in \mathcal{B}.
\end{aligned} \tag{4.12}
$$

We employ a greedy algorithm similar to the knapsack problem to solve Equation (4.11). The weight matrix δ_k (required data rate over the required

bandwidth) is calculated (*Steps* $1-6$), one solution Ω_1 is achieved from the heuristic algorithm (*Steps* $7-12$), another solution Ω_2 is obtained (*Step* 13), and the final solution is decided based on the performance of Ω_1 and Ω_2 (*Step* 14).

Algorithm 4: Greedy Algorithm for joint-BPU

Input : $v_j^{'}$, $h_j^{'}$ and other parameters in Table 4.2;

Output: $\omega_{i,j}$, $p_{i,j}$, and $b_{i,j}$;

1 **for** $j \in \mathcal{B}$ **do**
2 **for** $i \in \mathcal{U}$ **do**
3 calculate $b_{i,j}$ and $p_{i,j}$ for each UE;
4 sort $b_{i,j}$ in ascending order;
5 find $b_{i,j'} = \min(b_{i,j})$;
6 sort $\delta_i = r_i / b_{i,j'}$ in descending order;
7 $i' = 1, \mathcal{U}' = \mathcal{U}$, $\beta_j^{'} = 0, j = 1, ..|\mathcal{B}|$;
8 **while** $\beta_j^{'} \leq \beta_j^{max}$ & $\mathcal{U}' \neq \varnothing$ **do**
9 **if** $\beta_j^{'} + b_{i',j'} \leq \beta_j^{max}$ **then**
10 set $\omega_{i',j'} = 1$ and remove the kth UE in $\mathcal{U}'$;
11 $\Omega_1 = \Omega_1 \cup \{\omega_{i',j'}\}$ and $\beta_j^{'} = \beta_j^{'} + b_{i',j'}$;
12 **else**
13 repeat Steps 4-7 without calculating value $b_{i,j}$;
14 k=k+1;
15 calculate $\Omega_2 = \{\omega_{i',j'}$ that provides N maximum $r_i\}$;
16 return Ω_1 or Ω_2 which has higher throughput.

Theorem 2. *Algorithm 4 is a* $\frac{1}{2}$*-approximation algorithm for Equation* (4.11) *when not all UEs are provisioned; otherwise, the optimal throughput is achieved.*

Proof. (1) We first consider that one or more UEs are blocked (not all UEs are provisioned). Let $\Phi_1(\cdot)$ be the function of $\omega_{i,j}$ to calculate the objective value ($\Phi_1(\omega_{i,j}) = \sum_i \sum_j \omega_{i,j} r_i$). Assume the maximum number of items in Ω_1 is $(k-1)$, then $\Omega_1 = \cup_{i'=1}^{k-1}\{\omega_{i',j'}\}$. Assume UEs with the N largest data rates are marked with $k, k+1, \cdots, (k+N-1)$, then $\Omega_2 = \cup_{i'=k}^{k+N-1}\{\omega_{i',j'}\}$. Equation (4.12) is a linear programming (LP) relaxations of Equation (4.11). Equation (4.12) has the same objective function as Equation (4.11), and any solution to Equation (4.11) is also a solution to Equation (4.12). Let OPT be the optimal objective of Equation (4.11), and $(OPT)_{frac}$ be the optimal objective of Equation (4.12). Then, $(OPT)_{frac} \geq OPT$. Since we have assigned UEs to BSs one by one in the order of $r_i/b_{i,j'}$, and no remaining UEs can be added to Ω_1 in our solution, and thus we have $\Phi_1(\Omega_1) + \Phi_1(\Omega_2) \geq (OPT)_{frac}$. Therefore, we have $\Phi_1(\Omega_1) + \Phi_1(\Omega_2) \geq (OPT)_{frac} \geq OPT$. Thus, $\Phi_1(\Omega_1) + \Phi_1(\Omega_2) \geq OPT$, implying that whether $\Phi_1(\Omega_1)$ or $\Phi_1(\Omega_2)$ must be at least $OPT/2$. The final solution obtained by Algorithm 4 is Ω_1 or Ω_2, and it depends on which one is bigger. Thus, Algorithm 4 is a $\frac{1}{2}$-approximation algorithm for Equation (4.11).

(2) Now we consider all UEs are provisioned. In this case $\Phi_1(\Omega_1) = (OPT)_{frac} = OPT$, and $\Phi_1(\Omega_1) \geq \Phi_1(\Omega_2)$. The solution is Ω_1 for Equation (4.11), which provides the optimal throughput. □

4.3.2 The DBS Placement Problem

For the DBS placement, we exhaustively search for the optimal locations of all DBSs that achieve the highest throughput according to [16]. The algorithm is summarized

in Algorithm 5.

$$\max_{v_j,h_j,\omega_{i,j}} \quad \sum_j \sum_i \omega_{i,j} r_i$$

$$s.t.:$$

$$C1, C2, C3 \quad in \quad (4.11)$$

$$C4 : v_j \in \Lambda, \quad \forall j \in \mathcal{B}, j > 1,$$

$$C5 : h_j \in \Theta, \quad \forall j \in \mathcal{B}, j > 1. \quad (4.13)$$

Algorithm 5: Determining locations by exhaustive search

Input : parameters in Table 4.2;

Output: v_j^* and h_j^*;

```
for v_j ∈ Λ do
    for h_j ∈ Θ do
        calculate Φ_2(v_j, h_j) = Φ_1(ω_{i,j})|_{v'_j=v_j, h'_j=h_j} by Algorithm 4;
obtain v_j^*, h_j^* by (v_j^*, h_j^*) = argmax_{v_j,h_j} Φ_2(v_j, h_j);
return Ω_{i,j} associated with v_j^*, h_j^*.
```

Theorem 3. *Let v_j^*, h_j^* be the output of* Algorithm *5; the optimal location in the horizontal plane and the vertical plane is achieved by solving Equation* (4.13)*, which provides the highest throughput.*

Proof. Let $\Phi_2(v_j, h_j)$ be the function of v_j and h_j to calculate the objective value, $\Phi_2(v_j, h_j) = \Phi_1(\omega_{i,j})|_{v'_j=v_j, h'_j=h_j}$. Since we use the exhaustive search strategy (all locations for placing DBSs are checked), the maximum throughput is obtained, $\Phi_2(v_j^*, h_j^*) = \Phi_1(\omega_{i,j})\big|_{v'_j=v_j^*, h'_j=h_j^*}$ and $(v_j^*, h_j^*) = \underset{v_j,h_j}{\operatorname{argmax}} \Phi_2(v_j, h_j)$. Thus, the optimal locations of DBSs are achieved. □

Algorithm 6: Approximate Algorithm for DBSP-IBFD (*AA-DBSP*)

Input : parameters in Table 4.2;

Output: v_j, h_j, $\omega_{i,j}$, $b_{i,j}$, and $p_{i,j}$;

run *Algorithm* 5 to obtain v_j, h_j;

$L = 1$, $l = 0$, $\beta_j^l = \frac{P^D}{2^{l+1}}$;

while $L > 0$ & $l < l_{max}$ **do**

  $\beta_j^{max} = \sum_l \beta_j^l$ and $L_j = 1$;

  run *Algorithm* 4 to obtain $\Omega_{i,j}$;

  for $j \in \mathcal{B}, j > 1$ **do**

    if $|(\sum_i \sum_j \omega_{i,j} r_i - f_j)/f_j| < \varepsilon$ **then**

      $L_j = 0$;

      continue;

    if $\sum_i \omega_{i,j} r_i \leq f_j$ **then**

      $\beta_j^{l+1} = \frac{\beta_j}{2^{l+1}}$;

    else

      $\beta_j^{l+1} = -\frac{\beta_j}{2^{l+1}}$;

  $l = l + 1$, and $L = \sum_j L_j$;

obtain $b_{i,j}$ and $p_{i,j}$ associated with $\Omega_{i,j}$.

4.3.3 The DBSP-IBFD Problem

We propose an approximate algorithm to solve the DBSP-IBFD problem in Equation (4.9), named *AA-DBSP*, as summarized in *Algorithm* 6. Note that *Algorithm* 5 is used to determine the locations of all DBSs; then, the UE association is determined by *Algorithm* 4 with the determined placement of all DBSs; the bandwidth and power assignment are finally determined by the UE association.

Theorem 4. *Algorithm 6 is a* $\frac{1}{2}(1-\frac{1}{2^l})$*-approximation algorithm for Equation* (4.11) *when not all UEs are provisioned; otherwise, the optimal throughput is achieved. Here,* l *is the number of runs of Equation* (4.11)*.*

Proof. Theorem 4 can be concluded from Theorems 1, 2, and 3. □

The complexity of solving the DBSP-IBFD problem is $O(N^{|\mathcal{U}|}|\mathcal{U}|^2\mathrm{C}_{N_1}^{N_{bs}})$. Here, $N_1 = |\Lambda||\Theta|$. The complexity of Algorithm 6 is $O(N|\mathcal{U}|^3 log(|\mathcal{U}|)(l^{max} + \mathrm{C}_{N_1}^{N_{bs}}))$. The complexity of Algorithm 5 is $O(N|\mathcal{U}|^3 log(|\mathcal{U}|)\mathrm{C}_{N_1}^{N_{bs}})$. The complexity of Algorithm 4 is $O(N|\mathcal{U}|^3 log(|\mathcal{U}|))$. For Algorithm 4, the complexity of Steps 1-5 is $O(N|\mathcal{U}|))$, that of Step 6 is $O(|\mathcal{U}|log(|\mathcal{U}|))$, and that of Steps $7-16$ is $O(|\mathcal{U}|)$. The complexity of No-DBS algorithm is $O(|\mathcal{U}|^2 log(|\mathcal{U}|))$.

4.4 Performance Evaluation

MATLAB is used to run the simulation. The average result is obtained by running the simulation for 200 times. For each run, the coverage area of the MBS is set as $500m \times 500m$, and it is divided into 25 equal areas, implying that there are 25 candidate areas for placing the DBSs. Note that different DBSs are located at different locations if more than one DBS is used. In our simulation, the number of deployed DBSs is set as 3, i.e., $N = 4$ BSs (MBS and DBSs). We assume that all DBSs fly at the same height. The maximum transmission power of a DBS is set as 1W and that

of the MBS is set as 4W; the total bandwidth can be used in the network is 20 MHz, and all parameters are summarized in Table 4.2 [16, 34].

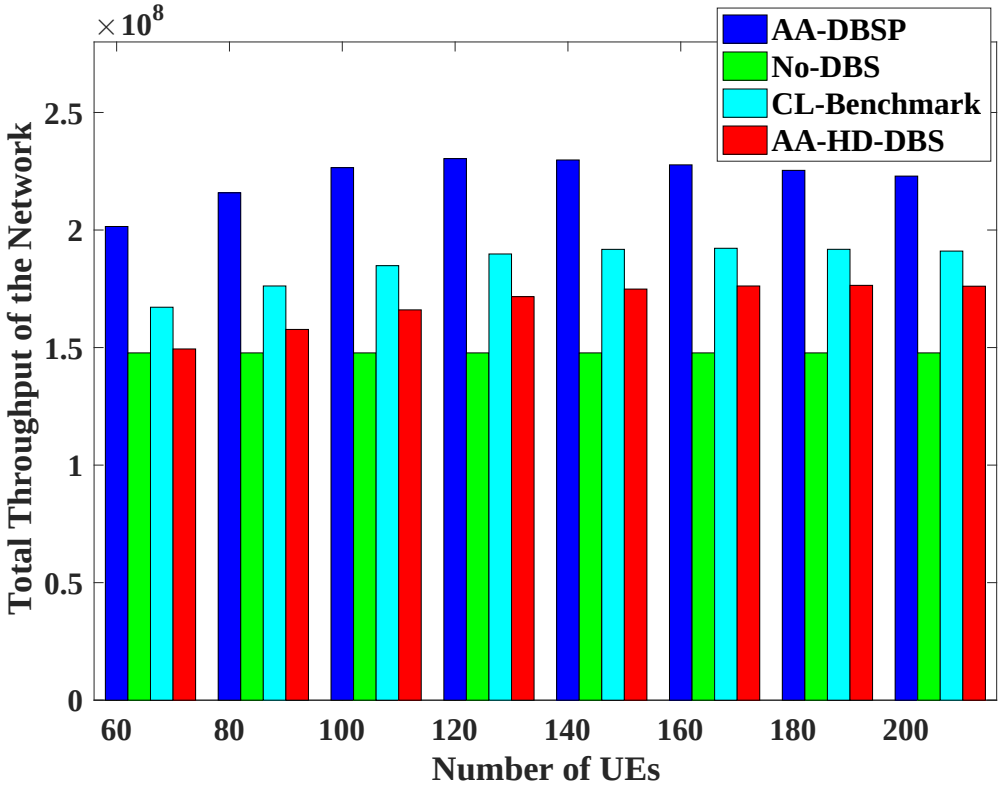

Figure 4.2 Throughput versus altitude with 220 UEs.

Three benchmark algorithms are compared to demonstrate the efficiency of the proposed AA-DBSP algorithm. The first one is named *No-DBS*, by which all UEs are associated with the MBS. The second one is named approximation algorithm with HD-enabled DBSs (*AA-HD-DBS*), which utilizes the same DBS placement strategy, the same UE association strategy and the same power and bandwidth assignment strategy as the AA-DBSP algorithm; however, the total available bandwidth of the access link and the backhaul link of each DBS is half that of the AA-DBSP algorithm because the total bandwidth of each BS is equally divided for these two links in using HD-enabled DBSs. The last one is named *CL-Benchmark*, which performs the best among algorithms compared in [23]. The DBS placement strategy of the

CL-Benchmark algorithm and that of the AA-DBSP algorithm are different, and the UE association strategies of these two algorithms are also different. The AA-DBSP algorithm provisions UEs based on the descending weight sequence (the best weight strategy), and the weight is defined as the data rate over the required bandwidth. The CL-Benchmark algorithm provisions UEs based on the best SINR (the best SINR strategy).

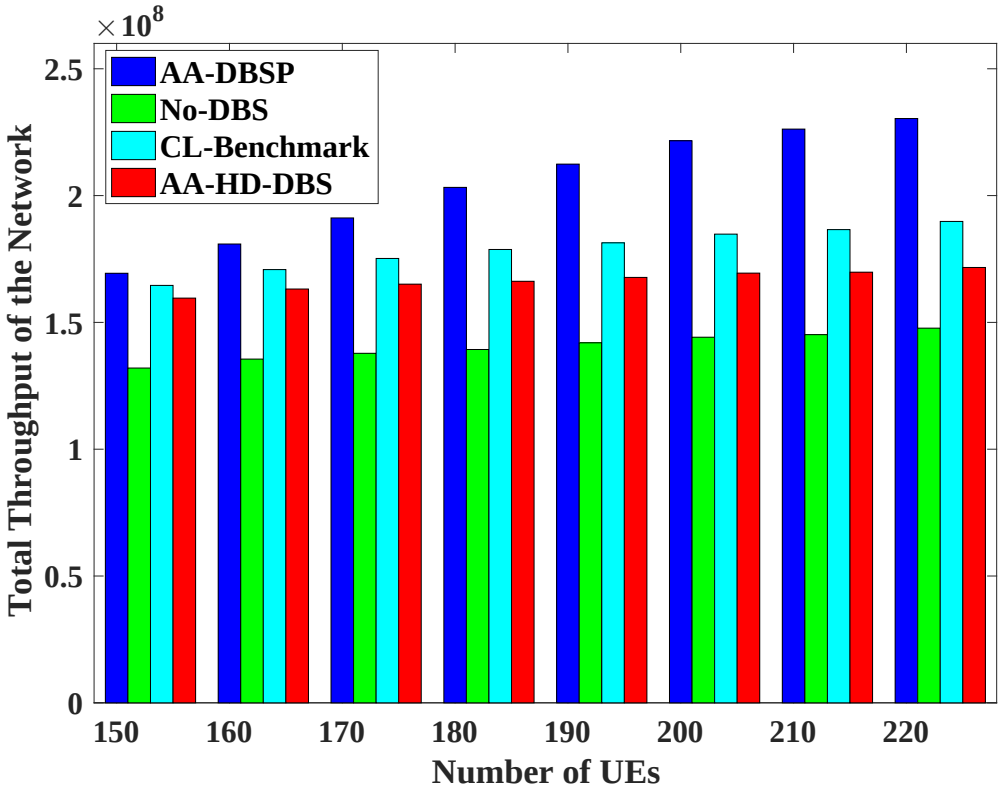

Figure 4.3 Throughput versus UEs at a fixed altitude (120m).

Figure 4.2 shows the total throughput performance of the network versus the altitude with 220 UEs. The maximum throughput results are obtained with altitude of 120m and 140m, respectively. The total throughputs achieved by the AA-DBSP and CL-Benchmark algorithms increase with the altitude $h < 120$m, and decrease when $h > 140$m. This is attributed to the fact that for $h < 120$m, NLoS is the main path loss and NLoS decreases as the altitude increases, and for $h > 140$m, LoS is the

main path loss and it increases as the altitude increases. The throughput performance of the No-DBS algorithm is the same for all altitudes because DBS is not deployed. The total throughput achieved by the AA-DBSP algorithm surpasses those by the CL-Benchmark algorithm, the AA-HD-DBS algorithm and the No-DBS algorithm by up to 21%, 34% and 56%, respectively.

Figure 4.3 illustrates the total throughput performance of the network versus different numbers of UEs at 120m altitude. The throughput performance of all algorithms increases as the number of UEs increases. This is attributed to the fact that BSs serve nearby UEs instead of remote UEs when there is not enough radio resource, thus leading to the increase of the total throughput (usually a nearby UE has better SINR than a remote UE does). AA-DBSP provides higher throughput than CL-Benchmark does because the AA-DBSP algorithm has better DBS placement strategy and better UE assignment strategy. The AA-DBSP algorithm, the CL-Benchmark algorithm and the AA-HD-DBS algorithm provide better throughput performance than the No-DBS algorithm because DBSs improve connections to UEs. The total throughput achieved by the AA-DBSP algorithm and that by the CL-Benchmark algorithm are higher than that of the AA-HD-DBS algorithm because full duplex enabled DBSs provide better throughput performance than half duplex enabled DBSs.

Figure 4.4 shows the results of the data rate block ratio, which is defined by the total data rate requirement of blocked UEs over that of all UEs. Since different UEs may have different data rate requirements, it is more precise to calculate the data block ratio instead of computing the number of blocked UEs. The AA-DBSP algorithm achieves the lowest data rate block ratio, and the No-DBS algorithm exhibits the highest data rate block ratio. This is because SINR of remote UEs to the MBS have been improved by IBFD-enabled DBSs, and AA-DBSP provides better DBS placement and better UE assignment than CL-Benchmark does. The data rate

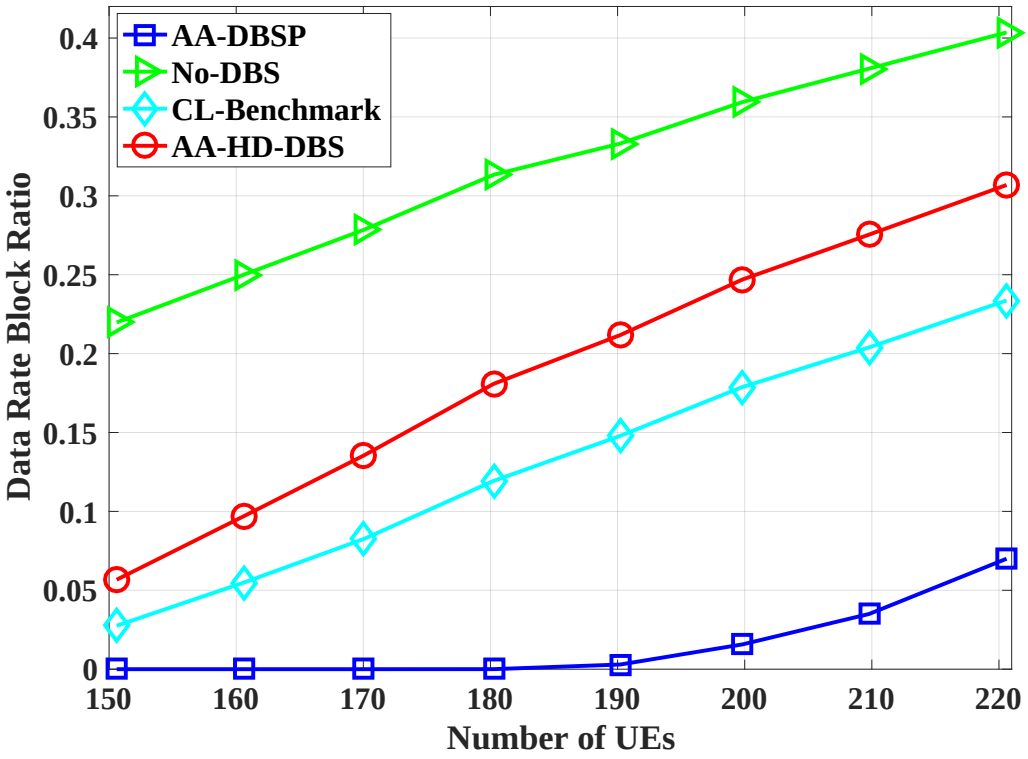

Figure 4.4 Performance of the data rate block ratio.

block ratio of all algorithms increases as the number of UEs increases because limited ratio resources cannot accommodate too many UEs. The data rate block ratio of the AA-DBSP algorithm and that of the CL-Benchmark algorithm are lower than that of the AA-HD-DBS algorithm because the same radio resource can be reused in the access links and backhaul links of full duplex enabled DBSs.

Here are some insight of our simulation results: the AA-DBSP algorithm achieves the optimal throughput result when all UEs are served; 2) the AA-DBSP algorithm provides 3-D locations of DBS deployment, and the optimal locations of all DBSs are achieved; 3) the AA-DBSP algorithm provides guaranteed performance, and the approximation ratio is $\frac{1}{2}(1-\frac{1}{2^l})$ (l is the number of simulation runs). All simulation results show that IBFD-enabled DBSs can improve the throughput performance of the network.

Table 4.1 Important Notations and Variables of the DBSP-IBFD Problem

Symbol	Definiton
N	the number of all BSs, including the MBS and DBSs.
N_{bs}	the number of deployed DBSs.
Λ	the set of candidate areas for placing DBSs in the horizontal plane.
Θ	the set of candidate altitudes for placing DBSs in the vertical plane.
r_i	the data rate requirement of the ith UE.
(x_i^{ue}, y_i^{ue})	the location of the ith UE.
P^M	the maximum transmission power of the MBS.
P^D	the maximum transmission power of a DBS.
$P_{j,1}$	the backhaul transmission power of the jth DBS assigned by the MBS.
ξ_j	the power spectral density of the jth BS.
β^M	the total available bandwidth in the network.
h_{min}	the minimum altitude of a DBS.
h_{max}	the maximum altitude of a DBS.
$\omega_{i,j}$	the UE-BS assignment indicator; 1 if the ith UE is associated with the jth BS, and 0, otherwise.
β_j	the total available bandwidth for the jth BS, and it is the backhaul bandwidth for the jth DBS when $j > 1$.
$p_{i,j}$	the assigned power from the jth BS towards the ith UE.
$b_{i,j}$	the assigned bandwidth from the jth BS towards the ith UE.
v_j	the location of the jth BS in the horizontal plane, $v_j \in \Lambda$.
h_j	the location of the jth BS in the vertical plane, $h_j \in \Theta$.
$d_{i,j}$	the achieved data rate of the ith UE via the jth DBS.

Table 4.2 Simulation Parameters for the DBSP-IBFD Problem

(a, b, η_L, η_N), environment parameters	$(9.61, 0.16, 1, 20)$
C_m, coverage area of the MBS	$500m \times 500m$
h_{min}	60 m
h_{max}	200 m
G2G (MBS to UE) path loss	$34.5 + 35log_{10}(d[m])$ [34]
shadow fading between the MBS and a UE	6 dB
N_0	-174 dBm/Hz
G_0	130 dB [15]
$\|\mathcal{U}\|$	$\{150, 160, \cdots, 220\}$
r_i	$\{0.5, 1, 1, 2\}$ Mbps
P^M	4 W
P^D	1 W
β^M	20 MHz
l^{max}	10
ε	0.0001

CHAPTER 5

OPTIMIZING THE DEPLOYMENT AND UPLINK THROUGHPUT OF DBS-ASSISTED HETNET

Many works related to DBS communications, viz., Unmanned Aerial Vehicle Base Station (*UAV-BS*) communications [16,40–47], have been reported. Alzenad *et al.* [16] studied the UAV-BS placement problem with the target to maximize the number of served UEs, and they proposed an exhaustive search algorithm to obtain the optimal altitude and coverage radius under a given path loss threshold. Bor-Yaliniz *et al.* [40] highlighted the properties of the 3-D DBS placement problem with the objective to maximize the revenue, which is proportional to the number of covered UEs. Lyu *et al.* [41] investigated the UAV-BS placement problem, and the objective is to minimize the number of required DBSs while each UE is at least covered by one DBS. Lai *et al.* [42] investigated the UAV-BS placement problem in a hot spot area and the goal is to maximize the number of covered UEs under given data rate requirements. Mei *et al.* [43] proposed to utilize cooperative beamforming to alleviate the downlink interference as the DBS reuses the frequency spectra already assigned to the ground BSs, and the target is to maximize the received SINR in the DBS. Cheng *et al.* [44] studied the UAV-aided computing offloading problem in the space-air-ground network, where the UAVs provide edge computing services and the satellites provide backhaul communications to the cloud core. Li *et al.* [45] surveyed recent research activities in UAV communications toward 5G/beyond 5G, and they advocated the importance of UAV-BS communications in the future 5G network owing to the following characteristics: good channel conditions, high maneuverability and flexible deployment. Shi *et al.* [46] studied the 3-D trajectory planning of multiple DBSs in the drone-aided radio access networks with the target to minimize the average path loss of the DBS to UEs. Wu *et al.* [47] considered the UE assignment, power control

and trajectories of multiple DBSs in a drone-assisted network, and the objective is to maximize the minimum throughput among all UEs.

IBFD communications, which provisions simultaneous transmission and reception over the same radio resources at the same time, has attracted significant attention in both academia and industry because it can theoretically double the throughput capacity, reduce the end-to-end delay and increase the spectrum utilization flexibility [13, 48]. Owing to the serious self-interference (*SI*) caused by the transmission and reception over the same frequency in an FD-enabled device, it is difficult to achieve IBFD communications in the past but some new innovative hardware design has validated the feasibility of FD communications by repressing the SI power [14]. Nam *et al.* [49] maximized the total throughput of all FD-enabled UEs in an FD orthogonal frequency division multiple access (*OFDMA*) network with only one BS. Goyal *et al.* [50] studied the spectral efficiency of a mixed multi-cell network, viz., mixed FD and HD cells while all UEs are half-duplex (*HD*) enabled. Chen *et al.* [51] maximized the total sum-rate of uplink and downlink communications within one FD BS under a heavy workload scenario. Zhang *et al.* [23, 36] studied the downlink throughput maximization problem and 3-D DBS placement with IBFD communications in a HetNet. However, few works have addressed the uplink communications in the HetNet with IBFD enabled DBSs.

Since DBSs can flexibly provision UEs with communication services and IBFD can theoretically double the spectrum efficiency, it is therefore conceivable to employ IBFD-enabled DBSs in the HetNets and we study the uplink communications in this research. We investigated the throughput maximization of the downlink communications in a HetNet with in-band full-duplex (*IBFD*) enabled DBSs in [23, 36]. In this research, we study the backhaul-aware uplink communications in a full-duplex DBS-aided HetNet (*BUD*) problem [52]. The preliminary results of BUD will be reported in [53] (Globecom 2019), and the differences between this

work and [53] are summarized as follows: 1) we have further studied the number of required DBSs in provisioning UEs in this work while that of [53] is fixed; 2) we have reformulated the BUD problem because the objective of this work is to maximize the total throughput of the network and at the same time minimize the number of deployed DBSs, while the objective of [53] is to maximize the total throughput of the network; 3) the AA-BUD algorithm is proposed to solve the BUD problem, and it gives a $(1-\varepsilon)$ approximation ratio ($\varepsilon \leq \frac{1}{2}$), which is better than that obtained in [53]; 4) we have also shown the evaluation results with the variation of the number of deployed DBSs in this work: the total throughput of the network increases as the number of deployed DBSs increases while the blocking ratio decreases.

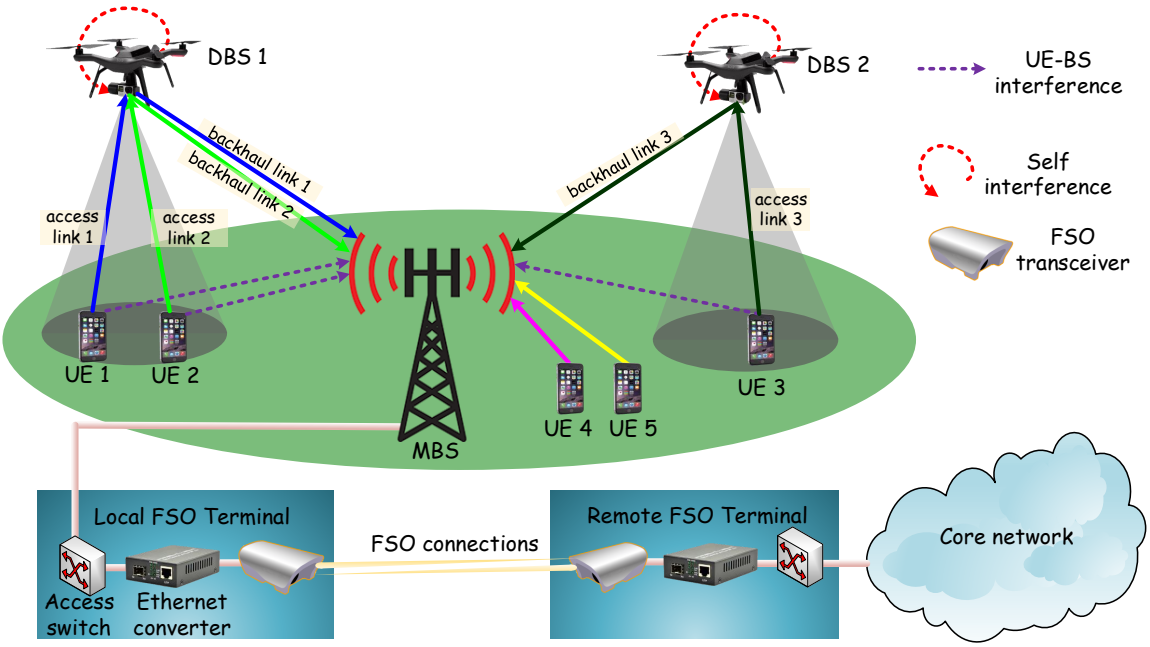

Figure 5.1 The IBFD DBS-aided HetNet framework.

The main contributions of this research are delineated as follows: 1) we propose an IBFD-enabled DBS-aided HetNet for uplink communications, and the DBSs can provide dynamic coverage to UEs by adjusting their vertical and horizontal positions; 2) the macro-BS (*MBS*) is connected to the core network through free space optics (*FSO*) links, implying that this network can be easily deployed to provide

communications to temporary events or fast communications recovery in emergency situations; 3) we propose two approximation algorithms to solve the sub-problems and another one named AA-BUD algorithm to solve the BUD problem. The AA-BUD algorithm with the approximation ratio of $(1-\varepsilon)$ is shown capable of acquiring the optimal locations of all DBSs. Here, $\varepsilon \leq \frac{1}{2}$.

5.1 System Model

Figure 5.1 shows a DBS-aided HetNet, in which the frequency division duplex (*FDD*) OFDMA framework is adopted [49]. DBS 1 and DBS 2 are FD-enabled, and the MBS and all UEs are HD-enabled. The MBS is connected to the core network through the local FSO terminal and the remote FSO terminal. Both the local FSO terminal and the remote FSO terminal include an access switch, an Ethernet converter (Ethernet/FSO signal conversion) and an FSO transceiver. The distance between the local FSO terminal and the remote FSO terminal can be a few kilometers while a high data rate transmission can still be achieved [54]. For example, Sarkar *et al.* [55] designed a 64-QAM FSO transceiver for one hop transmission, and the transceiver demonstrates a 120 Gb/s reliable communication data rate over a 1 km link. The access link is a UE-to-BS (UE-to-DBS) link while the backhaul link is the DBS-to-MBS link.

As shown in Figure 5.1, different UEs utilize different frequency spectra for communications, no matter whether the UEs are associated with the DBS (UE 1 and UE 2) or the MBS (UE 4 and UE 5); different DBSs are assigned with different frequency spectra (UE 1, UE2 and UE 3); the backhaul link of a DBS reuses the frequency spectra of its access link (access link 1 and backhaul link 1). In this work, we focus on the uplink communications. In other words, we focus on data transmission from a UE to the MBS directly or via a FD-enabled DBS. For the uplink communications, the basic (minimum) unit of the frequency spectrum is

one subcarrier (SC); one UE can be provisioned by one or multiple SCs while one subcarrier can only be assigned to one UE in order to avoid UE-UE interference.

Here, we briefly discuss the deployment of the proposed DBS-aided HetNet framework. We consider two different time slots in this research. One is a large time slot in terms of minutes even tens of minutes, and is utilized to relocate all DBSs based on the traffic load. The other one is a small time slot in terms of seconds, and is employed to assign the UEs to the BSs and allot the radio resources (including the power and bandwidth resource) to the UEs. In the following description, we focus on the resource management in one large time slot. We need to find the number of deployed DBSs, place all DBSs to their target positions, assign the UEs to the BSs, and allot the power and bandwidth resources to the UEs.

5.1.1 Path Loss Model

For the path loss of the proposed framework in Figure 5.1, we consider air-to-ground ($A2G$) path loss (DBS-MBS) and ground-to-air ($G2A$) path loss (UE-DBS). For both A2G and G2A path loss, we consider line-of-sight (LoS) and none-line-of-sight ($NLoS$) path loss [23, 24, 56]. Denote $\psi_{i,j}^{L}$ and $\psi_{i,j}^{N}$ as the probabilities of a LoS and NLoS connection of an A2G (G2A) link, as shown in Equation (5.1). Here, a and b are environment coefficients (i.e., suburban, urban or dense urban); $\theta_{i,j} = arctan(\frac{h_j}{d_{i,j}})$ is the elevation angle; h_j $(j > 1)$ is the altitude of the jth DBS and $d_{i,j}$ $(j > 1)$ is the 3-D distance between the ith UE and the jth DBS [16, 24].

$$\begin{cases} \psi_{i,j}^{L} = \dfrac{1}{1 + a\psi_0}, \quad \psi_0 = exp(-b(\dfrac{180\theta_{i,j}}{\pi} - a)), \\ \psi_{i,j}^{N} = 1 - \psi_{i,j}^{L}. \end{cases} \tag{5.1}$$

Let $\eta_{i,j}$ be the path loss between the ith UE and the jth DBS, as described in Equation (5.2). Here, ζ^L and ζ^N are the additional path losses of LoS and NLoS, respectively; f_0 is the carrier frequency and c_0 is the transmission speed of light. The

first item and the second item are the Los and NLoS of the excessive path loss, and the third item is the mean free-space path loss (including LoS and NLoS free-space path loss).

$$\eta_{i,j} = \psi_{i,j}^{L}\zeta^{L} + \psi_{i,j}^{N}\zeta^{N} + 20log(4\pi f_0 d_{i,j}/c_0). \tag{5.2}$$

After substituting Equation (5.1) into Equation (5.2), we have

$$\eta_{i,j} = \psi_{i,j}^{L}(\zeta^{L} - \zeta^{N}) + 20log(4\pi f_0 d_{i,j}/c_0) + \zeta^{N}. \tag{5.3}$$

5.1.2 Communications Model

Let $s_{i,j}^{1}$ and $s_{i,j}^{2}$ $(j > 1)$ be the signal to interference plus noise ratio ($SINR$) of the access link and the backhaul link from the ith UE to the MBS via the jth DBS, as expressed in Equations (5.4)-(5.5). Here, $j = 1$ implies that the UE connects to the MBS directly; P_U is the transmission power of a UE; $\sigma_j^2 = \tau_0 b_{i,j} N_0$ is the thermal noise power, τ_0 is the bandwidth of one SC, $b_{i,j}$ is the assigned bandwidth for the ith UE to the jth BS in terms of SCs, and N_0 is the thermal noise power spectral density; $\alpha_{i,j} = p_{i,j}/\tau^{SI}$ is the self interference (SI) at the jth DBS incurred by the FD communications, $p_{i,j}$ is the assigned power by the jth DBS for the backhaul link (the jth DBS to the MBS) in provisioning the ith UE, and τ^{SI} is the SI cancellation capability [57].

$$s_{i,j}^{1} = \begin{cases} \frac{P_U \Gamma_{i,j}}{\sigma_{i,j}^2}, & \forall i \in \mathcal{U}, j \in \mathscr{B}, j = 1, \\ \frac{P_U \eta_{i,j}}{\alpha_{i,j} + \sigma_{i,j}^2}, & \forall i \in \mathcal{U}, j \in \widetilde{\mathscr{B}}. \end{cases} \tag{5.4}$$

Equation (5.5) shows the SINR of the backhaul link for the ith UE from the jth DBS to the MBS. Here, $\tilde{\eta}_{1,j}$ is the channel gain from the jth DBS to the MBS; $\Gamma_{i,1}$ is the channel gain from the ith UE to the MBS; $\sigma_{i,1}^2$ is the thermal noise power

at the MBS owing to the transmission of the ith UE.

$$s_{i,j}^2 = \frac{p_{i,j}\tilde{\eta}_{1,j}}{P_U\Gamma_{i,1} + \sigma_{i,1}^2}, \quad \forall i \in \mathcal{U}, j \in \widetilde{\mathscr{B}}. \tag{5.5}$$

Let $\beta_{i,j}$ be the data rate from the ith UE to the jth BS, expressed as:

$$\beta_{i,j} = \begin{cases} \beta_{i,j}^1, & \forall i \in \mathcal{U}, j \in \mathscr{B}, j = 1, \\ \min(\beta_{i,j}^1, \beta_{i,j}^2), & \forall i \in \mathcal{U}, j \in \widetilde{\mathscr{B}}, \end{cases} \tag{5.6}$$

where $\beta_{i,j}^1$ is the data rate of the access link (UE-BS) and $\beta_{i,j}^2$ is the data rate of the backhaul link (DBS-BS), expressed as:

$$\begin{cases} \beta_{i,j}^1 = \tau_0 b_{i,j} log_2(1 + s_{i,j}^1), & \forall i \in \mathcal{U}, j \in \mathscr{B}, \\ \beta_{i,j}^2 = \tau_0 b_{i,j} log_2(1 + s_{i,j}^2)], & \forall i \in \mathcal{U}, j \in \widetilde{\mathscr{B}}. \end{cases} \tag{5.7}$$

5.2 Problem Formulation

We focus on the uplink communications in an FD DBS-aided HetNet, and each UE is provisioned by one BS. Two important variables are presented here to formulate the BUD problem.

$x_{i,j}$: the UE-BS indicator, which is 1 if the ith UE is provisioned by the jth BS, and 0 otherwise.

y_j: the DBS indicator, which is 1 if the jth DBS ($j > 1$) is used, and 0 otherwise. As the MBS is always used, $y_1 = 1$.

Let $\Phi(x_{i,j}, y_j, p_{i,j}, b_{i,j}, \gamma_j, h_j) = \sum_i \sum_j x_{i,j} r_i$ be the throughput of the network and N be the total number of deployed DBSs, $N = \sum_j y_j$. Important notations and variables are listed in Tables 5.1 and 5.2.

The BUD problem is formulated to maximize the total throughput of the network for the uplink communications while minimizing the number of deployed DBSs as a multi-objective optimization problem:

$$
\begin{aligned}
\mathscr{P}_0 : & \max_{x_{i,j}, y_j, p_{i,j}, b_{i,j}, \gamma_j, h_j} \Phi \quad \& \quad \max_{y_j}(-N) \\
s.t. : & \\
& C1 : \sum_j x_{i,j} \leq 1, \quad \forall i \in \mathscr{U}, \\
& C2 : \sum_i x_{i,j} b_{i,j} \leq f_j^{max}, \quad \forall j \in \mathscr{B}, \\
& C3 : \sum_i x_{i,j} p_{i,j} \leq P_D, \quad \forall j \in \widetilde{\mathscr{B}}, \\
& C4 : x_{i,j} r_i \leq \beta_{i,j}, \quad \forall i \in \mathscr{U}, j \in \mathscr{B}, \\
& C5 : \gamma_j \in \mathscr{V}_1, \quad \forall j \in \widetilde{\mathscr{B}}, \\
& C6 : h_j \in \mathscr{V}_2, \quad \forall j \in \widetilde{\mathscr{B}}, \\
& C7 : y_j \leq \sum_i x_{i,j} \leq y_j |\mathscr{U}|, \quad j \in \widetilde{\mathscr{B}}. \\
& C8 : x_{i,j} \in \{0,1\}, \quad \forall i \in \mathscr{U}, j \in \mathscr{B}. \\
& C9 : y_j \in \{0,1\}, \quad \forall j \in \widetilde{\mathscr{B}}.
\end{aligned} \tag{5.8}
$$

We negate N in the objective function in order to transform the minimization problem into the maximization problem. C1 and C8 are the UE provisioning constraints, which impose one UE to be provisioned by at most one BS. C2 is the bandwidth capacity constraint for each BS and imposes the assigned bandwidth by a BS to its associated UEs not to exceed the BS' bandwidth capacity. C3 is the power capacity constraint of each DBS for the backhaul link, and it imposes the total power used by a DBS not to exceed its power capacity. C4 is the data rate provisioning constraint, implying that the achieved data rate of a UE is equal or larger than the required data rate. C5–C6 are the DBS placement constraints, and they impose all DBSs to be placed on the candidate locations in the horizontal plane and vertical

plane. C7–C9 are the constraints for the number of deployed DBS to ensure that a DBS is used only if there is one or more UEs provisioned by this DBS.

Table 5.1 Notations of the BUD Problem

Symbol	Definition
$\mathscr{B}$	the set of BSs ($\widetilde{\mathscr{B}}$ is the set of DBSs).
$\widetilde{\mathscr{B}}$	the set of DBSs.
N	the number of total used DBSs, $N = \sum_j y_j$.
N_{max}	the maximum number of available BSs, $N \leq N_{max}$.
$\mathscr{U}$	the set of UEs.
$\mathscr{V}_1$	the set of horizontal candidate locations.
$\mathscr{V}_2$	the set of vertical candidate locations.
τ_0	the bandwidth of one SC.
r_i	the data rate requirement of the ith UE.
f^{max}	the total available bandwidth of all BSs in terms of SCs.
f_j^{max}	the total available bandwidth for the jth BS in term of SCs.
P_D	the power capacity of the jth BS.
P_U	the power capacity of the ith UE.
κ_j	the power spectral density of the jth DBS, $j \in \widetilde{\mathscr{B}}$.
$d_{i,j}$	the 3-D distance between the ith UE and the jth DBS.
$\eta_{i,j}$	the path loss between the ith UE and the jth DBS.
$\tau_{i,j}^{SI}$	the SI power at the jth DBS for provisioning the ith UE.

Table 5.2 Variables of the BUD Problem

Symbol	Definition
$x_{i,j}$	the UE-BS association indicator.
$y_{i,j}$	the used DBS indicator.
$\beta_{i,j}$	the achieved data rate of the ith UE towards the jth BS.
$b_{i,j}$	the assigned SCs by the jth BS towards the ith UE.
$p_{i,j}$	the assigned power by the jth DBS for the DBS-MBS transmission (backhaul data transmission for the ith UE).
γ_j	the horizontal location of the jth BS, $\gamma_j \in \mathscr{V}_1$.
h_j	the vertical location of the jth BS, $h_j \in \mathscr{V}_2$.

5.3 Problem Analysis

Any instance of the Max-Generalized Assignment Problem (*Max-GAP*) problem [58] can be reduced into the BUD problem for a given number of DBSs, and the BUD problem is NP-hard because the Max-GAP problem is a well-known NP-hard problem. Then, we decompose the BUD problem into three sub-problems: the joint UE association, power and bandwidth assignment (*Joint-UPB*) problem, the DBS placement problem and the problem of determining the number of DBSs to be deployed. We first solve the sub-problems one by one, and then we use the solutions of these sub-problems to solve the BUD problem.

5.3.1 Solving the Joint-UPB Problem

For given vertical and horizontal positions [37] of all DBSs, i.e., $\tilde{y}_j$, $\hat{\gamma}_j$ and $\hat{h}_j$, $\mathscr{P}_0$ can be transformed into $\mathscr{P}_1$.

$$
\begin{aligned}
\mathscr{P}_1: \quad & \max_{x_{i,j},p_{i,j},b_{i,j}} \quad \Phi_1 \\
s.t.: \quad & \\
& C1: \sum_j x_{i,j} \leq 1, \quad \forall i \in \mathscr{U}, \\
& C2: \sum_i x_{i,j} b_{i,j} \leq f_j^{max}, \quad \forall j \in \mathscr{B}, \\
& C3: \sum_i x_{i,j} p_{i,j} \leq P_D, \quad \forall j \in \widetilde{\mathscr{B}}, \\
& C4: x_{i,j} r_i \leq \beta_{i,j}, \quad \forall i \in \mathscr{U}, j \in \mathscr{B}, \\
& C5: x_{i,j} \in \{0,1\}, \quad \forall i \in \mathscr{U}, j \in \mathscr{B}.
\end{aligned} \tag{5.9}
$$

Here, $\Phi_1(x_{i,j}, p_{i,j}, b_{i,j}) = \Phi|_{\gamma_j=\hat{\gamma}_j, h_j=\hat{h}_j, y_j=\hat{y}_j} = \sum_i \sum_j x_{i,j} r_i$ is the objective function of problem $\mathscr{P}_1$, which is the total throughput of the network for given UE association indicator ($x_{i,j}$), and power and bandwidth assignment ($p_{i,j}$, $b_{i,j}$). To ensure analytical tractability, we assume the power assignment is proportional to the bandwidth assignment, viz., $p_{i,j} = b_{i,j}\kappa_j$. Note that the MBS does not assign power and bandwidth to the UEs while the DBSs need to assign power and bandwidth to the backhaul links. Then, constraint $C3$ is relaxed. The required bandwidth to provision the ith UE by the jth BS can be calculated as $\hat{b}_{i,j} = \underset{b_{i,j}}{\operatorname{argmin}} (\beta_{i,j} - x_{i,j} r_i \geq 0), x_{i,j} = 1, \forall i \in \mathscr{U}, j \in \mathscr{B}$. Obviously, constraint $C4$ is also relaxed. Then, $\mathscr{P}_1$ can be transformed into $\mathscr{P}_2$.

$$\mathscr{P}_2: \quad \max_{x_{i,j}} \quad \sum_i \sum_j x_{i,j} r_i$$

$$s.t.:$$

$$C1: \sum_j x_{i,j} \leq 1, \quad \forall i \in \mathscr{U},$$

$$C2: \sum_i x_{i,j} b_{i,j} \leq f_j^{max}, \quad \forall j \in \mathscr{B},$$

$$C3: x_{i,j} \in \{0,1\}, \quad \forall i \in \mathscr{U}, j \in \mathscr{B}. \tag{5.10}$$

Since approximation algorithms can solve an NP-hard problem efficiently in polynomial time and achieve sub-optimal solutions with determined deviation from the optimal one, we propose an approximation algorithm to solve problem $\mathscr{P}_2$ as depicted in Algorithm 7, referred to as Approximation Algorithm for the joint-UPB problem (*AA-UPB*). The parameters are initialized in *Step* 1. BS $\tilde{j}$, which uses the least bandwidth resource to provision the ith UE, is determined through *Steps* $2-6$. The weight z_i of the ith UE and the least required bandwidth to provision the ith UE are calculated by *Step* 7. Here, the weight $z_i^{'}$ is a ratio of the data rate over the required bandwidth, i.e., $z_i^{'} = \frac{r_i}{\tau_0 b_{i,j}}$; as τ_0 is a constant, we can use $z_i = r_i/b_{i,j}$ instead of $z_i^{'}$. Considering two UEs with the same bandwidth requirement and different weights, provisioning the UE with a larger weight results in a larger throughput than the other; the same bandwidth resource in the network can achieve a larger throughput if UEs with larger weights are provisioned. This is the reason why we need to calculate the weights of all UEs. The weights are then sorted in a decreasing order in *Step* 7 and this new order represents a new sequence of the same UEs. Note that two solutions are determined by *Steps* $9-19$ and *Steps* $20-24$, and we may use these two solutions to find the lower bound of problem $\mathscr{P}_2$. In Algorithm 7, the first solution $\Lambda_1 = \cup\{x^1_{\tilde{i},\tilde{j}}\}$, which includes the UEs with larger weights is obtained

through *Steps* $9-19$, and the other solution $\Lambda_3 = \cup\{x^2_{\hat{i},\hat{j}}\}$, which contains $|\mathscr{B}|$ UEs with the maximum data rate, is achieved through *Steps* $20-24$. Finally, the one ($\cup\{\tilde{x}_{i,j}\}$, viz., either Λ_1 or Λ_3) which produces a higher throughput is returned by *Step* 25, and the corresponding $\tilde{b}_{i,j}$ and $\tilde{p}_{i,j}$ are also returned by *Step* 26.

Since data requirements of all UEs are not equal, some special UEs with lower weights may have larger data rate requirements than the other UEs. This is the reason why we need to find another solution to avoid poor radio resource assignment. Here, the special UEs are defined as the $|\mathscr{B}|$ UEs with the maximum data rate requirement in the UE set $\mathscr{U}$, and the number of special UEs equals to the number of BSs. In this scenario, the throughput of the network may be compromised if special UEs are not provisioned. Hence, we need to find one solution, which includes the UEs with larger weights, and the other solution, which includes only the $|\mathscr{B}|$ special UEs with the largest data rate requirement; we then choose the one with a higher throughput between these two solutions. For a better illustration, we present an example here with three UEs and one BS, and the bandwidth capacity is set as 5. The respective data rate, bandwidth, and weight of all UEs are shown in Table 5.3; then, UE 1 and UE 2 are selected by the first solution and UE 3 (the special UE) is selected by the second solution (only two solutions are determined); the throughput of the first solution is 4.5 but the throughput of the second solution is 5; the second solution is returned as it yields a larger throughput than that of the first solution.

Theorem 5. *The AA-UPB algorithm is a* $\frac{1}{2}$*-approximation algorithm of problem* $\mathscr{P}_2$*. In particular, this algorithm achieves the optimal throughput when all UEs are provisioned.*

Proof. As we want to find a non-integer solution to problem $\mathscr{P}_2$, $x_{i,j}$ is relaxed to a continuous variable in order to transform problem $\mathscr{P}_2$ into problem $\mathscr{P}_3$. Here, we define $\Phi_2(x_{i,j}) = \Phi_1|_{p_{i,j}=\tilde{p}_{i,j},b_{i,j}=\tilde{b}_{i,j}}$ for $x_{i,j} \in \{0,1\}$ as the objective function of $\mathscr{P}_2$,

and $\Phi_3(x_{i,j}) = \Phi_1|_{p_{i,j}=\tilde{p}_{i,j}, b_{i,j}=\tilde{b}_{i,j}}$ for $0 \leq x_{i,j} \leq 1$ as the objective function of $\mathscr{P}_3$. Note that the objective of problem $\mathscr{P}_3$ is usually bigger than that of problem $\mathscr{P}_2$; they are equal only when all UEs are provisioned. In this proof, we assume that the number of UEs is more than the number of deployed BSs, $|\mathscr{B}| < |\mathscr{U}|$.

$$\begin{aligned}
\mathscr{P}_3: \quad & \max_{x_{i,j}} \quad \sum_i \sum_j x_{i,j} r_i \\
s.t.: \quad & \\
& C1, C2 \quad in \quad \mathscr{P}_2 \\
& C3: 0 \leq x_{i,j} \leq 1, \quad \forall i \in \mathscr{U}, j \in \mathscr{B}.
\end{aligned} \tag{5.11}$$

1) If all UEs are provisioned, $|\Lambda_1| > |\Lambda_3|$ because Λ_3 only includes the $|\mathscr{B}|$ UEs with the maximum data rate. Note that Λ_1 may include all UEs but Λ_3 does not because $|\Lambda_3| = |\mathscr{B}| < |\mathscr{U}|$. The achieved total throughput by Algorithm 7 is $\max(\Phi_2(\Lambda_1), \Phi_2(\Lambda_3)) = \Phi_2(\Lambda_1) = \sum_i \sum_j x_{i,j} r_i = \sum_i r_i$; the optimal solutions of $\mathscr{P}_2$ and $\mathscr{P}_3$ are $\Phi_2(x^*_{i,j}) = \sum_i \sum_j x^*_{i,j} r_i = \sum_i r_i$ and $\Phi_3(x^*_{i,j}) = \sum_i \sum_j x^*_{i,j} r_i = \sum_i r_i$. Here, $\sum_j x_{i,j} = 1$ and $\sum_j x^*_{i,j} = 1$. Algorithm 7 produces the results equivalent to the optimal solutions of problem $\mathscr{P}_2$ and $\mathscr{P}_3$.

2) Here, we discuss the scenario with one or more blocked UEs. We first find the relationship between the optimal value of problem $\mathscr{P}_3$, $\Phi_2(\Lambda_1)$ and $\Phi_2(\Lambda_3)$. Then, the lower bound of $\max(\Phi_2(\Lambda_1), \Phi_2(\Lambda_3))$ is determined, which is leveraged to prove the approximation ratio of the AA-UPB algorithm. Note that Algorithm 7 puts all UEs in a sequence by the decreasing order of their weights (the data rate over the required bandwidth), and all UEs provisioned by this order are included in Λ_1; provisioning more UEs means that a larger throughput is achieved. Let $(k-1)$ be the index of the last UE which is provisioned in Λ_1, i.e., $|\Lambda_1| = k - 1$. $\Phi_3(\cup x^*_{i,j}) = \Phi_2(\Lambda_1) + \Phi_2(\cup_{\hat{i}=k}^{k-1+|\mathcal{B}|} \tau_j \hat{x}'_{\hat{i},\hat{j}})$. Here, $\Lambda_1 = \cup\{x^1_{\tilde{i},\tilde{j}}\}$, and $\cup_{\tilde{i}=k}^{k-1+|\mathcal{B}|} \hat{x}'_{\tilde{i},\tilde{j}}$ includes $|\mathscr{B}|$ UEs with the

maximum data rate requirement among the UEs with the starting index k and the end index $|\mathscr{U}|$; $\tau_j = (f_j^{max} - \sum_{\tilde{i}=1}^{k-1} \tilde{x}_{\tilde{i},\tilde{j}} \tilde{b}_{\tilde{i},\tilde{j}})/(\hat{x}'_{\hat{i},\hat{j}} \hat{b}'_{\hat{i},\hat{j}})$ and $0 \leq \tau_j < 1$. Note that $\Lambda_3 = \cup_{\hat{i}=1}^{|\mathscr{B}|} \{x^2_{\hat{i},\hat{j}} = \underset{x_{i,j}}{\operatorname{argmax}}\, x_{i,j} r_i\}$, which represents the $|\mathscr{B}|$ UEs with the maximum data rate requirement among all UEs. Thus, the objective value of Λ_3 should be equal or bigger than $\Phi_2(\cup_{\hat{i}=k}^{k-1+|\mathcal{B}|} \hat{x}'_{\hat{i},\hat{j}})$. Then, $\Phi_2(\cup_{\hat{i}=k}^{k-1+|\mathcal{B}|} \hat{x}'_{\hat{i},\hat{j}}) \leq \Phi_2(\Lambda_3)$, and $\Phi_2(\cup_{\hat{i}=k}^{k-1+|\mathcal{B}|} \tau_j \hat{x}'_{\hat{i},\hat{j}}) < \Phi_2(\Lambda_3)$. Therefore, we have $\Phi_3(\cup x^*_{i,j}) < \Phi_2(\Lambda_1) + \Phi_2(\Lambda_3)$, implying that the objective values of set Λ_1 and Λ_3 are bigger than that of $\Phi_3(\cup x^*_{i,j})$. Meanwhile, the objective value of problem $\mathscr{P}_2$ is smaller or equal to that of problem $\mathscr{P}_3$, $\Phi_2(\cup x^*_{i,j}) \leq \Phi_3(\cup x^*_{i,j})$. We have $\Phi_2(\cup x^*_{i,j}) < \Phi_2(\Lambda_1) + \Phi_2(\Lambda_3)$, implying that either $\Phi_2(\Lambda_1) \geq \frac{1}{2}\Phi_2(\cup x^*_{i,j})$ or $\Phi_2(\Lambda_3) \geq \frac{1}{2}\Phi_2(\cup x^*_{i,j})$. Thus, $\max(\Phi_2(\cup x^1_{\tilde{i},\tilde{j}}), \Phi_2(\cup x^2_{\hat{i},\hat{j}})) \geq \frac{1}{2}\Phi_2(\cup x^*_{i,j})$, which means that the lower bound of the AA-UPB algorithm is bigger than $\frac{1}{2}$ of the optimal value of problem $\mathscr{P}_2$ and the approximation ratio of the AA-UPB algorithm is $\frac{1}{2}$. □

Lemma 1. *The AA-UPB algorithm has an* $(1-\varepsilon)$ *approximation ratio of solving problem* $\mathscr{P}_2$ *if* $b_i \leq \varepsilon f^{max}$. *In other words, the lower bound of Algorithm 7 is* $(1-\varepsilon)OPT$. *Here,* $\varepsilon \leq \frac{1}{2}$, $b_i = b_{i,j}$ *if* $x_{i,j} = 1$.

Proof. We have proved that the total throughput achieved by Algorithm 7 is optimal when all UEs are provisioned. Here, we try to prove a better lower bound achieved by Algorithm 7 while at least one UE is blocked by the network.

We have made the assumption that $(k-1)$ is the index of the last provisioned UE, and then k is the index of the first blocked UE. Since $\frac{r_i}{b_i} \leq \frac{r_k}{b_k}$ for $1 \leq i \leq k$, we

have

$$\frac{r_1 + r_2 + \cdots + r_{k-1} + r_k}{b_1 + b_2 + \cdots + b_{y-1} + b_k} \geq \frac{r_k}{b_k}$$
$$r_k \leq b_y \frac{r_1 + r_2 + \cdots + r_{k-1} + r_k}{b_1 + b_2 + \cdots + b_{k-1} + b_k}$$
$$r_k \leq \frac{b_k}{f^{max}}(r_1 + r_2 + \cdots + r_{k-1} + r_k)$$
$$r_k \leq \frac{\varepsilon f^{max}}{f^{max}}(r_1 + r_2 + \cdots + r_{k-1} + r_k)$$
$$r_k \leq \varepsilon(r_1 + r_2 + \cdots + r_{k-1} + r_k)$$
$$r_k \leq \frac{\varepsilon}{1-\varepsilon}(r_1 + r_2 + .. + r_{k-1}) \tag{5.12}$$

Note that $b_i \leq \varepsilon f^{max}$, $b_1 + b_2 + \cdots + b_{k-1} + b_k \geq f^{max}$ and $b_1 + b_2 + \cdots + b_{k-1} \leq f^{max}$ because k is the index of the first blocked UE. Let $OPT = \Phi_2(x^*_{i,j})$; then, we have

$$r_1 + r_2 + \cdots + r_{k-1} + r_k \geq OPT$$
$$(r_1 + r_2 + \cdots + r_{k-1}) + (r_1 + r_2 + \cdots + r_{k-1})\frac{\varepsilon}{1-\varepsilon} \geq OPT$$
$$r_1 + r_2 + \cdots + r_{k-1} \geq (1-\varepsilon)OPT \tag{5.13}$$

Note that the output of Algorithm 7 is $max(\Phi_2(\Lambda_1), \Phi_2(\Lambda_3))$, and then $max(\Phi_2(\Lambda_1), \Phi_2(\Lambda_3)) = r_1+r_2+\cdots+r_{k-1} \geq (1-\varepsilon)OPT$. Meanwhile, we have proved that $\max(\Phi_2(\cup x^1_{\tilde{i},\tilde{j}}), \Phi_2(\cup x^2_{\hat{i},\hat{j}})) \geq \frac{1}{2}\Phi_2(\cup x^*_{i,j})$; then, we have $(1-\varepsilon) \geq \frac{1}{2}$ and $\varepsilon \leq \frac{1}{2}$. Thus, the lower bound of Algorithm 7 is $(1-\varepsilon)OPT$ and the AA-UPB algorithm has an approximation ratio $(1-\varepsilon)$. □

5.3.2 Solving the DBS Placement Problem

The UE association, and power and bandwidth allocation are determined in the last subsection. Here, we try to find the best locations to place all DBS which can maximize the total throughput of the network. For the horizontal placement, every DBS is placed at a unique position, implying that two different DBSs are not placed at the same position. For the vertical placement, all DBSs are placed at the same

altitude. Problem $\mathscr{P}_0$ is transformed into problem $\mathscr{P}_4$ for given $\tilde{x}_{i,j}$, $\tilde{y}_j$, $\tilde{p}_{i,j}$ and $\tilde{b}_{i,j}$, which is to determine the candidate placement of DBSs that yields the maximum throughput (all constraints including $\tilde{x}_{i,j}$, $\tilde{y}_j$, $\tilde{p}_{i,j}$ and $\tilde{b}_{i,j}$ are removed).

$$\begin{aligned}
\mathscr{P}_4 : & \max_{\gamma_j, h_j} \quad \Phi_4(\gamma_j, h_j) \\
s.t. : & \\
& C1 : \gamma_j \in \mathscr{V}_1, \quad \forall j \in \widetilde{\mathscr{B}}, \\
& C2 : h_j \in \mathscr{V}_2, \quad \forall j \in \widetilde{\mathscr{B}}.
\end{aligned} \tag{5.14}$$

where $\Phi_4(\gamma_j, h_j) = \Phi|_{x_{i,j}=\tilde{x}_{i,j}, y_j=\tilde{y}_j, p_{i,j}=\tilde{p}_{i,j}, b_{i,j}=\tilde{b}_{i,j}}$ and $\tilde{y}_j$ is the given DBS indicator. We propose an optimal DBS placement algorithm (*Opt-DBS-Placement*), which utilizes the exhaustive search method [16] to solve problem $\mathscr{P}_4$, as depicted in Algorithm 8.

Theorem 6. *The Opt-DBS-Placement algorithm produces the optimal 3-D positions of all DBSs.*

Proof. Since $\Phi_4(\gamma_j, h_j)$ is the objective value of $\mathscr{P}_4$, $\Phi_4(\hat{\gamma}_j, \hat{h}_j)$ is the total throughput of the network for given positions of all DBSs in the horizontal and vertical dimensions ($\hat{\gamma}_j$ and $\hat{h}_j$), and determined UE association power and bandwidth assignment ($\tilde{x}_j$, $\tilde{p}_{i,j}$ and $\tilde{b}_{i,j}$). Meanwhile, $\Phi_4(\hat{\gamma}_j^*, \hat{h}_j^*) = \Phi\Big|_{\gamma_j=\hat{\tau}_j^*, h_j=\hat{h}_j^*} = \max_{\hat{\gamma}_j, \hat{h}_j} \Phi_4(\hat{\gamma}_j, \hat{h}_j)$, $(\hat{\gamma}_j^*, \hat{h}_j^*) = \operatorname{argmax}_{\hat{\gamma}_j, \hat{h}_j} \Phi_4(\hat{\gamma}_j, \hat{h}_j)$, and Algorithm 8 has checked all candidate horizontal and vertical positions ($\mathscr{V}_1$ and $\mathscr{V}_2$). Thus, the optimal horizontal and vertical positions are achieved by Algorithm 8 (the Opt-DBS-Placement algorithm). □

5.3.3 Determining the Number of Required DBSs

Now, we focus on minimizing the number of required DBSs for given UE assignment and DBS placement results as formulated in problem $\mathscr{P}_5$.

$$\begin{aligned}
&\mathscr{P}_5 : \min_{y_j} \quad N \\
&s.t. : \\
&\qquad C1 : y_j \leq \sum_i x_{i,j} \leq y_j |\mathscr{U}|, \quad j \in \tilde{\mathscr{B}}, \\
&\qquad C2 : T \geq T_{th}, \\
&\qquad C3 : y_j \in \{0,1\}, \quad \forall j \in \widetilde{\mathscr{B}}.
\end{aligned} \tag{5.15}$$

Here, T_{th} is the pre-defined throughput threshold of the network; $T_{th} = \min\{T_{max}, \sum_i r_i\}$ and T_{max} is the maximum throughput achieved by solving problem $\mathscr{P}_1$. Constraint C2 is used to ensure that the network's throughput exceeds the pre-defined threshold T_{th}. In other words, we want to serve as many UEs as we can, and then to minimize the number of deployed DBSs.

Theorem 7. *The optimal objective N^* of problem $\mathscr{P}_5$ can be achieved, implying that the minimum number of DBSs is utilized in provisioning UEs.*

Proof. Let $\Phi_5(y_j) = N = \sum_j y_j$ be the objective function of problem $\mathscr{P}_5$. After solving problem $\mathscr{P}_1$, the UE-BS indicator $x_{i,j}$ is determined, and y_j^* is determined by $x_{i,j}$ based on constraint C1 in problem $\mathscr{P}_5$. If none of the UEs is provisioned by the jth DBS, $x_{i,j}$ equals to 0 ($\forall i \in \mathscr{U}, j \geq 1$), and 1 otherwise. Here, we discuss how we map the UE provisioning results $x_{i,j}$ into the DBS selection results y_j based on three different serving situations of the jth DBS: 1) No UE is provisioned by the jth DBS. $x_{i,j} = 0, \forall i \in \mathscr{U}$ and $y_j = 0$ because $y_j \leq \sum_i x_{i,j}$ and $\sum_i x_{i,j} = 0$, which means that the jth DBS is not used; 2) One UE is provisioned by the jth DBS, implying that $\sum_i x_{i,j} = 1$. Then, $x_{i,j} = 1$ and $y_j = 1$ because $\sum_i x_{i,j} \leq y_j |\mathscr{U}|$, $\sum_i x_{i,j} > 0$ and

$|\mathscr{U}| > 1$, which means that the jth DBS is used; 3) More than one UE is provisioned by the jth DBS, implying that $\sum_i x_{i,j} > 1$. Then, $x_{i,j} = 1$ and $y_j = 1$ because $\sum_i x_{i,j} \leq y_j|\mathscr{U}|$, $\sum_i x_{i,j} > 1$ and $|\mathscr{U}| > 1$. From the above discussions, $y_j = 0$ if none of the UEs is served by this DBS and $y_j = 1$ if one or more UEs are provisioned by the DBS. Then, $N^* = \Phi_5(y_j) = \sum_j y_j$, which is the optimal number of used DBSs. □

5.3.4 Solving the BUD Problem

Here, we propose an approximation algorithm, which is named Approximation Algorithm for the BUD problem (*AA-BUD*) to solve problem $\mathscr{P}_0$, as depicted in Algorithm 9. The AA-BUD algorithm is designed based on Algorithm 7 and Algorithm 8. Here, N_{used} is the number of used BSs and N_b is the number of blocked UEs. We pre-set $N_{used} = 1$ and $N_b = 0$; we then find the best positions to place the DBSs, which provide the highest throughput based on the deployed DBSs and workload; afterward, we check the service situation and add one more DBS to the network if one or more UEs are blocked; this iterative process continues until all UEs are provisioned or the maximum number of DBSs are deployed.

Theorem 8. *The AA-BUD algorithm is a* $(1-\varepsilon)$*-approximation algorithm of problem* $\mathscr{P}_0$*. Here,* $\varepsilon \leq \frac{1}{2}$.

Proof. It is easy to derive *Theorem* 4 from *Theorem* 1 –*Theorem* 3 and *Lemma* 1. In other words, the lower bound of Algorithm 9 is bigger than $(1-\varepsilon)$ of the optimal value of problem $\mathscr{P}_0$ and the approximation ratio of the AA-BUD algorithm is $(1-\varepsilon)$. □

5.4 Performance Evaluation

We use MATLAB to evaluate the performance of the AA-BUD algorithm, and run each simulation 200 times to acquire the average results [59–61]. In this section, we first evaluate the proposed algorithm with a fixed number of DBSs, etc., three DBSs are assumed to be used in the network ($N = 3$); we then evaluate the proposed

algorithm with a varying number of DBSs ($1 \leq N \leq N_{max}$). All DBS are placed at the same altitude. The locations of UEs are generated through a Matérn cluster process [34]. The parameters that are used in the simulation are listed in Table 5.4.

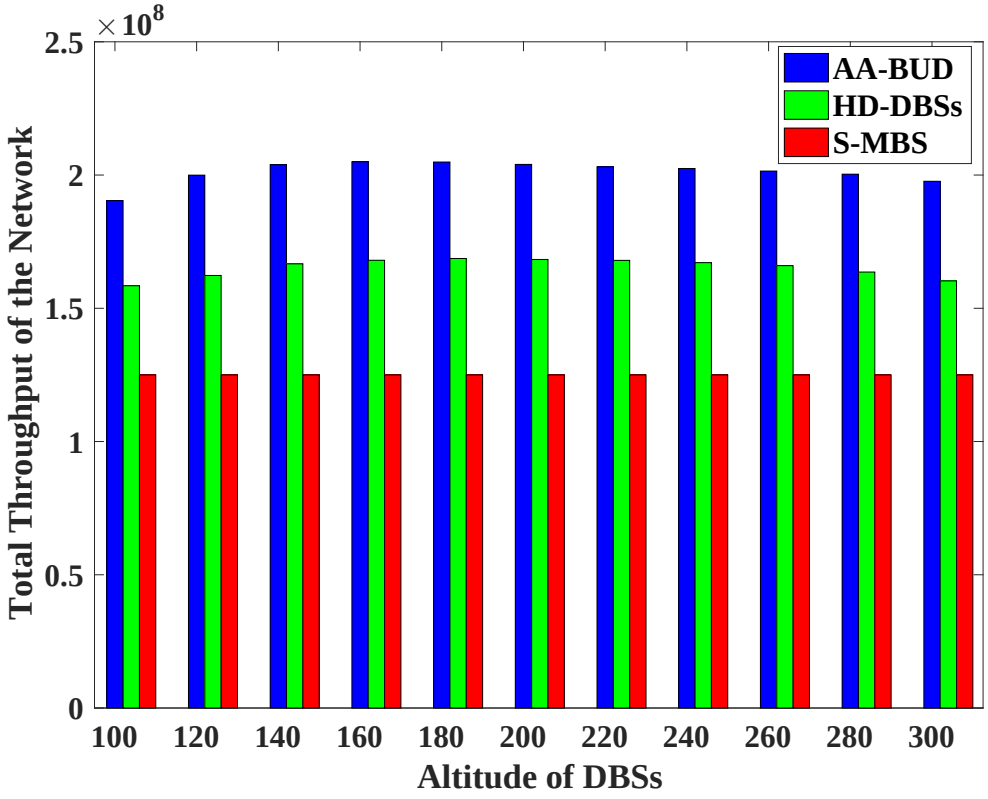

Figure 5.2 Total throughput versus altitude with 170 UEs and three DBSs ($N = 3$).

We evaluate the performance of the AA-BUD algorithm and compare it with two baseline algorithms. One is the single MBS algorithm without any DBSs (*S-MBS*), and the other algorithm named *HD-DBSs* with half-duplex enabled DBSs. The HD-DBSs algorithm is quite similar to the AA-BUD algorithm. The main difference between these two is that the HD-enabled DBSs are used in the former and FD-enabled DBSs are used in the latter.

The total throughput performance versus the altitude with 170 UEs and three DBSs ($N = 3$) is shown in Figure 5.2. The HD-DBSs algorithm obtains the maximum throughput at 120m while the AA-BUD algorithm achieves the maximum throughput at 160m. For the HD-DBSs algorithm, the bottlenecks of the uplink communications

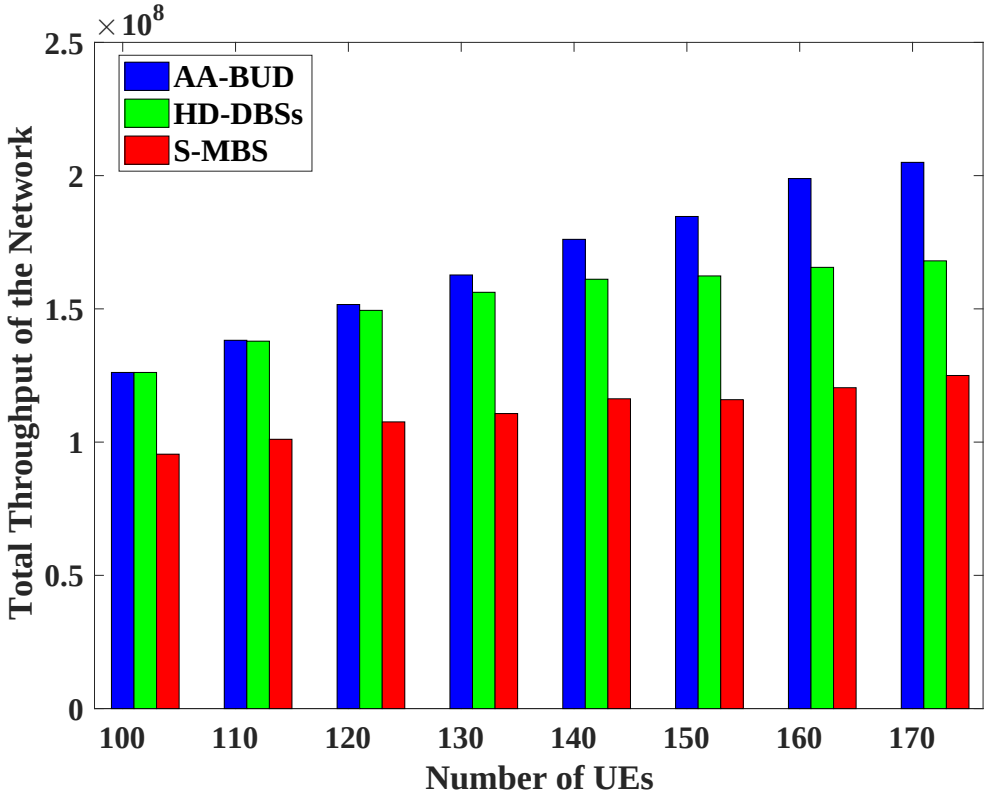

Figure 5.3 Total throughput versus the number of UEs at 160m altitude and three DBSs ($N = 3$).

are the backhaul links (DBS-MBS links) while those of the AA-BUD algorithm are the access links (UE-DBS links or UE-MBS links). This is because the UEs can utilize more frequency spectra when FD-enabled DBSs are operated by the AA-BUD algorithm. For altitude lower than $160m$ of the AA-BUD algorithm, the path loss is dominated by NLoS-path-loss, which decreases as the altitude increases. For altitude higher than $160m$ using the AA-BUD algorithm, the path loss is dominated by LoS-path-loss, which increases as the altitude increases.

The total throughput results versus the workload with 160m altitude and three DBSs ($N = 3$) are shown in Figure 5.3. The AA-BUD algorithm achieves up to 23% and 62% improvement of the total throughput as compared to the S-MBS algorithm and HD-DBSs algorithm, respectively. All algorithms have better throughput performance as the workload increases because all algorithms try to serve

UEs with better channel conditions first and then provision the remaining UEs. Hence, less radio resources can be used to provision the same number of UEs but with better channel conditions, and then more UEs can be provisioned by the remaining radio resources.

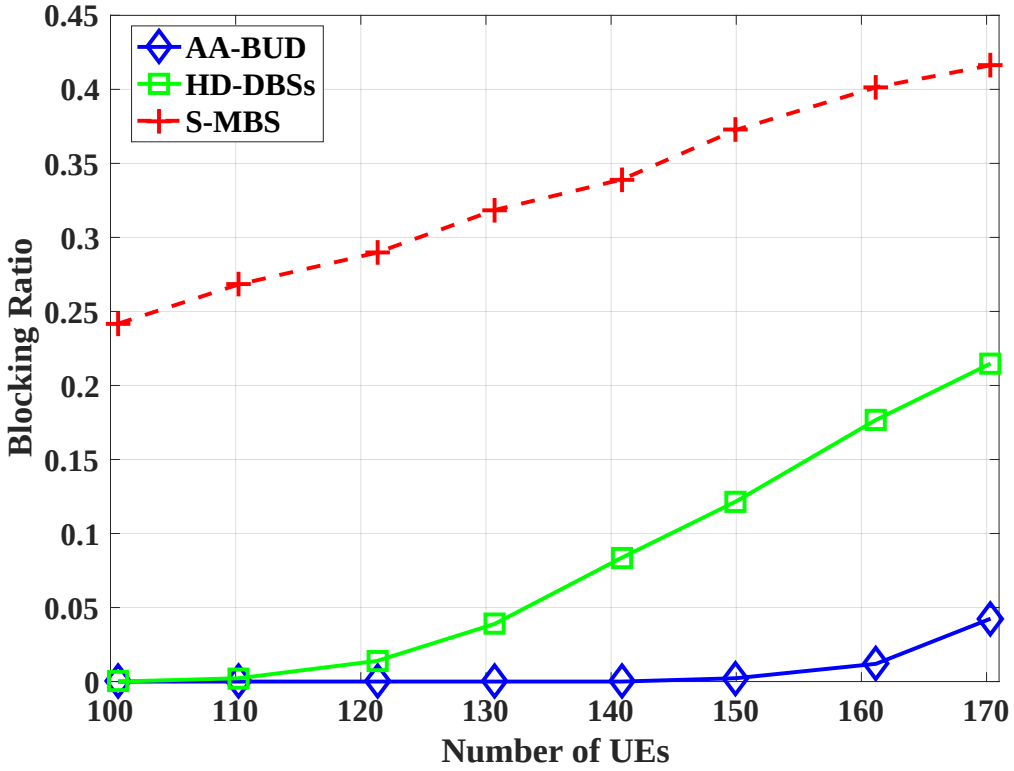

Figure 5.4 Blocking ratio at 160m altitude and three DBSs ($N = 3$).

The blocking ratio versus workload at 160m altitude and three DBSs ($N = 3$) is shown in Figure 5.4. Here, the blocking ratio is the data rate requirement of un-provisioned UEs of the uplink communications over the total uplink data rate requirement of all UEs. We use the "blocking ratio" to show the fraction of data rates of all UEs that cannot be provisioned; it is more accurate in terms of communications resources as compared to the number of blocked UEs because not all UEs have the same data rate requirement. Obviously, the AA-BUD algorithm exhibits the best performance with the lowest blocking ratio, and all UEs are provisioned until the number of UEs reaches 150.

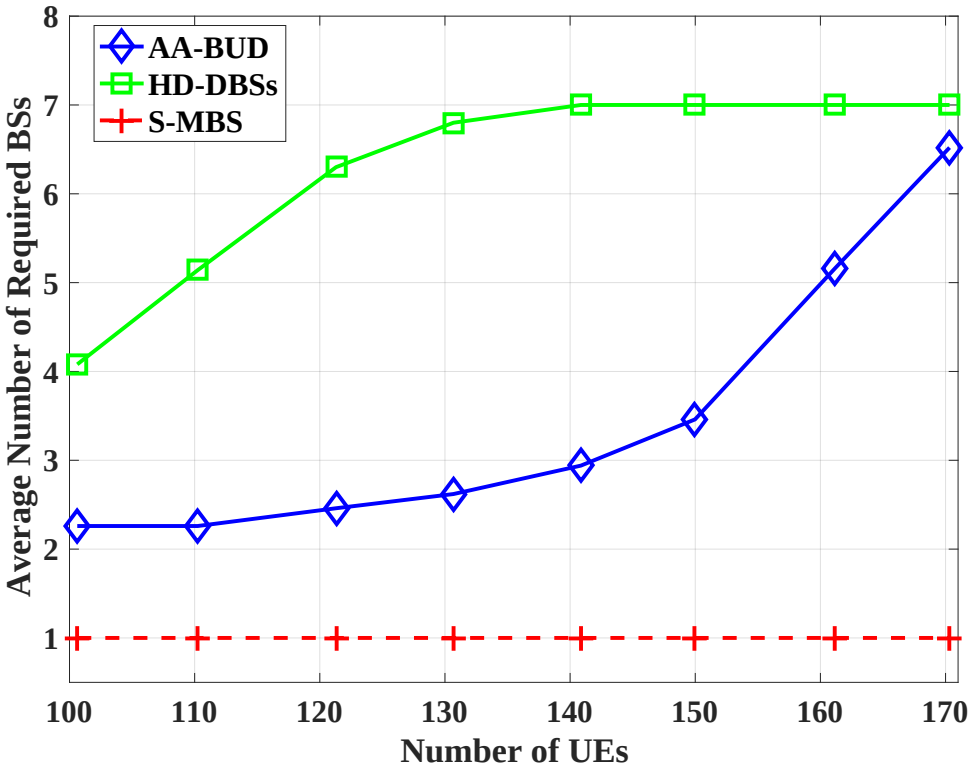

Figure 5.5 The number of required BSs at 160m altitude.

Figure 5.5 shows the number of required DBSs (including the MBS) to be deployed versus different workload at 160m altitude. The number of required DBSs increases as the workload increases because more DBSs can provide better channel conditions to the UEs and then more UEs can be provisioned in the network. Meanwhile, the number of required DBSs of the AA-BUD algorithm is less than that of the HD-DBSs algorithm because IBFD-enabled DBSs are used in the former and HD-enabled DBSs are used in the latter. In other words, the IBFD-enabled DBSs can use the bandwidth resource more efficiently than the HD-enabled DBSs do.

Figure 5.6 shows the performance of the total throughput versus the number of UEs and the number of deployed DBSs at 160m altitude. The total throughput of the network increases as the workload increases because all algorithms try to provision UEs with better channel conditions. The total throughput of the network increases

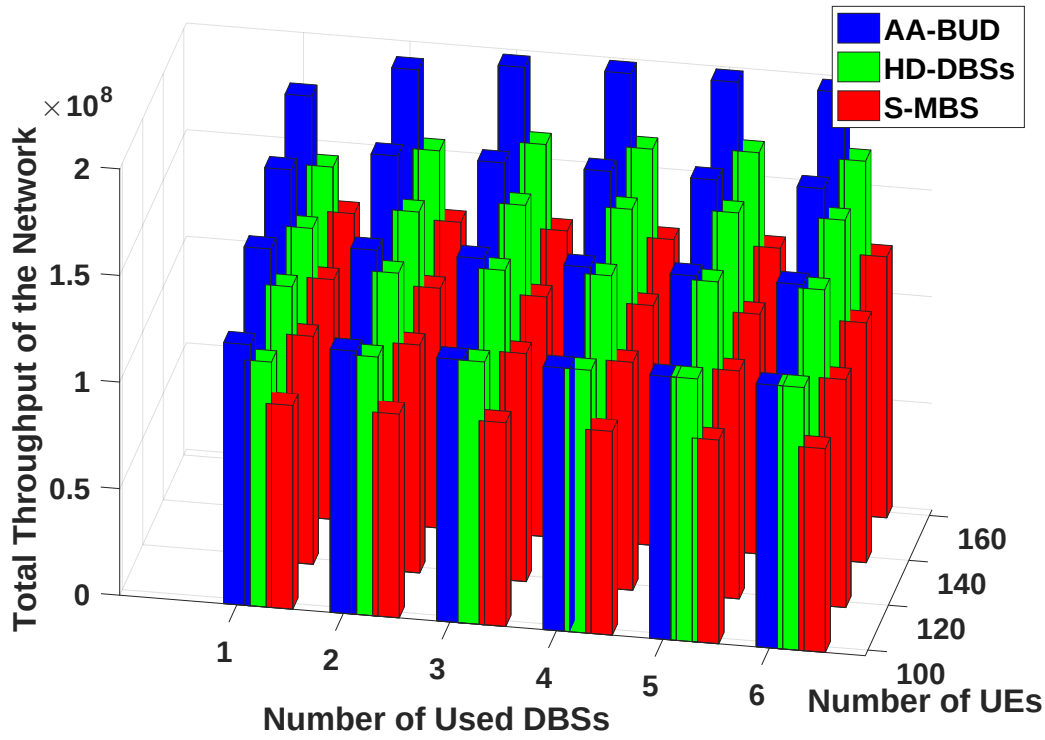

Figure 5.6 Total throughput versus the number of UEs and the number of used DBSs at 160m altitude.

as the number of deployed DBSs increases. This is because UEs are closer to BSs and have better channel conditions when more DBSs are deployed; the same radio resources can be used to provision more UEs and hence the total throughput of the network increases. As the number of DBSs increases, the total throughput of the AA-BUD algorithm and that of the HD-DBSs algorithm have 14.5% and 15.6% improvement as compared to the one DBS scenario.

Figure 5.7 shows the blocking ratio versus the number of UEs and the number of used DBSs at 160m altitude. The blocking ratio decreases as the number of deployed DBSs increases for a given number of UEs, but it increases as the number of UEs increases for a given number of DBSs. As the number of deployed DBSs increases, the blocking ratios of the AA-BUD algorithm and the HD-DBSs algorithm decrease by more than 73% and 33%, respectively, as compared to the one DBS scenario. Evaluation results have demonstrated that the AA-BUD algorithm performs

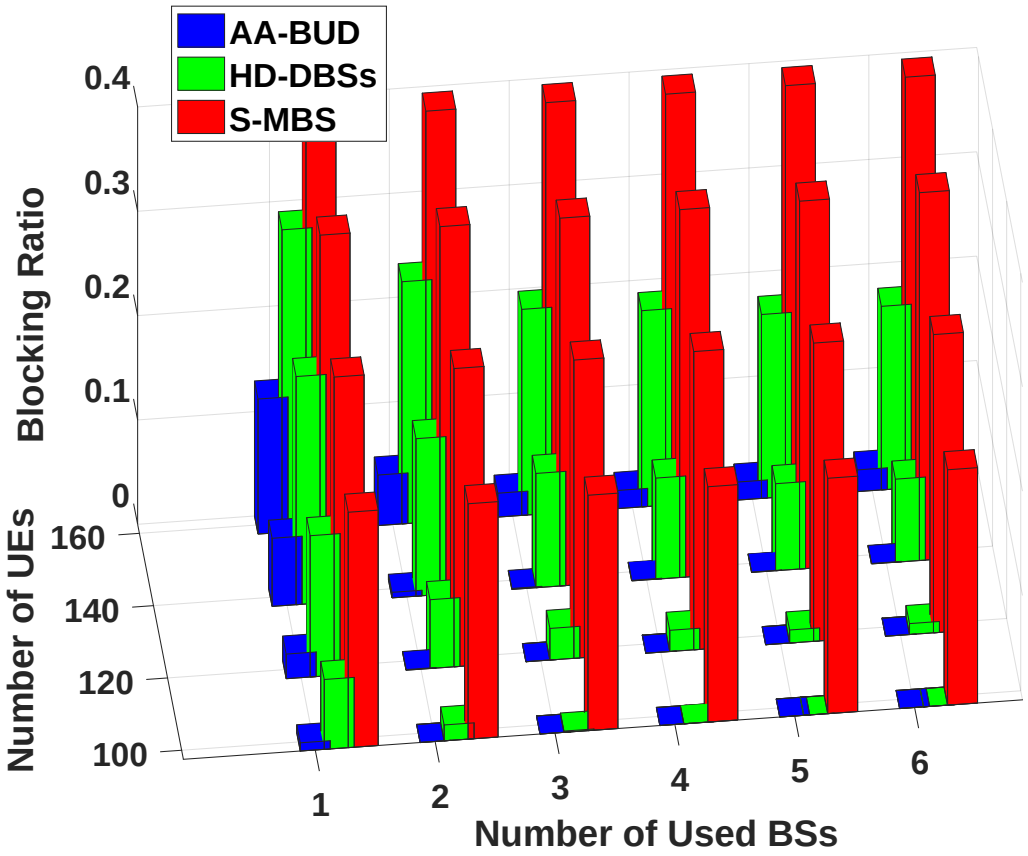

Figure 5.7 Blocking ratio versus the number of UEs and the number of used DBSs at 160m altitude.

better than the baseline algorithms; both the total throughput and the blocking ratio improve as the number of deployed DBSs increases; the total throughput of the network improves and the blocking ratio worsens as the workload increases.

Algorithm 7: AA-UPB

Input : $\mathscr{B}$, $\mathscr{U}$, f_j^{max}, κ_j, r_i, $\hat{y}_j$, $\hat{\gamma}_j$ and $\hat{h}_j$;

Output: $\tilde{x}_{i,j}$, $\tilde{b}_{i,j}$ and $\tilde{p}_{i,j}$;

$f_j^{used} = 0$, $\Lambda_0 = \mathscr{U}$, $\Lambda_1 = \varnothing$, $\forall j \in \mathscr{B}$;

for $i \in \Lambda_0$ **do**

  for $j \in \mathcal{B}$ **do**

    $\hat{b}_{i,j} = \underset{b_{i,j}}{\operatorname{argmin}} \left(\beta_{i,j} - r_i \geq 0\right)$ and $\hat{p}_{i,j} = \hat{b}_{i,j}\kappa_j$;

  obtain $\tilde{j} = \underset{j}{\operatorname{argmin}}\, \hat{b}_{i,j}$, $\forall i$;

  get $b_{i,\tilde{j}} = \min(\hat{b}_{i,j})$ and $z_i = r_i / b_{i,\tilde{j}}$;

$\Lambda_2 = \Lambda_0$ and sort the UEs in a descending order $\tilde{i}$ by z_i;

while $f_j^{used} \leq f_j^{max}$ & $\Lambda_2 \neq \varnothing$ **do**

  if $f_j^{used} + b_{\tilde{i},\tilde{j}} \leq f_j^{max}$, $\forall \tilde{i} \in \Lambda_2$ **then**

    $x^1_{\tilde{i},\tilde{j}} = 1$, $f_j^{used} = f_j^{used} + b_{\tilde{i},\tilde{j}}$, $\Lambda_1 = \Lambda_1 \cup \{x^1_{\tilde{i},\tilde{j}}\}$ and $\Lambda_2 = \Lambda_2 \setminus \tilde{i}$;

  else

    $\Lambda_0 = \Lambda_2$ and go to step 2;

  $\tilde{i} = \tilde{i} + 1$;

$\Lambda_3 = \varnothing$, $\Lambda_4 = \mathscr{U}$;

for $i \leq |\mathcal{B}|$ **do**

  find $\hat{i} = \operatorname{argmax} r_i, \forall i \in \Lambda_4$;

  $\Lambda_3 = \Lambda_3 \cup \{x^2_{\hat{i},\hat{j}} = \underset{x_{i,j}}{\operatorname{argmax}}\, x_{i,j} r_i\}$, $\forall i \in \Lambda_4$;

  $\Lambda_4 = \Lambda_4 \setminus \hat{i}$;

return Λ_1 or Λ_3 which produces a higher throughput;

obtain $\tilde{b}_{i,j}$ and $\tilde{p}_{i,j}$.

Table 5.3 Information of UEs

	Data rate, r_i	Bandwidth, $b_{i,j}$	Weight, z_i
UE 1	2	1	2
UE 2	2.5	2	1.25
UE 3	5	5	1

Algorithm 8: The optimal DBS placement algorithm (*Opt-DBS-Placement*)

Input : $\mathscr{B}$, $\mathscr{U}$, $\mathscr{V}_1$, $\mathscr{V}_2$, $\tilde{x}_{i,j}$, $\tilde{y}_j$, $\tilde{p}_{i,j}$ and $\tilde{b}_{i,j}$;

Output: $\hat{\gamma_j}^*$ and $\hat{h}_j^*$;

for $\hat{\gamma}_j \in \mathscr{V}_1$ **do**
  for $\hat{h}_j \in \mathscr{V}_2$ **do**
    update the locations of all DBSs $(\hat{\gamma}_j, \hat{h}_j)$;
    update $\tilde{x}_{i,j}$, $\tilde{p}_{i,j}$ and $\tilde{b}_{i,j}$;
    obtain the objective value, $\Phi_4(\hat{\gamma}_j, \hat{h}_j)$;

calculate $(\hat{\gamma}_j^*, \hat{h}_j^*) = \underset{\hat{\gamma}_j, \hat{h}_j}{\operatorname{argmax}} \Phi_4(\hat{\gamma}_j, \hat{h}_j)$;

return $\hat{\gamma}_j^*$, $\hat{h}_j^*$.

Algorithm 9: Approximation Algorithm for the BUD problem (*AA-BUD*)

Input : $\mathscr{B}$, $\mathscr{U}$, f_j^{max}, κ_j, r_i, $\mathscr{V}_1$ and $\mathscr{V}_2$;

Output: $\tilde{x}_{i,j}$, $\tilde{b}_{i,j}$, $\tilde{p}_{i,j}$, $\tilde{y}_j$, $\hat{\gamma}_j$ and $\hat{h}_j$;

$N_{used} = 1$, $N_b = 0$;

while $N_{used} \leq N_{max}$ & $N_b = 1$ **do**

  for $\hat{\gamma}_j \in \Lambda_1$ **do**

    for $\hat{h}_j \in \Lambda_2$ **do**

      $N_b = 0$;

      update the locations of all DBSs $(\hat{\gamma}_j, \hat{h}_j)$;

      obtain $\max(\Phi_2(\cup x^1_{\tilde{i},\tilde{j}}), \Phi_2(\cup x^2_{\hat{i},\hat{j}}))$ by *Algorithm* 7;

      update N_b, $\tilde{x}_{i,j}$, $\tilde{y}_j$, $\tilde{p}_{i,j}$ and $\tilde{b}_{i,j}$;

  obtain $\Phi_4(\hat{\gamma}_j, \hat{h}_j)$;

  compute $(\hat{\gamma}_j^*, \hat{h}_j^*) = \underset{\hat{\gamma}_j, \hat{h}_j}{\operatorname{argmax}} \Phi_4(\hat{\gamma}_j, \hat{h}_j)$;

  $\tilde{\gamma}_j = \hat{\gamma}_j^*$, and $\tilde{h}_j = \hat{h}_j^*$;

  if $N_b > 0$ **then**

    $N_{used} = N_{used} + 1$;

return N_{used}, $\tilde{x}_{i,j}$, $\tilde{y}_j$, $\tilde{p}_{i,j}$ and $\tilde{b}_{i,j}$.

Table 5.4 Parameters for Simulations of the BUD Problem

N_{max}	6 DBSs
coverage area of the MBS	$1000m \times 1000m$
f_0	2 GHz
P_D	40 dBm
P_U	23 dBm
$\lvert\mathscr{U}\rvert$	$\{100, 110, \cdots, 170\}$
(a, b, ζ^L, ζ^N)	$(4.88, 0.43, 0.1, 21)$ [40]
path loss between a UE and the MBS	$136.8 + 39.1log10(d_{i,j})$, $d_{i,j}$ in km [62]
Rayleigh fading between a UE and the MBS	-8 dB [50]
$\lvert\mathscr{V}_1\rvert$	36
$\mathscr{V}_2$	$\{100, 120, \cdots, 300\}$ m
N_0	-174 dBm/Hz
τ_0	15 kHz
τ^{SI}	130 dB [15]
r_i	$\{0.5, 1, 1.5, 2\}$ Mbps
f^{max}	1200 SCs
f_j^{max}	300

CHAPTER 6

FUTURE WORK

While we have solved a number of challenging problems in DBS-assisted networking, there remain many interesting issues to be investigated, among which we will look into the following issues.

6.1 DBS-assisted Mobile Edge Computing

Advances in 5G technologies are enabling many new emerging applications such as autonomous driving, augmented reality (AR), agriculture monitoring and Internet of Things (IoT) [63]. The number of connected devices in the whole world exceeded 17 billion including 7 billion IoT devices by 2018, and the numbers of total devices and IoT devices are estimated to be 34.2 billion and 22 billion by 2025, respectively [64]. Some IoT devices may have limited or no computing capability and some IoT applications (autonomous driving and AR) require low latency in the control, communication and computing service [63, 65]. Moreover, the internet is greatly burdened to accommodate such huge IoT traffic generated by the IoT devices and destined to the mobile cloud [66].

Owing to the large amount of data and tremendous devices, mobile edge computing (MEC) has been proposed to improve the Quality-of-Service (QoS), and the concept of cloudlets is an early adoption to provide edge computing service [63, 67, 68]. In MEC, the cellular base station, viz., the macro base station (MBS), is equipped with computing resources to provision services to IoT users (UEs) or wireless devices [63]. Many UEs receive computing service locally without traversing the remote core network, and thus the latency of UEs can be reduced. DBS-aided/UAV-aided MEC can provide better wireless connections (line-of-sight) to UEs and more flexibility in the implementation as compared to the traditional

MEC where the computing facilities are only available at the MBS on the ground [69]. Then, it is interesting to study the DBS-aided/UAV-aided MEC problem to minimize the average latency of all users.

6.2 FSO for Both Charging and Communications

Despite the advantages of DBS-assisted HetNet with IBFD, there remain challenges for realizing spectrum-efficient communications in such networks. First, how to achieve the optimal power and bandwidth allocation in both the backhaul link and the access link remains a challenging issue. Inefficient power and bandwidth allocation in the MBS will lead to bottleneck in the backhaul link or the access link, and inefficient power and bandwidth allocation in the DBS will result in low spectrum efficiency in the access link. Second, how to overcome the endurance problem (a temporary event may be longer than the maximum serving time of a DBS) is still an open issue. One possible solution to overcome the endurance problem is to enlarge the battery capacity of the DBS, but at the expense of a heavier payload that may limit the flying time of the DBS. Another possible solution is to charge DBSs through radio frequency or solar energy. Note that high altitude platforms can better harvest solar energy than low altitude platforms (DBSs), but DBSs can harvest energy from radio frequency (low charging rate) [8]. One more possible solution is to employ another fully charged DBS to replace the DBS with drained battery, and then to steer the former DBS back to the charging station to recharge its battery. The last solution is preferred currently because it is low cost and facilitates a high charging rate. Other solutions may emerge in the future because all solutions highly depend on the development of various technologies.

Note that a laser beam may have a very high throughput capacity such as 10 Gbps. A laser beam can be used to carry both data and energy and then transmit them to the DBS. Then, it is interesting to utilize the free space optics (*FSO*) as

the backhaul and the energizer for a DBS in the DBS-aided HetNet. The target is to maintain a high charging efficiency while maximizing the total throughput of the network. Then, the backhaul throughput capacity can be increased and the endurance problem can also be alleviated.

CHAPTER 7

CONCLUSION

Drone-mounted base stations (DBSs) are promising solutions to provide ubiquitous connections to users and support various emerging applications in mobile networks while full-duplex communications has the potential to improve the spectrum efficiency. DBSs are especially useful for supporting unexpected and temporary events. In this research, the droNe-mounted bAse-station PlacEment (*NAPE*) problem with consideration of 3-D DBS placement and IBFD-enabled DBS communications for both access links and backhaul links of DBSs have been studied. The objective is to minimize the required number of DBSs in providing service to UEs. Simulation results have demonstrated that the required number of DBSs is minimized by the proposed D-NAPE algorithm, and the total network throughput is increased and the data rate block ratio is decreased as compared to those of other strategies.

Then, the three-dimensional DBS Placement with in-band full-duplex communications have been investigated, and the drone-base-station placement with IBFD communications (DSP-IBFD) problem have been formulated. Since the DSP-IBFD problem is a non-linear non-convex combinatorial optimization problem, it is then decomposed into the DBS placement problem and the joint bandwidth and power allocation problem. Two heuristic algorithms have been proposed based on different DBS placement strategies to solve the DSP-IBFD problem. Simulation results have demonstrated that the network throughput achieved by Dynamic-DSP is 45% and 8% more than that of without DBSs and that by the Fixed-DSP strategy, respectively.

After that, the joint radio resource assignment and DBS placement problem have been studied. Since full-duplex communications has the potential to improve the spectrum efficiency and DBSs can be used to improve the services of the UEs for future

5G networks, the *D*rone-mounted *B*ase-*S*tation *P*lacement with in-band full-duplex communication (*DBSP-IBFD*) problem has been investigated. Both access links and backhaul links of DBSs are considered, in which one UE can be provisioned by the MBS directly or via a DBS. The objective is to maximize the total throughput of the network. The DBSP-IBFD problem is decomposed into two sub-problems: the joint-BPU problem and the DBS placement problem. Then, approximation algorithms have been proposed to solve the sub-problems. Finally, a $\frac{1}{2}(1-\frac{1}{2^l})$-approximation algorithm has been proposed to solve the DBSP-IBFD problem (l is the number of simulation runs) that has been demonstrated to be superior to the benchmark algorithms by up to 56% total throughput improvement via various simulation scenarios.

Then, the backhaul-aware uplink communications in a full-duplex DBS-aided HetNet (*BUD*) problem with the target to maximize the total throughput of the network for the uplink communications with the minimum number of deployed DBSs has been studied. The DBSs are full-duplex enabled, and the MBS and all UEs are half-duplex enabled. Free space optics (*FSO*) terminals are used to connect the MBS to the core network. Since the BUD problem is NP-hard, we have proposed an approximation algorithm, named AA-BUD algorithm, to solve the BUD problem. The AA-BUD algorithm has been proved to be a $(1-\varepsilon)$-approximation algorithm that is capable of obtaining the optimal horizontal and vertical dimensions of DBSs ($\varepsilon \leq \frac{1}{2}$). Evaluation results have validated that the proposed AA-BUD algorithm is superior to the other baseline algorithms with up to 62% improvement of the uplink throughput. Moreover, the total throughput of the AA-BUD algorithm increases and the blocking ratio decreases as the number of deployed DBSs increases.

Finally, two future research endeavors have been identified. Firstly, DBSs/UAVs are deployed to provide both communications and computing service to users because DBSs/UAVs have high mobility, high flexibility, and high maneuverability. DBS-aided/UAV-aided MEC can provide better wireless connections to users as compared

to the traditional MEC where the computing facilities are only available at the MBS on the ground. Secondly, the DBS's serving time is limited by its battery and the typical flying time is around 30 minutes. To overcome this issue, an FSO beam will be utilized as both the backhaul and the energizer for a DBS in the DBS-aided HetNet, and the objective is to maintain a high charging efficiency while maximizing the total throughput of the network.

BIBLIOGRAPHY

[1] X. Ge, S. Tu, G. Mao, C. X. Wang, and T. Han, "5G ultra-dense cellular networks," *IEEE Wireless Communications*, vol. 23, no. 1, pp. 72–79, Feb. 2016.

[2] H. Zhang, N. Liu, X. Chu, K. Long, A. H. Aghvami, and V. C. M. Leung, "Network slicing based 5G and future mobile networks: Mobility, resource management, and challenges," *IEEE Communications Magazine*, vol. 55, no. 8, pp. 138–145, 2017.

[3] "Cisco visual networking index: Global mobile data traffic forecast update, 2016 – 2021 white paper." [Online]. Available: https://www.cisco.com/c/en/us/solutions/collateral/service-provider/visual-networking-index-vni/mobile-white-paper-c11-520862.html

[4] L. Zhang and N. Ansari, "A framework for 5G networks with in-band full-duplex enabled drone-mounted base-stations," *IEEE Wireless Communications*, vol. 26, no. 5, pp. 121–127, Oct. 2019.

[5] L. Zhang, M. Xiao, G. Wu, M. Alam, Y. Liang, and S. Li, "A survey of advanced techniques for spectrum sharing in 5G networks," *IEEE Wireless Communications*, vol. 24, no. 5, pp. 44–51, 2017.

[6] F. Tang, Z. M. Fadlullah, N. Kato, F. Ono, and R. Miura, "AC-POCA: Anticoordination game based partially overlapping channels assignment in combined UAV and D2D-based networks," *IEEE Transactions on Vehicular Technology*, vol. 67, no. 2, pp. 1672–1683, Feb. 2018.

[7] Y. Zeng, R. Zhang, and T. J. Lim, "Wireless communications with unmanned aerial vehicles: opportunities and challenges," *IEEE Communications Magazine*, vol. 54, no. 5, pp. 36–42, May 2016.

[8] S. Sekander, H. Tabassum, and E. Hossain, "Multi-tier drone architecture for 5G/B5G cellular networks: challenges, trends, and prospects," *IEEE Communications Magazine*, vol. 56, no. 3, pp. 96–103, Mar. 2018.

[9] I. Bucaille, S. Hethuin, A. Munari, R. Hermenier, T. Rasheed, and S. Allsopp, "Rapidly deployable network for tactical applications: Aerial base station with opportunistic links for unattended and temporary events absolute example," in *IEEE Military Communications Conference*, Nov. 2013.

[10] Y. Takahashi, Y. Kawamoto, H. Nishiyama, N. Kato, F. Ono, and R. Miura, "A novel radio resource optimization method for relay-based unmanned aerial vehicles," *IEEE Transactions on Wireless Communications*, vol. 17, no. 11, pp. 7352–7363, Nov. 2018.

[11] A. Pregler, "AT&T flying COW (cell tower on wings)," National Public Safety Telecommunications Council, Jun. 2017. [Online]. Available: https://policyforum.att.com/wp-content/uploads/2018/01/COW-ONe-Pager_d10.pdf

[12] I. B. Times, "Nokia and EE trial mobile base stations floating on drones to revolutionise rural 4G coverage," International Business Times, Aug. 2016. [Online]. Available: https://www.ibtimes.co.uk/nokia-ee-trial-mobile-base-stations-floating-drones-revolutionise-rural-4g-coverage-1575795

[13] C. D. Nwankwo, L. Zhang, A. Quddus, M. A. Imran, and R. Tafazolli, "A survey of self-interference management techniques for single frequency full duplex systems," *IEEE Access*, vol. 6, pp. 30 242–30 268, Nov. 2017.

[14] D. Nguyen, L. N. Tran, P. Pirinen, and M. Latva-aho, "On the spectral efficiency of full-duplex small cell wireless systems," *IEEE Transactions on Wireless Communications*, vol. 13, no. 9, pp. 4896–4910, Sept. 2014.

[15] Y. S. Choi and H. Shirani-Mehr, "Simultaneous transmission and reception: Algorithm, design and system level performance," *IEEE Transactions on Wireless Communications*, vol. 12, no. 12, pp. 5992–6010, Dec. 2013.

[16] M. Alzenad, A. El-Keyi, and H. Yanikomeroglu, "3-D placement of an unmanned aerial vehicle base station for maximum coverage of users with different QoS requirements," *IEEE Wireless Communications Letters*, vol. 7, no. 1, pp. 38–41, Feb. 2018.

[17] E. Kalantari, M. Z. Shakir, H. Yanikomeroglu, and A. Yongacoglu, "Backhaul-aware robust 3D drone placement in 5G+ wireless networks," in *IEEE International Conference on Communications Workshops (ICC Workshops)*, May 2017, pp. 1–6.

[18] Y. Chen, W. Feng, and G. Zheng, "Optimum placement of UAV as relays," *IEEE Communications Letters*, vol. 22, no. 2, pp. 248–251, Feb. 2018.

[19] M. Mozaffari, W. Saad, M. Bennis, and M. Debbah, "Efficient deployment of multiple unmanned aerial vehicles for optimal wireless coverage," *IEEE Communications Letters*, vol. 20, no. 8, pp. 1647–1650, Aug. 2016.

[20] U. Siddique, H. Tabassum, and E. Hossain, "Downlink spectrum allocation for in-band and out-band wireless backhauling of full-duplex small cells," *IEEE Transactions on Communications*, vol. 65, no. 8, pp. 3538–3554, Aug. 2017.

[21] S. Goyal, P. Liu, and S. S. Panwar, "User selection and power allocation in full-duplex multicell networks," *IEEE Transactions on Vehicular Technology*, vol. 66, no. 3, pp. 2408–2422, Mar. 2017.

[22] A. Al-Hourani, S. Kandeepan, and A. Jamalipour, "Modeling air-to-ground path loss for low altitude platforms in urban environments," in *IEEE Global Communications Conference*, Dec. 2014, pp. 2898–2904.

[23] L. Zhang, Q. Fan, and N. Ansari, "3-D drone-base-station placement with in-band full-duplex communications," *IEEE Communications Letters*, vol. 22, no. 9, pp. 1902–1905, Sept. 2018.

[24] A. Al-Hourani, S. Kandeepan, and S. Lardner, "Optimal LAP altitude for maximum coverage," *IEEE Wireless Communications Letters*, vol. 3, no. 6, pp. 569–572, Dec. 2014.

[25] X. Huang, T. Han, and N. Ansari, "Smart grid enabled mobile networks: Jointly optimizing BS operation and power distribution," *IEEE/ACM Transactions on Networking*, vol. 25, no. 3, pp. 1832–1845, June 2017.

[26] T. Han and N. Ansari, "Enabling mobile traffic offloading via energy spectrum trading," *IEEE Transactions on Wireless Communications*, vol. 13, no. 6, pp. 3317–3328, Jun. 2014.

[27] I. Bor-Yaliniz and H. Yanikomeroglu, "The new frontier in RAN heterogeneity: Multi-tier drone-cells," *IEEE Communications Magazine*, vol. 54, no. 11, pp. 48–55, Nov. 2016.

[28] Z. Kaleem and M. H. Rehmani, "Amateur drone monitoring: State-of-the-art architectures, key enabling technologies, and future research directions," *IEEE Wireless Communications*, vol. 25, no. 2, pp. 150–159, Apr. 2018.

[29] X. Sun and N. Ansari, "Latency aware drone base station placement in heterogeneous networks," in *IEEE Global Communications Conference*, Dec. 2017, pp. 1–6.

[30] L. Wang, B. Hu, and S. Chen, "Energy efficient placement of a drone base station for minimum required transmit power," *IEEE Wireless Communications Letters*, pp. 1–1, Feb. 2018.

[31] Q. Fan and N. Ansari, "Green energy aware user association in heterogeneous networks," in *IEEE Wireless Communications and Networking Conference*, Apr. 2016, pp. 1–6.

[32] M. Alzenad, A. El-Keyi, F. Lagum, and H. Yanikomeroglu, "3-D placement of an unmanned aerial vehicle base station (UAV-BS) for energy-efficient maximal coverage," *IEEE Wireless Communications Letters*, vol. 6, no. 4, pp. 434–437, Aug. 2017.

[33] V. Sharma, M. Bennis, and R. Kumar, "UAV-assisted heterogeneous networks for capacity enhancement," *IEEE Communications Letters*, vol. 20, no. 6, pp. 1207–1210, Jun. 2016.

[34] L. Zhang and N. Ansari, "On the number and 3-D placement of in-band full-duplex enabled drone-mounted base-stations," *IEEE Wireless Communications Letters*, vol. 8, no. 1, pp. 221–224, Feb. 2019.

[35] A. Sharma, R. K. Ganti, and J. K. Milleth, "Joint backhaul-access analysis of full duplex self-backhauling heterogeneous networks," *IEEE Transactions on Wireless Communications*, vol. 16, no. 3, pp. 1727–1740, Mar. 2017.

[36] L. Zhang and N. Ansari, "Approximate algorithms for 3-D placement of IBFD enabled drone-mounted base-stations," *IEEE Transactions on Vehicular Technology*, vol. 68, no. 8, pp. 7715–7722, Aug. 2019.

[37] X. Guo, N. R. Elikplim, N. Ansari, L. Li, and L. Wang, "Robust WiFi localization by fusing derivative fingerprints of RSS and multiple classifiers," *IEEE Transactions on Industrial Informatics*, vol. 16, no. 5, pp. 3177–3186, May 2020.

[38] C. Saha, M. Afshang, and H. S. Dhillon, "3GPP-inspired HetNet model using poisson cluster process: Sum-product functionals and downlink coverage," *IEEE Transactions on Communications*, vol. 66, no. 5, pp. 2219–2234, May 2018.

[39] M. Afshang, C. Saha, and H. S. Dhillon, "Nearest-neighbor and contact distance distributions for matérn cluster process," *IEEE Communications Letters*, vol. 21, no. 12, pp. 2686–2689, Dec. 2017.

[40] R. I. Bor-Yaliniz, A. El-Keyi, and H. Yanikomeroglu, "Efficient 3-D placement of an aerial base station in next generation cellular networks," in *IEEE International Conference on Communications (ICC)*, Jul. 2016, pp. 1–5.

[41] J. Lyu, Y. Zeng, R. Zhang, and T. J. Lim, "Placement optimization of UAV-mounted mobile base stations," *IEEE Communications Letters*, pp. 1–4, Mar. 2017.

[42] C. Lai, C. Chen, and L. Wang, "On-demand density-aware UAV base station 3D placement for arbitrarily distributed users with guaranteed data rates," *IEEE Wireless Communications Letters*, vol. 8, no. 3, pp. 913–916, Jun. 2019.

[43] W. Mei and R. Zhang, "Cooperative downlink interference transmission and cancellation for cellular-connected UAV: A divide-and-conquer approach," *IEEE Transactions on Communications*, vol. 68, no. 2, pp. 1297–1311, Feb. 2020.

[44] N. Cheng, F. Lyu, W. Quan, C. Zhou, H. He, W. Shi, and X. Shen, "Space/aerial-assisted computing offloading for IoT applications: A learning-based approach," *IEEE Journal on Selected Areas in Communications*, vol. 37, no. 5, pp. 1117–1129, May 2019.

[45] B. Li, Z. Fei, and Y. Zhang, "UAV communications for 5G and beyond: Recent advances and future trends," *IEEE Internet of Things Journal*, vol. 6, no. 2, pp. 2241–2263, Apr. 2019.

[46] W. Shi, J. Li, N. Cheng, F. Lyu, S. Zhang, H. Zhou, and X. Shen, "Multi-drone 3-D trajectory planning and scheduling in drone-assisted radio access networks," *IEEE Transactions on Vehicular Technology*, vol. 68, no. 8, pp. 8145–8158, Aug. 2019.

[47] Q. Wu, Y. Zeng, and R. Zhang, "Joint trajectory and communication design for multi-UAV enabled wireless networks," *IEEE Transactions on Wireless Communications*, vol. 17, no. 3, pp. 2109–2121, Mar. 2018.

[48] D. Kim, H. Lee, and D. Hong, "A survey of in-band full-duplex transmission: From the perspective of PHY and MAC layers," *IEEE Communications Surveys Tutorials*, vol. 17, no. 4, pp. 2017–2046, Fourthquarter 2015.

[49] C. Nam, C. Joo, and S. Bahk, "Joint subcarrier assignment and power allocation in full-duplex OFDMA networks," *IEEE Transactions on Wireless Communications*, vol. 14, no. 6, pp. 3108–3119, Jun. 2015.

[50] S. Goyal, C. Galiotto, N. Marchetti, and S. Panwar, "Throughput and coverage for a mixed full and half duplex small cell network," in *IEEE International Conference on Communications (ICC)*, May 2016, pp. 1–7.

[51] L. Chen, C. Zhong, H. Lin, and Z. Zhang, "Joint user pairing and power allocation design for heavy loaded full-duplex small cell systems," *IEEE Transactions on Vehicular Technology*, vol. 67, no. 9, pp. 8989–8993, Sept. 2018.

[52] L. Zhang and N. Ansari, "Optimizing the deployment and throughput of DBSs for uplink communications," *IEEE Open Journal of Vehicular Technology*, vol. 1, pp. 18–28, Jan. 2020.

[53] ——, "Backhaul-aware uplink communications in full-duplex DBS-aided HetNets," in *IEEE Global Communications Conference (GLOBECOM)*, Dec. 2019, pp. 1–6.

[54] M. Curran, M. Rahman, H. Gupta, K. Zheng, J. Longtin, S. Das, and T. Mohamed, "FSONet: A wireless backhaul for multi-gigabit picocells using steerable free space optics," in *the 23rd Annual International Conference on Mobile Computing and Networking (MobiCom)*, Oct. 2017, pp. 154–166.

[55] S. Sarkar, V. Janyani, G. Singh, T. Ismail, and H. A. Selmy, "Design of 64 QAM transceiver model and its performance analysis for FSO communication," in *Proc. of International Conference on Signal Processing and Integrated Networks*, Feb. 2018, pp. 630–634.

[56] N. Ansari and L. Zhang, "Flexible backhaul-aware DBS-aided HetNet with IBFD communications," *ICT Express*, vol. 6, no. 1, pp. 48–56, Mar. 2020.

[57] M. S. Elbamby, M. Bennis, W. Saad, M. Debbah, and M. Latva-aho, "Resource optimization and power allocation in in-band full duplex-enabled non-orthogonal multiple access networks," *IEEE Journal on Selected Areas in Communications*, vol. 35, no. 12, pp. 2860–2873, Dec. 2017.

[58] L. Fleischer, M. Goemans, V. Mirrokni, and M. Sviridenko, "Tight approximation algorithms for maximum general assignment problems," in *Proceedings of the 17th Annual ACM-SIAM Symposium on Discrete Algorithms*, Jan. 2006, pp. 611–620.

[59] L. Zhang, T. Han, and N. Ansari, "Renewable energy-aware inter-datacenter virtual machine migration over elastic optical networks," in *IEEE 7th International Conference on Cloud Computing Technology and Science (CloudCom)*, Dec. 2015, pp. 440–443.

[60] L. Zhang, N. Ansari, and A. Khreishah, "Anycast planning in space division multiplexing elastic optical networks with multi-core fibers," *IEEE Communications Letters*, vol. 20, no. 10, pp. 1983–1986, Oct. 2016.

[61] L. Zhang, T. Han, and N. Ansari, "Energy-aware virtual machine management in inter-datacenter networks over elastic optical infrastructure," *IEEE Transactions on Green Communications and Networking*, vol. 2, no. 1, pp. 305–315, Mar. 2018.

[62] M. Andrews, A. Ghosh, R. N. Pupala, and S. Vasudevan, "Performance evaluation of self backhauled small cell heterogeneous networks," *IEEE Transactions on Wireless Communications*, vol. 16, no. 5, pp. 3102–3110, May 2017.

[63] X. Cao, F. Wang, J. Xu, R. Zhang, and S. Cui, "Joint computation and communication cooperation for energy-efficient mobile edge computing," *IEEE Internet of Things Journal*, vol. 6, no. 3, pp. 4188–4200, Jun. 2019.

[64] K. L. Lueth, "State of the IoT 2018: Number of IoT devices now at 7B – market accelerating," Aug. 2018. [Online]. Available: https://iot-analytics.com/state-of-the-iot-update-q1-q2-2018-number-of-iot-devices-now-7b/

[65] Y. Du, K. Wang, K. Yang, and G. Zhang, "Energy-efficient resource allocation in UAV based MEC system for IoT devices," in *IEEE Global Communications Conference (GLOBECOM)*, 2018, pp. 1–6.

[66] X. Sun and N. Ansari, "EdgeIoT: Mobile edge computing for the internet of things," *IEEE Communications Magazine*, vol. 54, no. 12, pp. 22–29, Dec. 2016.

[67] P. Wang, C. Yao, Z. Zheng, G. Sun, and L. Song, "Joint task assignment, transmission, and computing resource allocation in multilayer mobile edge computing systems," *IEEE Internet of Things Journal*, vol. 6, no. 2, pp. 2872–2884, Apr. 2019.

[68] N. Ansari and X. Sun, "Mobile edge computing empowers Internet of Things," *IEICE Transactions on Communications*, vol. E101-B, no. 3, pp. 604–619, Mar. 2018.

[69] J. Zhang, L. Zhou, Q. Tang, E. C. . Ngai, X. Hu, H. Zhao, and J. Wei, "Stochastic computation offloading and trajectory scheduling for UAV-assisted mobile edge computing," *IEEE Internet of Things Journal*, vol. 6, no. 2, pp. 3688–3699, Apr. 2019.